

Supplementary Material to
Age-specific transmission dynamics of SARS-CoV-2
during the first two years of the pandemic

Otilia Boldea, PhD¹, Amir Alipoor, MSc¹, Sen Pei, PhD², Jeffrey Shaman, PhD^{2,3}, and Ganna Rozhnova, PhD^{*4,5,6}

¹Department of Econometrics and OR and CentER, Tilburg School of Economics and Management, Tilburg University, Tilburg, The Netherlands

²Department of Environmental Health Sciences, Mailman School of Public Health, Columbia University, New York, USA

³Columbia Climate School, Columbia University, New York, USA

⁴Julius Center for Health Sciences and Primary Care, University Medical Center Utrecht, Utrecht University, Utrecht, The Netherlands

⁵BioISI—Biosystems & Integrative Sciences Institute, Faculdade de Ciências, Universidade de Lisboa, Lisbon, Portugal

⁶Center for Complex Systems Studies (CCSS), Utrecht University, Utrecht, The Netherlands

December 6, 2022

*Corresponding author:

Dr Otilia Boldea
Department of Econometrics and OR, and CentER
Tilburg School of Economics and Management, Tilburg University
P.O. Box 90153, Tilburg, The Netherlands
E-mail: o.boldea@tilburguniversity.edu, phone: +31 134663219

Dr. Ganna Rozhnova
Julius Center for Health Sciences and Primary Care
University Medical Center Utrecht
P.O. Box 85500 Utrecht, The Netherlands
Email: g.rozhnova@umcutrecht.nl, phone: +31 631117965

Contents

1 Data	4
1.1 Population N_{ik}	4
1.2 Reported cases $I_{newik}^{obs}(t)$	4
1.3 Hospital admissions $H_{newik,(1)}^{obs}(t), H_{newi,(2)}^{obs}(t), H_{newk,(3)}^{obs}(t)$	6
1.4 Seroprevalence data $t_h^{ser}, ser_{hk}, n_{hk}, h = 1, \dots, 4$ rounds	10
1.5 Mobility $M_{ij}(t)$	10
1.6 Vaccinations $V_{ik}(t)$	12
1.7 Booster transition function $g_{B,k}(t)$	15
1.8 Variants of concern transition functions $g_\alpha(t), g_\delta(t), g_o(t)$	15
1.9 Elementary and secondary school contact matrices $c_{ikk^*,ES}(t), c_{ikk^*,SS}(t)$, all-setting contact matrix $c_{kk^*}^{(r)}$, and non-school contact matrix $c_{kk^*,NS}^{(r)}$ from surveys $r = 1, 2, 3$, among age categories $k, k^* = 1, 2, 3$	16
2 Model	19
2.1 Model without vaccination	19
2.2 Model with vaccination	22
2.3 Modelling time-varying parameters	22
2.4 Modelling time variation in non-school contact matrices as a result of NPIs	24
3 Inference	26
3.1 Calibrated parameters	27
3.2 Estimated parameters and their priors	31
3.3 Estimation via the ensemble adjustment Kalman filter	32
3.4 Algorithm	34
4 Parameter Estimates	35
4.1 Time Evolution of Posterior Distributions	35
4.2 Parameter estimates over variant periods	39
5 Supplement to Main Text, Section “Results”	41
5.1 Time-dependent burden of hospital admissions	41
5.2 Time-dependent burden of confirmed cases and seroprevalence	45
5.3 Age distribution of total infections and hospital admissions by VoC	56
5.4 Age-specific burden stratification by immune status and VoC	58
6 Parameter and system identifiability	59
6.1 Simulated model fit	59
6.2 Parameter identification	64
7 Sensitivity analysis	67
7.1 Sensitivity to seroprevalence	67
7.2 Sensitivity to waning rates	67

7.3	Sensitivity to higher transmissibility of Omicron	68
7.4	Sensitivity to seasonality factor	69

1 Data

Table 1 (main text) gives an overview of the data, notation, and sources. In this section, we explain how we constructed each dataset or estimated some logistic transition functions to be further used in the model fitting.

1.1 Population N_{ik}

The population data is retrieved from the Dutch Central Bureau of Statistics (CBS), stratified by province and age into groups of one year on January 1, 2020. We assume for simplicity that the population in each age category and province is constant over the entire study period considered.

1.2 Reported cases $I_{new}^{obs}(t)$

We use daily data on reported positive PCR tests by age and province from the RIVM (National Institute for Public Health and the Environment, Bilthoven, The Netherlands) Dashboard, from February 27, 2020, when the first case was reported, until January 31, 2022. The data are by self-reported date of symptoms if that date is known, otherwise by the date of positive lab result, or, if that is unknown, by date of reporting. Since the recommendation in the Netherlands throughout most of the pandemic was to test if symptomatic, and the capacity for contact tracing remained limited so that asymptomatic testing was not very frequent in most periods, most of the reported cases are by the self-reported first date of symptoms. However, there are many unreported symptomatic cases because although the testing capacity was substantially expanded over the pandemic, it remained limited in most waves. Note that the lowest administrative units for which these data are available are the twenty-five *safety regions* corresponding to all the decentralized public health organizations (GGDs) organizing PCR tests and reporting to the RIVM. However, we chose to use province-level data, because, for children and adolescents, the number of confirmed cases per safety region is very small and contains many zeros in the first half year since the onset of the pandemic. The data are plotted in Figures S1-S3, divided by the population in each province and multiplied by 1,000 individuals to facilitate comparison. The figures show substantial synchronization in the timing of the waves across provinces, in each age category, motivating the use of a metapopulation model with mobility across provinces to capture the rapid spread of SARS-CoV-2 across the country.

Figure S1: Adult: Daily reported cases per 1,000 people in each province

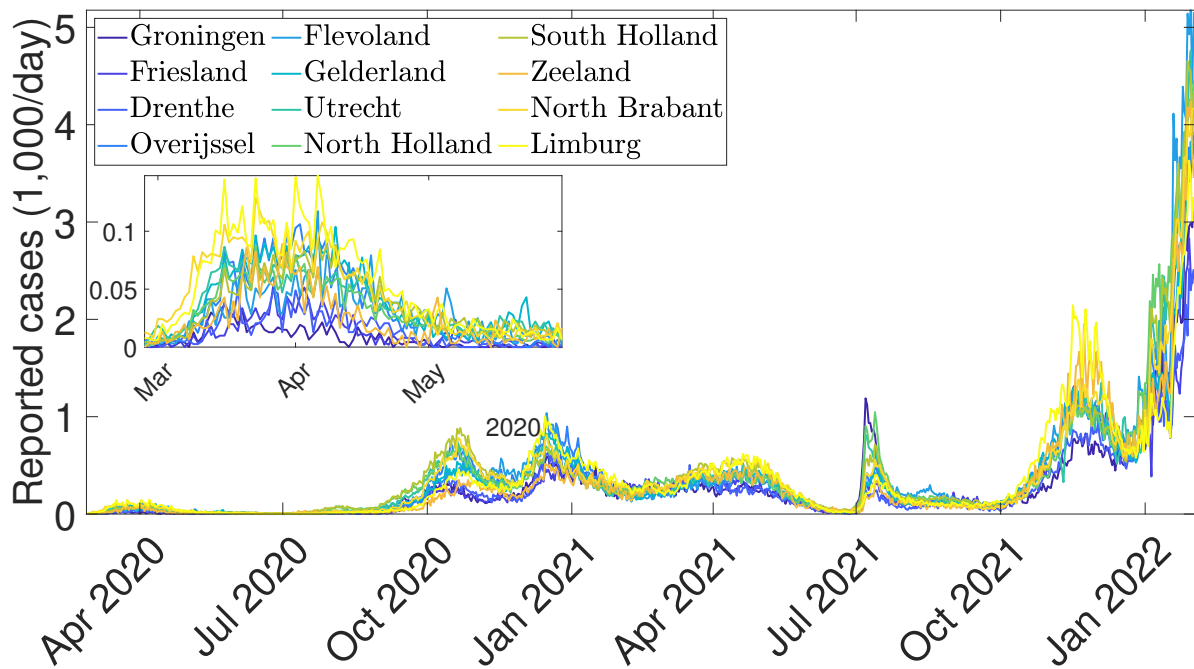


Figure S2: Adolescents: Daily reported cases per 1,000 people in each province

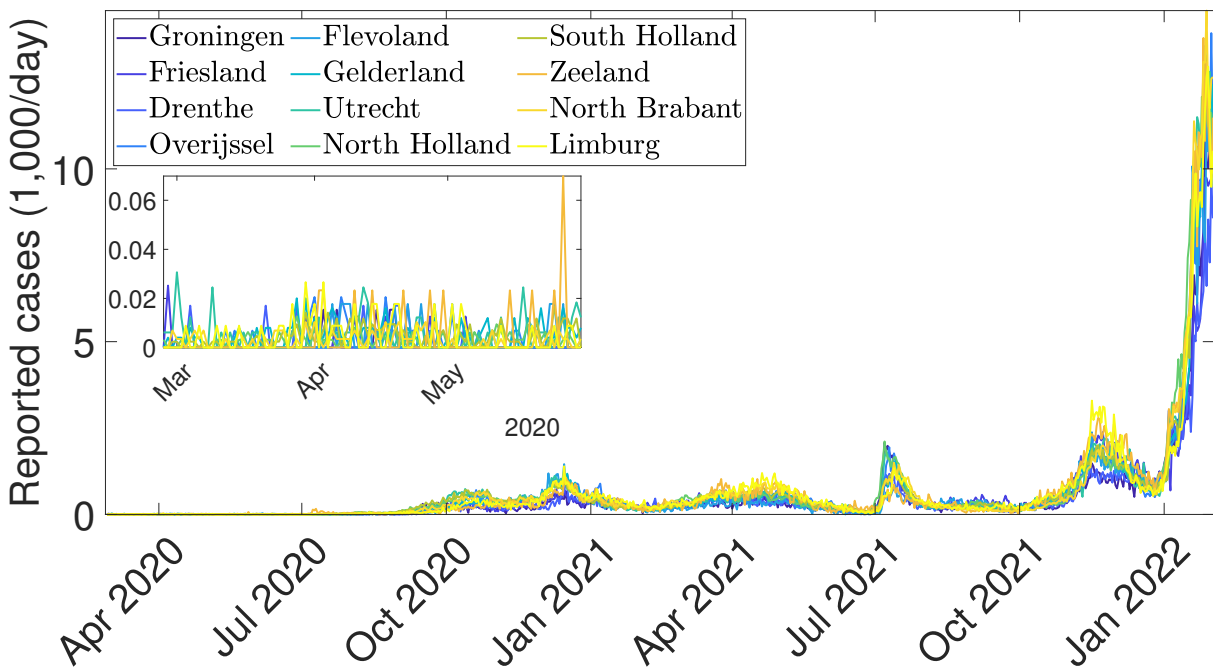
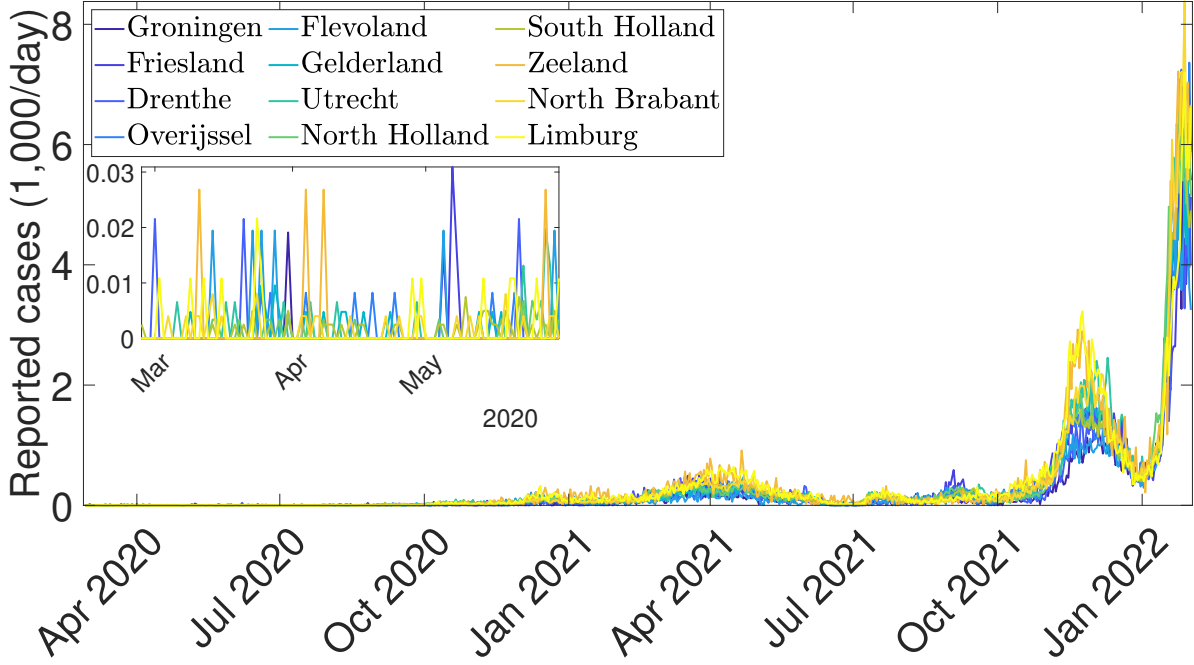


Figure S3: Young children: Daily reported cases per 1,000 people in each province



1.3 Hospital admissions $Hnew_{ik,(1)}^{obs}(t)$, $Hnew_{i,(2)}^{obs}(t)$, $Hnew_{k,(3)}^{obs}(t)$.

We use three sources of hospitalization data. Dataset 1, $Hnew_{ik,(1)}^{obs}(t)$, contains daily data on new hospital admissions by date of (first) hospitalization, age, and province of origin from February 27, 2020 until September 30, 2021, and was obtained from the RIVM. Since the number of new daily hospitalizations per province for children and adolescents was small, and often zero, for them, we fitted the model to the national new daily hospital admissions data, while for adults, we fitted the model to new daily hospital admissions per province. These data divided by the population in each province and age group and multiplied by 1,000 are plotted in Figures S4-S5. For fitting the model after September 30, 2021, we used Dataset 2, $Hnew_{i,(2)}^{obs}(t)$, featuring publicly available new daily hospital admissions per province. According to the data description, the hospitalizations should also largely be by date of new admission, but sometimes they are by date of reporting. Figures S6-S8 show substantial agreement across these two datasets. Dataset 3, $Hnew_{k,(3)}^{obs}(t)$, is also used in the estimation after September 30, 2021. To construct this dataset, we retrieved publicly available data on new weekly hospital admissions per age categories 0-14 and 15-19 (source is listed in Table 1, main text). Because most of these admissions in the 0-14 age category were likely to be among the younger children, as observed for other countries - [12], and there were much fewer hospitalizations in age category 15-19 than in age category 0-14, we multiplied the hospitalizations in age category 15-19 with the population age 10-19 and divided by the population age 15-19, to obtain weekly hospitalizations for adolescents. The weekly hospitalizations for children are obtained by subtracting these from the total new admissions for both age categories 0-14 and 15-19. We then divided these time series by 7 and took a seven-day moving average to obtain daily hospitalizations in children and adolescents. The resulting series is plotted against Dataset 1 and 2 in Figure S9, showing substantial agreement with both datasets at the national level.

Figure S4: Dataset 1: Daily hospital admissions per 1,000 adults in each province

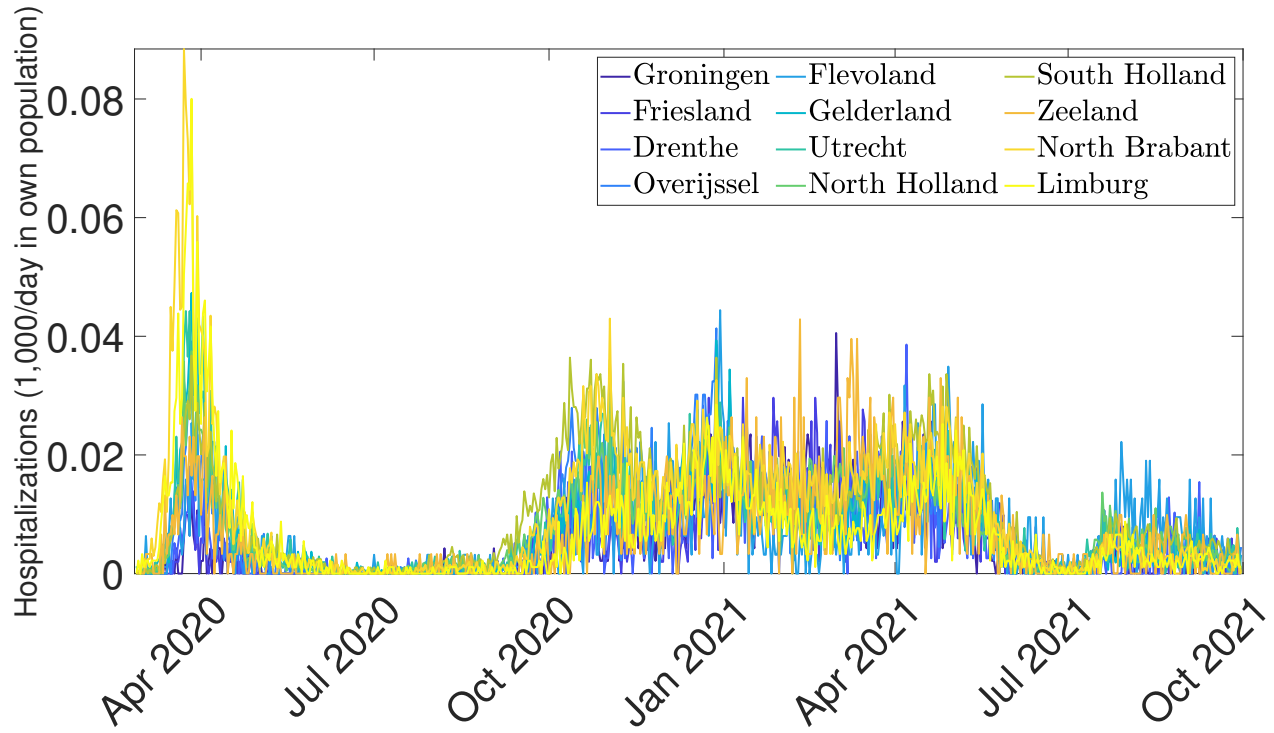


Figure S5: Dataset 1: Daily hospital admissions per 1,000 people in each age category

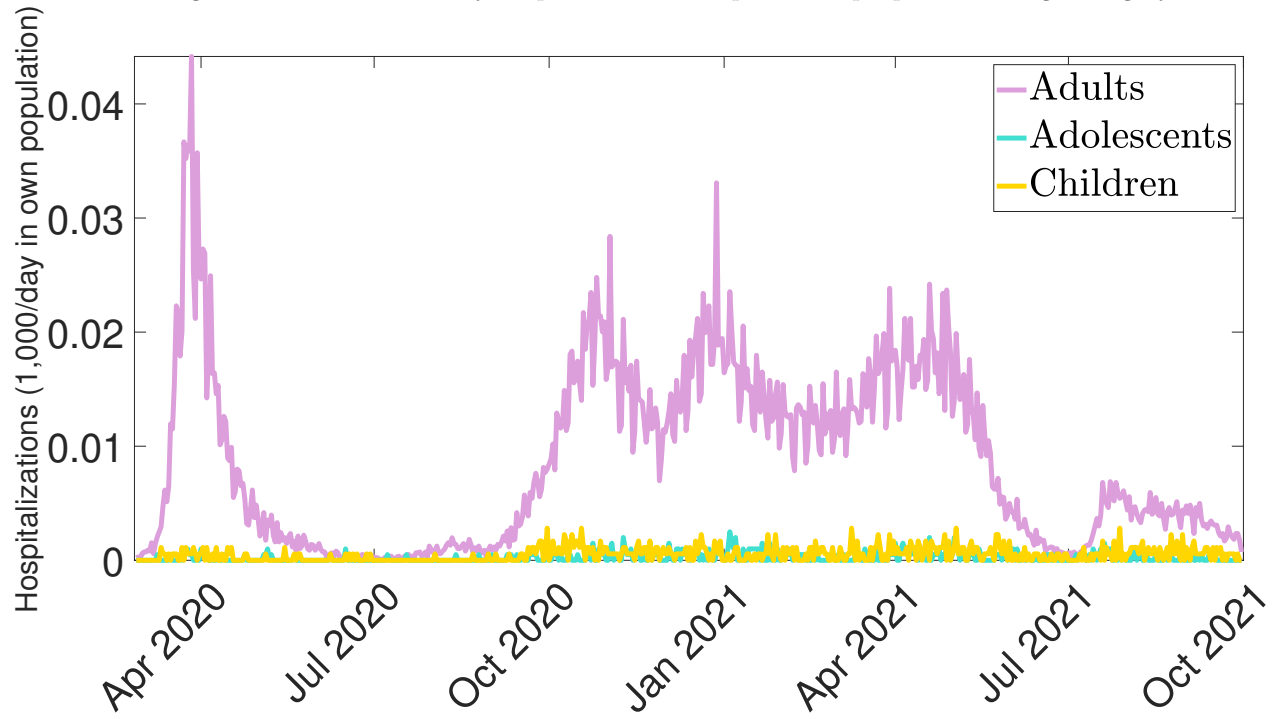
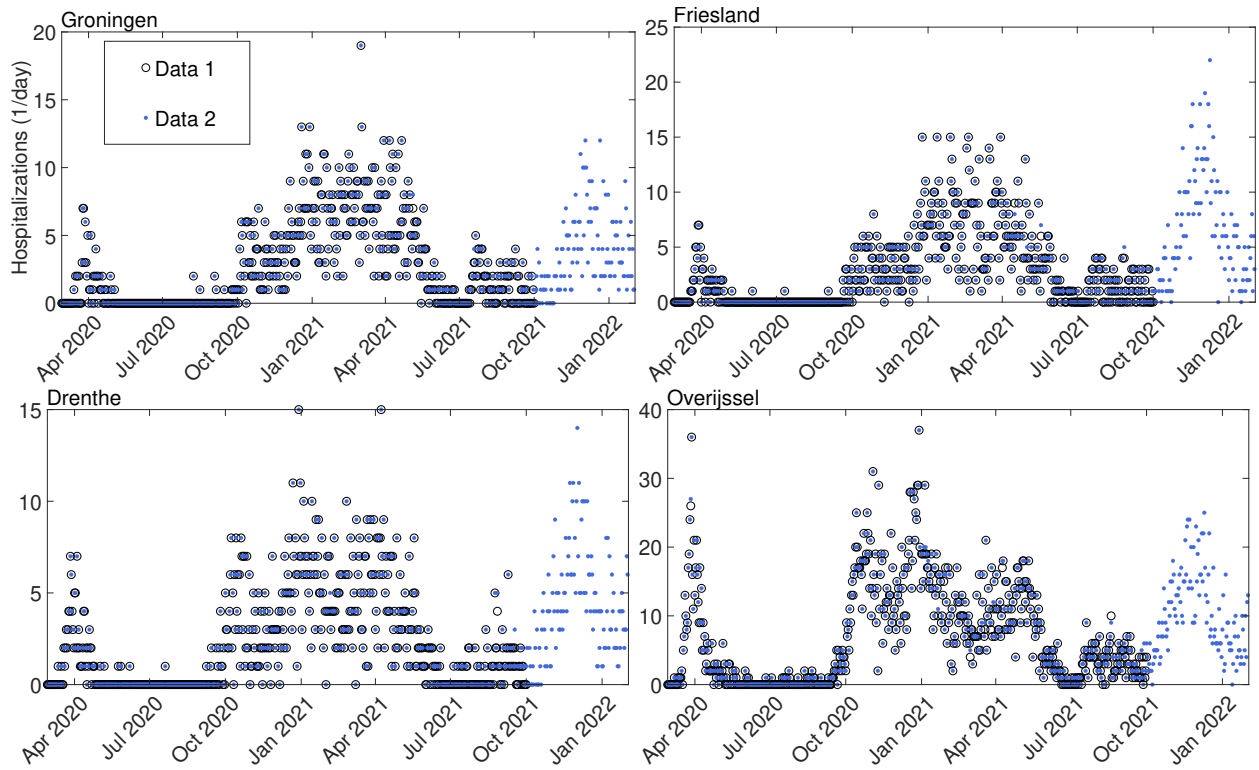
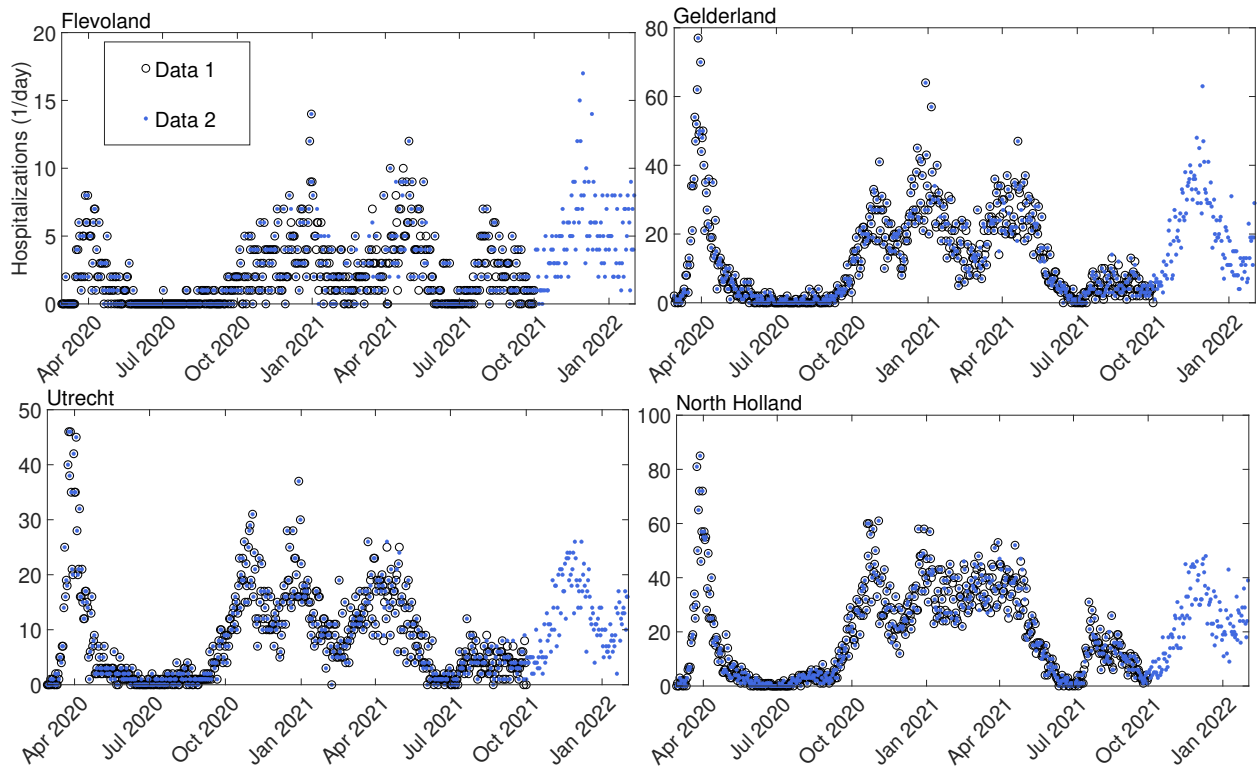


Figure S6: Daily hospital admissions: Dataset 1 (sum over age categories) versus Dataset 2. Part I



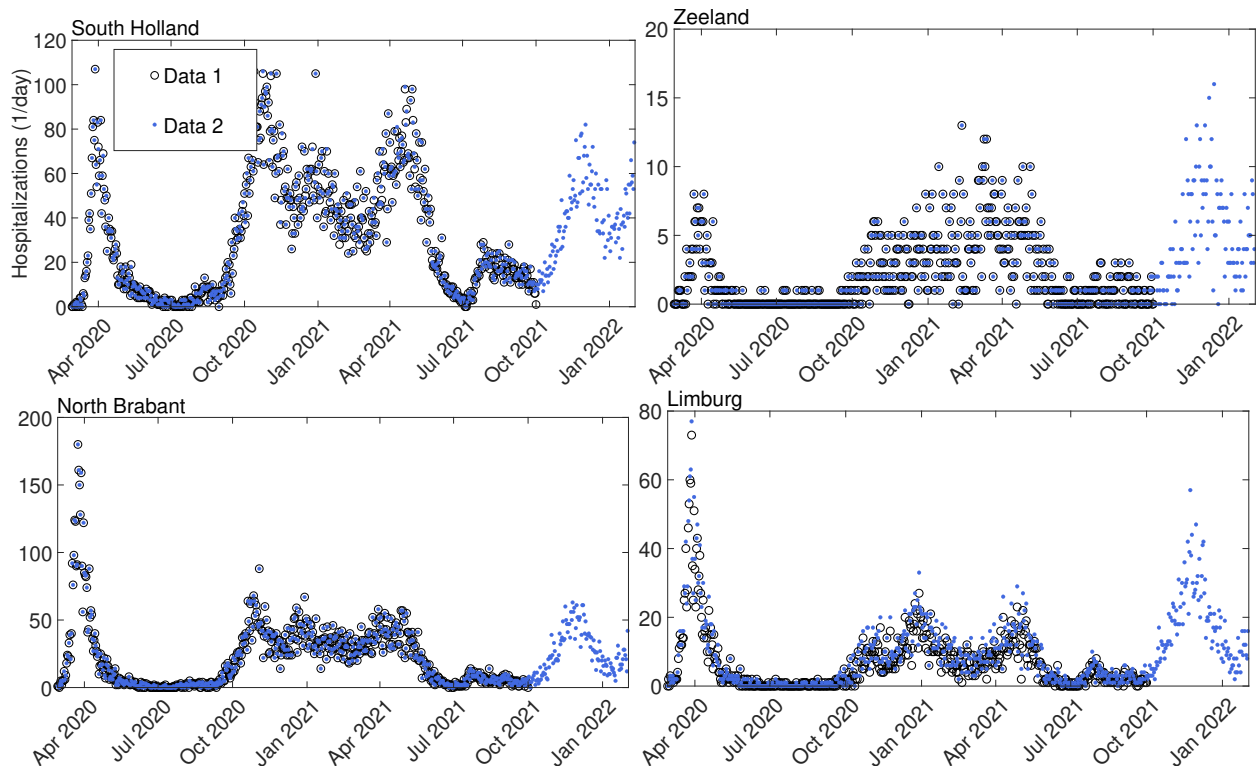
Note: Data 1 are used in the estimation until September 30, 2021, and Data 2 (RIVM Dashboard) are used afterwards.

Figure S7: Daily hospital admissions: Dataset 1 (sum over age categories) versus Dataset 2. Part II



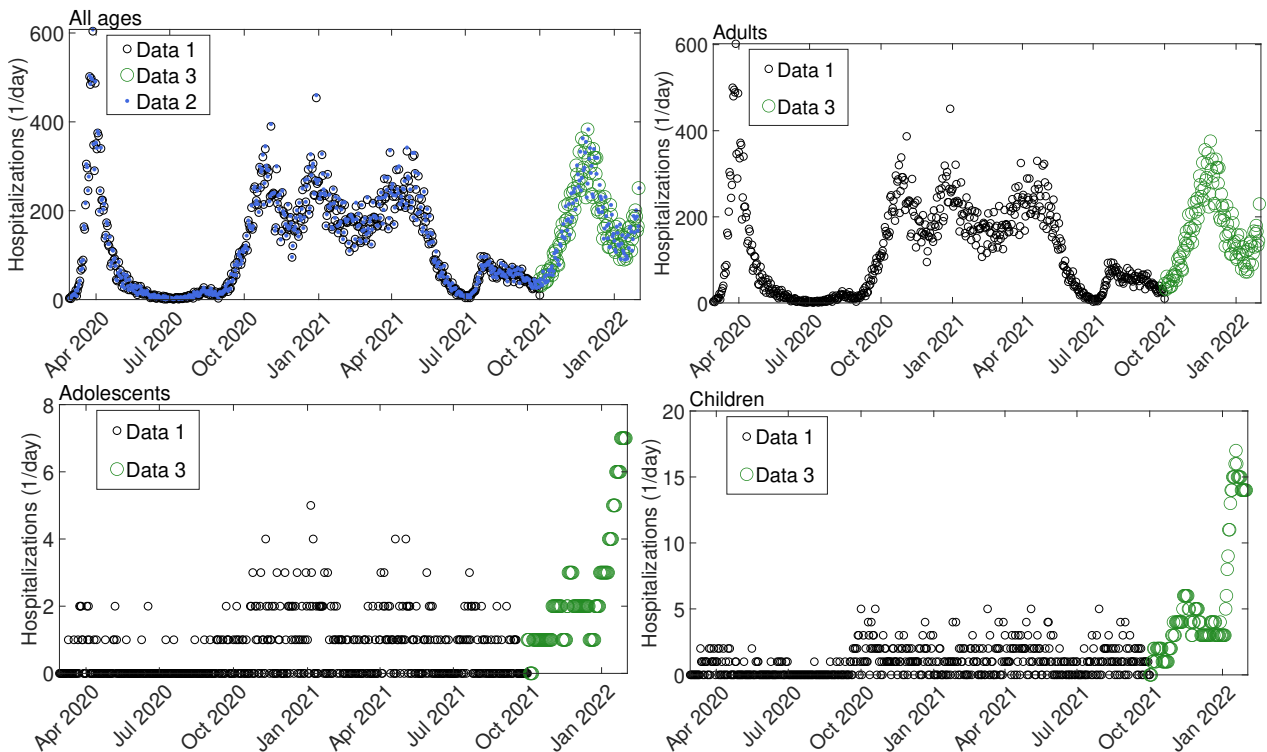
Note: Data 1 are used in the estimation until September 30, 2021, and Data 2 (RIVM Dashboard) are used afterwards.

Figure S8: Daily hospital admissions: Dataset 1 (sum over age categories) versus Dataset 2. Part III



Note: Data 1 are used in the estimation until September 30, 2021, and Data 2 (RIVM Dashboard) are used afterwards.

Figure S9: Daily hospital admissions: Dataset 1, 2 and 3 at the national level, and Dataset 1 versus Dataset 3 per age.



Note: Data 1 (RIVM) are used in the estimation until September 30, 2021, and Data 2 and 3 (RIVM Dashboard) are used afterwards.

1.4 Seroprevalence data $t_h^{ser}, ser_{hk}, n_{hk}, h = 1, \dots, 4$ rounds

We obtained from the RIVM seroprevalence data for four national random population serosurvey rounds of the PIENTER Corona Study (note that more rounds were conducted afterwards, but the underlying data are only available in graphical form, so we could not use them). The first four rounds of this survey were conducted before vaccination in April-May 2020 (median inclusion time April 3, 2020), June-July 2020 (median inclusion time June 4, 2020), September - November (median inclusion time September 28, 2020), and February 2021 (median inclusion time not available, we assumed it to be February 11, 2021, based on comparing the fraction of individuals fully vaccinated in the serological sample and in the population). The seroconversion date assumed when fitting the model was the median inclusion time minus 14 days to allow for seroconversion, and specification checks were done for 10 days instead of 14, or not using the seroprevalence data at all. The serosurvey data include the number of people who tested positive for antibodies and the total number of samples in age categories of 5 years. The cumulative seroprevalence for children, adolescents, and adults (ser_{hk}), the percentage of positive samples in the total samples (n_{hk}), and the seroconversion date (t_h^{ser}) are shown in Table S1.

Table S1: Seroprevalence data.

	Round 1		Round 2		Round 3		Round 4	
t_h^{ser}	$t_1^{ser} = \text{March 20, 2020}$		$t_2^{ser} = \text{June 6, 2020}$		$t_3^{ser} = \text{September 14, 2021}$		$t_4^{ser} = \text{January 28, 2021}$	
Age k	n_{1k}	ser_{1k}	n_{2k}	ser_{2k}	n_{3k}	ser_{3k}	n_{4k}	ser_{4k}
> 19	2549	0.030	5685	0.051	5196	0.054	6078	0.123
10-19	291	0.027	623	0.035	515	0.037	659	0.141
0-9	366	0.011	505	0.010	382	0.008	565	0.062

1.5 Mobility $M_{ij}(t)$

For the model, we need the number of commuters between the provinces rather than the percentage change in commuters, as reported by Google mobility data. To approximate the number of commuters, we obtained daily train mobility data from the National Railway Company (Nederlandse Spoorwegen - NS, effectively a monopoly for railway travel in the Netherlands), from February 1, 2020 until September 30, 2021. In the Netherlands, almost all individuals travel on trains with a card where they need to check-in at the origin and check-out at their destination. This allows NS to track the number of travelers at a given time in a given region.¹ The NS data contains the total number of check-ins and check-outs registered daily in a municipality, in periods of six hours (8 : 00 – 14 : 00, 14 : 00 – 20 : 00, 20 : 00 – 2 : 00, 2 : 00 – 8 : 00). The origin of the commuters is not available in the data we received.

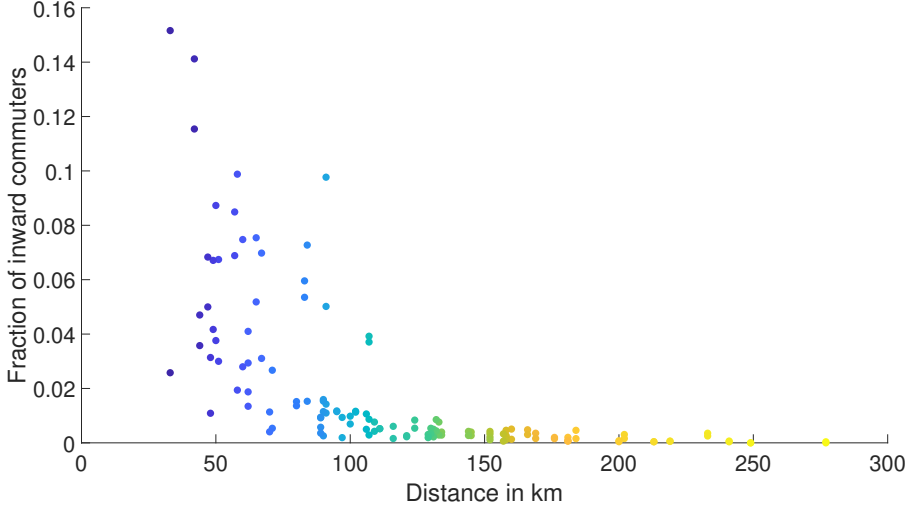
We first aggregated the data to the province level j by adding all municipalities in a province, then daily, by calculating $M_j^{in}(t)$ as the daily sum of all check-ins within the four six-hour intervals, and $M_j^{out}(t)$ as the daily sum of all check-outs within the same intervals, starting at 8 : 00 am. The data were available only if the number of check-ins or check-outs was 15 or more. Only 139 municipalities have at least one observation that is larger than 15, but most of them do not have a dedicated train station. For these municipalities, we simply assume that there are zero travelers when the travel data are not displayed.²

¹A small number of travelers such as young children may travel at particular hours on adults' travel cards without paying, and some people may forget to check in when buying a ticket, under-estimating the number of travelers. Since our model in Section 2 allows for a reporting error, we ignore these biases in the data construction.

²We could have drawn random integers between 0 and 15 to fill in the missing data. However, when adding up municipalities, we would induce possibly large measurement errors in the mobility data.

To construct the number of travelers across all province pairs, which we need in the model, we use pre-pandemic CBS data from 2019 on the fractions of employees living in province j but working in province i , w_{ij} . These data are static but computed for virtually the entire workforce in the Netherlands at the time of data collection. We construct two fractions of commuters from j to i and i to j , $w_{ij}^{(1)} = \frac{w_{ij}}{\sum_{i=1}^{12} w_{ij}}$ and $w_{ij}^{(2)} = \frac{w_{ji}}{\sum_{i=1}^{12} w_{ji}}$. The fractions $w_{ij}^{(1)}$ are plotted against the “as the crow flies” distance between provinces³ in Figure S10.

Figure S10: Fraction of inward commuters to each province from other provinces, $w_{ij}^{(1)}, i \neq j$.



Note: distances “as the crow flies” are calculated between the centers of each province. This is why the minimum distance traveled is shown as approximately 50 km, even though individuals also travel across municipalities that are closer to each other.

To take advantage of the fact that the railway data provide both inward and outward daily movements M_i^{in} and M_i^{out} , we constructed the number of people living in province j and commuting to province i in two ways: $M_{ij}^{(1)}(t) = w_{ij}^{(1)} M_j^{in}(t)$, and $M_{ij}^{(2)}(t) = w_{ji}^{(2)} M_i^{out}(t)$. Since $M_{ij}^{(1)}(t)$ and $M_{ij}^{(2)}(t)$ are slightly different, due to, among other reasons, replacing the missing train data with zeros as discussed above, people traveling multiple times or forgetting to check out⁴, we average across the two measurements: $M_{ij}(t) = (M_{ij}^{(1)}(t) + M_{ij}^{(2)}(t))/2$. Since the travel data do not include people traveling across provinces by other means, such as by car or train, we take this into account in our model in Section 2 via a reporting error that multiplies $M_{ij}(t)$ and accounts both for this under-reporting and for the fact that commuters between provinces do not commute every day to work but work part-time at home, as working from home a few days a week was common in the Netherlands before the pandemic. The implicit assumption when using train data in the model in Section 2 is that individuals travel proportionally to their work-commute pattern, which is a reasonable assumption for the Netherlands, as the country features a well-connected train network, and a large fraction of the population is commuting for work.

The train data are only available until September 30, 2021, but we fitted the model until January 31, 2022. To extrapolate the train data out of sample, we used the national Dutch Google mobility data near transit stations. Since the constructed train data measure the number of commuting people, while the Google mobility data near transit stations show the percentage change in transit, we first constructed the percentage change in $M_{ij}(t)$ over each day of the week relative to the average $M_{ij}(t)$ of those same weekdays in the two weeks from February 1, 2020 until February 14, 2020 before the pandemic. This makes it comparable to the Google mobility data, which

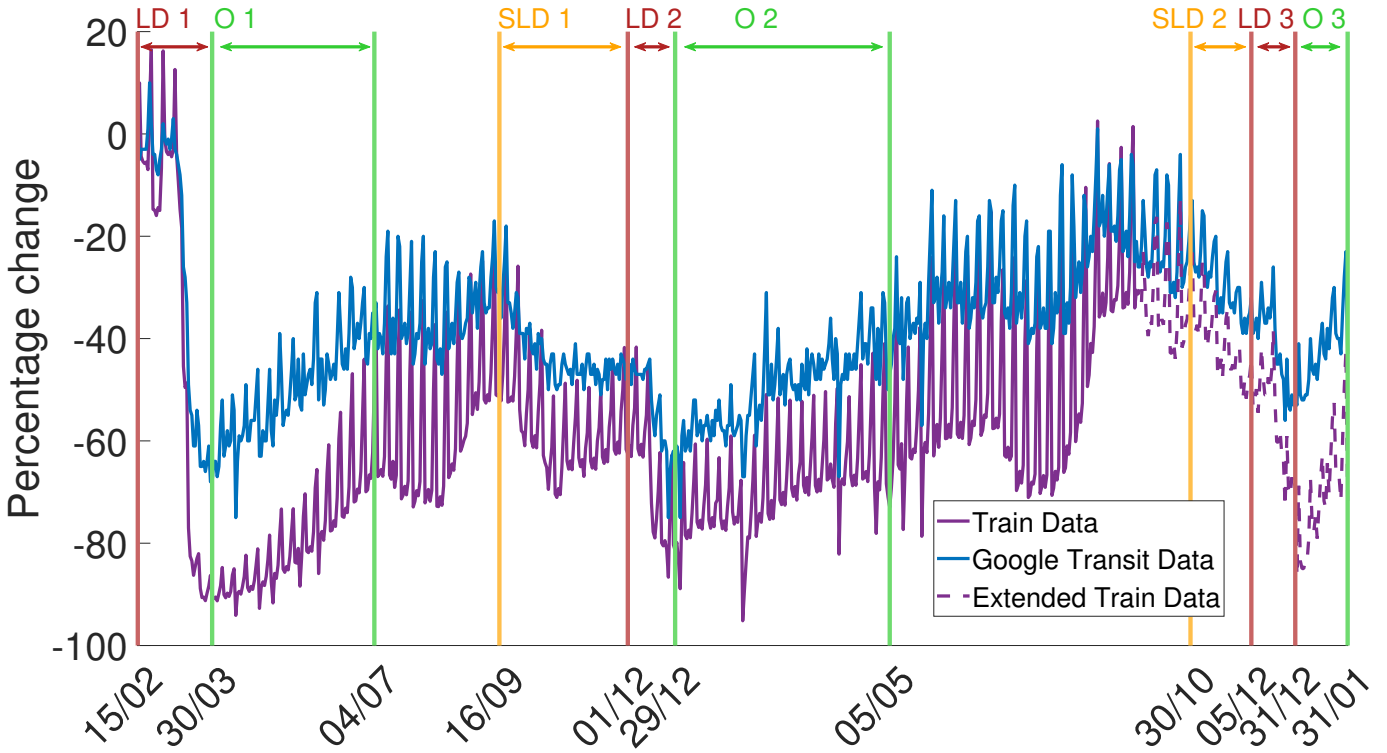
³These distances were retrieved from <https://nl.distance.to>.

⁴The latter should be a small proportion of the travelers because a fine is automatically added if a person did not check out after 24 hours.

is constructed as percentage changes relative to the median mobility on the same weekday of the first 5 weeks of 2020. The two series are plotted in Figure S11, and exhibit similar trends over time.

We make use of these similar trends to extrapolate the train data out of sample. We drop the period until March 30, 2020, and identify periods marked by the introduction of important policy changes. We construct three dummy variables indicating when the elementary schools open after a lockdown (regimes O 1-3 in Figure S11), when there is a semi-lockdown (SLD 1-2 in Figure S11), and when there is a lockdown (regimes LD 1-3 in Figure S11). We then regress the percentage change in the NS data (y_{NS}) on the percentage change in Google mobility data (y_G), an intercept, and interaction terms of y_G with the three dummy variables mentioned above, to account for slope changes when the regime changes, using ordinary least squares.⁵ We then evaluate the regression function at the Google mobility data from October 1, 2021 until January 31, 2022. The extended train data obtained in this way are shown in Figure S11. Since in the model we need the number of commuters rather than the percentage changes, we apply these daily percentage changes to the average number of train commuters in the corresponding weekdays from February 1, 2020 until February 14, 2020.

Figure S11: Google and train mobility near transit stations, and extrapolation of train mobility reduction from October 1, 2021 until January 31, 2022: percentage change relative to February 2020



Note: LD refers to a period transitioning into lockdown, SLD to one transitioning into semi-lockdown, and O indicates the opening of elementary schools after a lockdown. The length of each regime, indicated by the double arrows, is explained in detail in Section 3.1.

1.6 Vaccinations $V_{ik}(t)$

We only consider fully vaccinated individuals, defined as individuals who received the second dose of the Pfizer, Moderna, and AstraZeneca vaccines or a single dose for the Janssen vaccine at least two weeks ago. Note that since the national recommendation was to get only one vaccine dose if individuals had an infection in the previous six months, the individuals who received one dose within six months of a prior infection are included in all freely

⁵More explanation about the regimes can be found in Section 3.1, Figure S19 and Table S8.

available datasets on the RIVM Dashboard as “fully vaccinated”. Since in our model in Section 2 we group the individuals who lost immunity from a previous infection and those fully vaccinated into the same set of compartments, considering these individuals as fully vaccinated is inconsequential for our analysis.

To construct new daily vaccinations per age and province, we use two datasets freely available on the RIVM Dashboard (see Table 1, main text). The first dataset provides the fraction of weekly vaccinations in 5-year age categories (12 – 17 years old at the time of vaccinations, 18 – 22 years old, and so on). We multiply the fraction of weekly vaccinations by the CBS population data in categories of one year, assuming uniform vaccine coverage for individuals in each 5-year category. We transform the data into daily data by simply dividing the weekly vaccination levels per each age group by seven. The second dataset provides the cumulative fraction of fully vaccinated people in two age categories: 12 to 17 years old and above, per province downloaded on February 17, 2022. Therefore, from the cumulative fraction of fully vaccinated population aged 12 years or older per province, we calculate the population-weighted fraction of daily vaccines administered in each province for 12 to 17 years old adolescents, and the rest of the population, older than 17 years. We then assume this fraction is constant over time for adolescents and adults, apply it individually to daily vaccines in all one-year age categories, and aggregate the data to obtain the vaccination schedule for 10 to 19 years old adolescents and the rest of the population. The obtained vaccination schedule is plotted in Figures S12-S14. Note that vaccines for children aged 5 to 11 years old only became available at the end of our sample (end December 2021); therefore, for simplicity, we assume that in the sample, children were not fully vaccinated.

Figure S12: Daily number of fully vaccinated individuals by province and age: I

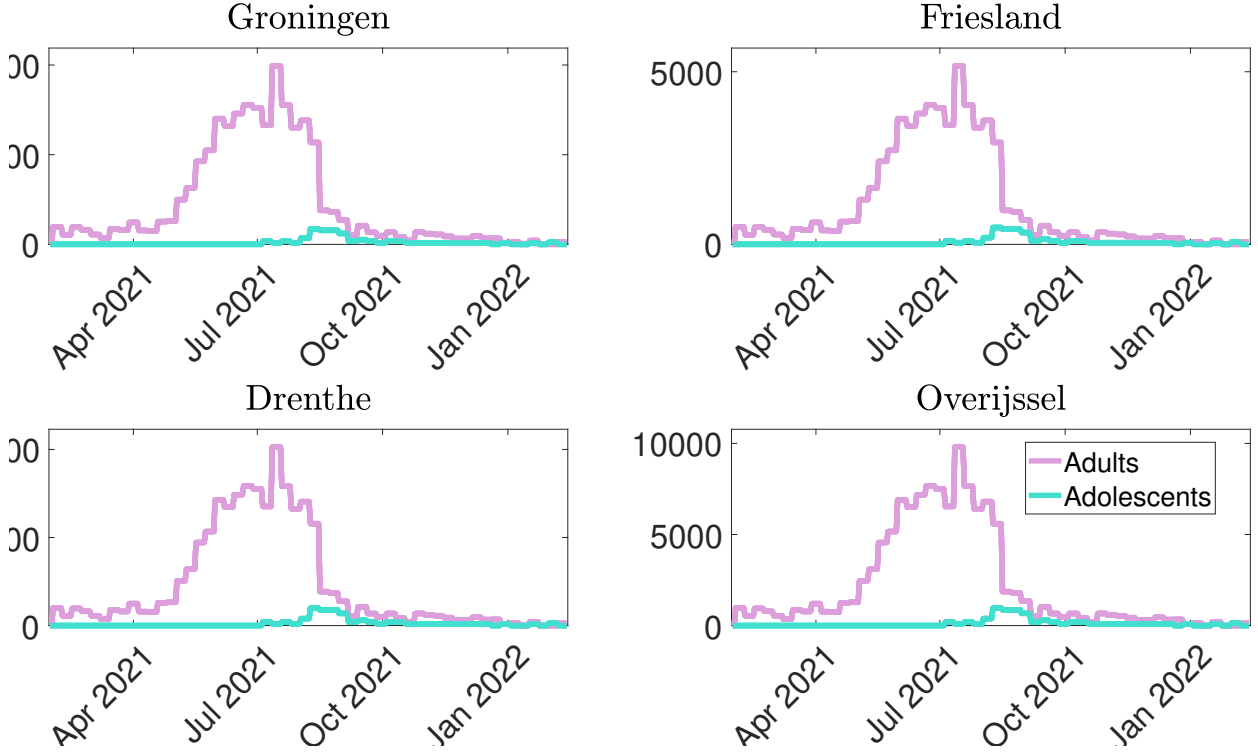


Figure S13: Daily number of fully vaccinated individuals by province and age: II

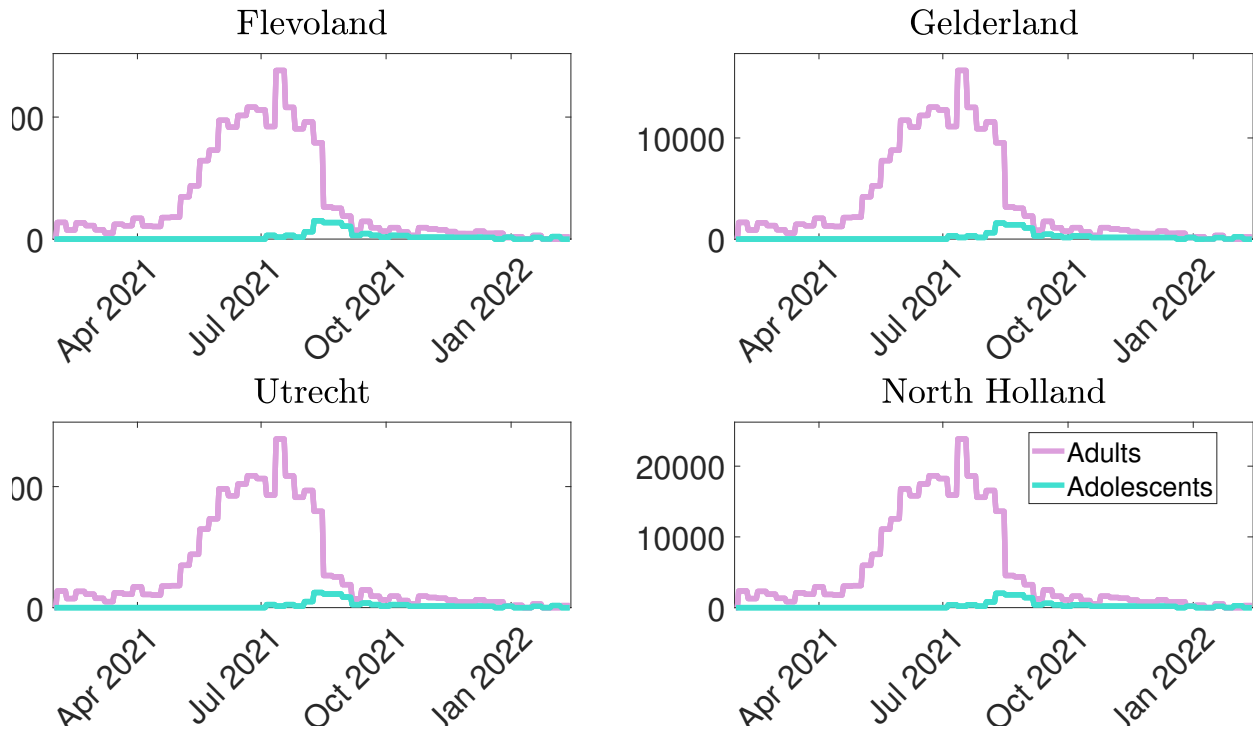
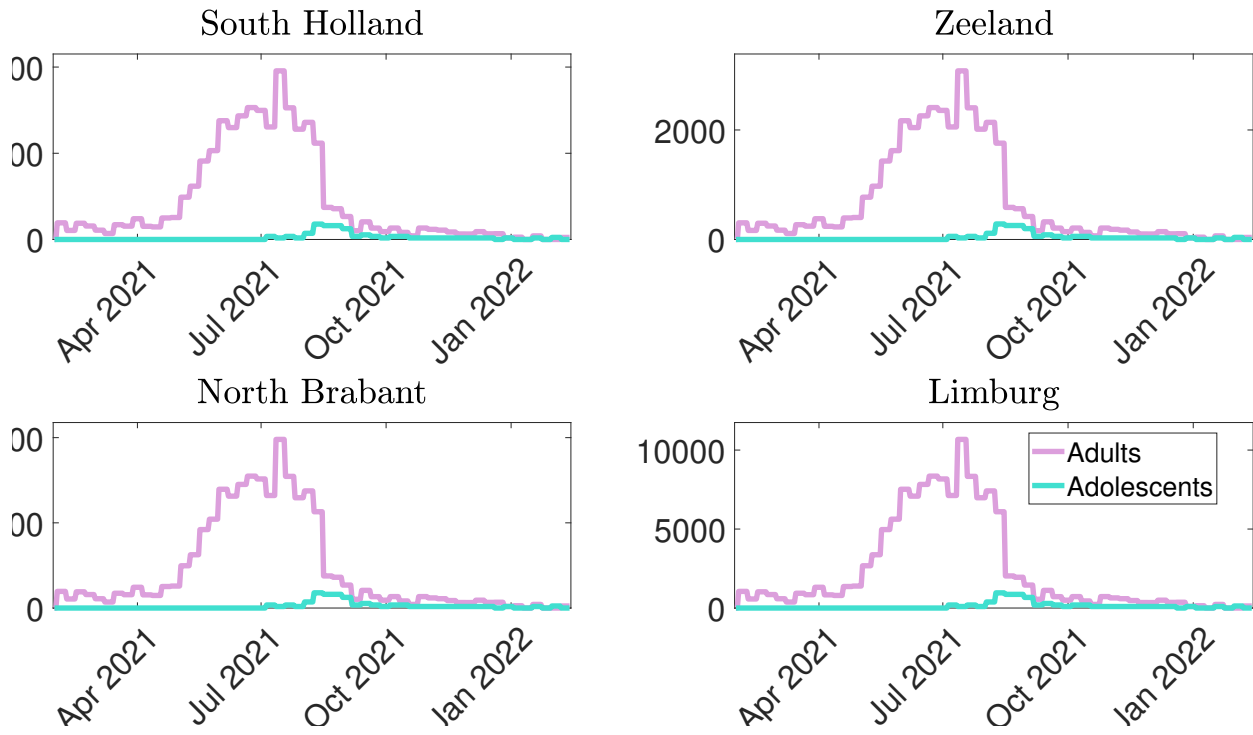


Figure S14: Daily number of fully vaccinated individuals by province and age: III



1.7 Booster transition function $g_{B,k}(t)$

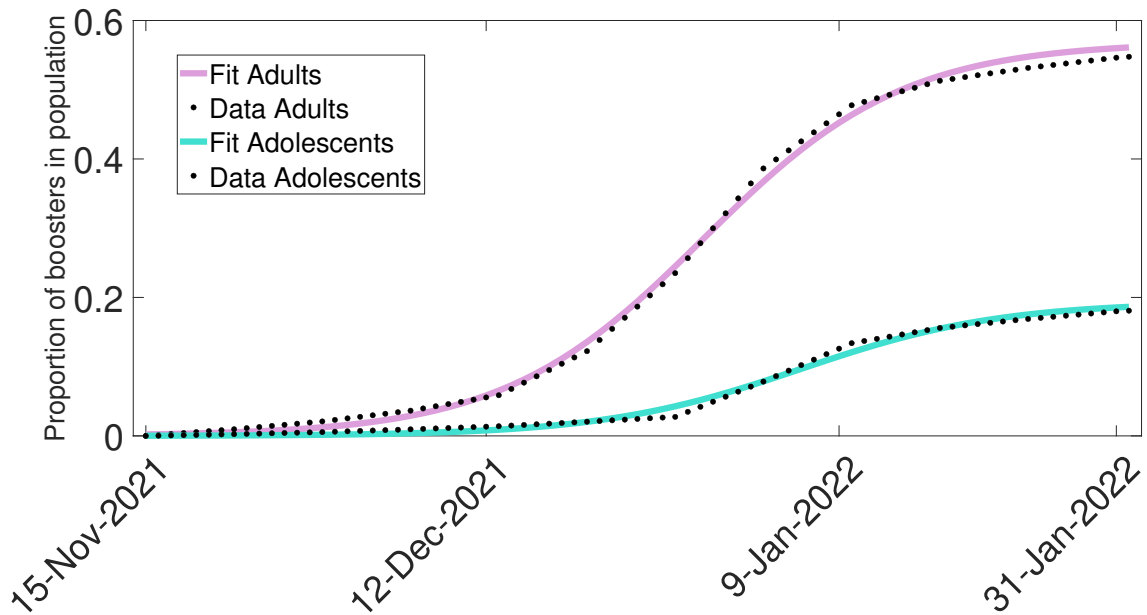
Boosters were only offered to adults and adolescents over our sample period. In the model, we use a booster transition function that reduces susceptibility as more boosters are given. Therefore, we retrieved the weekly proportion of administered boosters from the RIVM dashboard data and transformed them into daily data by assuming the number of daily new boosters is the same within a week. We then estimated by nonlinear least squares the logistic transition function that transits from no boosters to the maximum fraction of boosters administered in the population until January 31, 2022 ($m_1 = 0.5691$ for adults, and $m_2 = 0.1934$ for adolescents).

More precisely, let $t_{B,k}$ be the mid-time of transition, and $K_{B,k}$ the slope of the transition. Then the model

$$g_{B,k}(t) = \frac{m_k}{1 + \exp[-K_{B,k}(t - t_{B,k})]}$$

is fitted to the data for adults ($k = 1$) and adolescents ($k = 2$). The estimates are $t_{B,1} = \text{December 29, 2021}$, $K_{B,1} = 0.1258$ (for adults) and $t_{B,2} = \text{January 5, 2022}$, $K_{B,2} = 0.1262$ (for adolescents). The estimated transition functions are plotted against the constructed proportion of boosters in the population in Figure S15.

Figure S15: Nonlinear least squares fit to the data on the daily proportion of boosters administered in the population of adults and adolescents respectively



1.8 Variants of concern transition functions $g_\alpha(t), g_\delta(t), g_o(t)$

Every week, RIVM published data from about 1,500 random test samples that it receives from various labs across the country, which allows them to calculate the proportion of each variant of concern in the population. Since in our model the transmissibility increases with variants according to logistic transition functions, we fit to the proportion of each of these variants a logistic function over the time period they become dominant as follows

$$g_\ell(t) = \frac{1}{1 + \exp[-K_\ell(t - t_\ell)]},$$

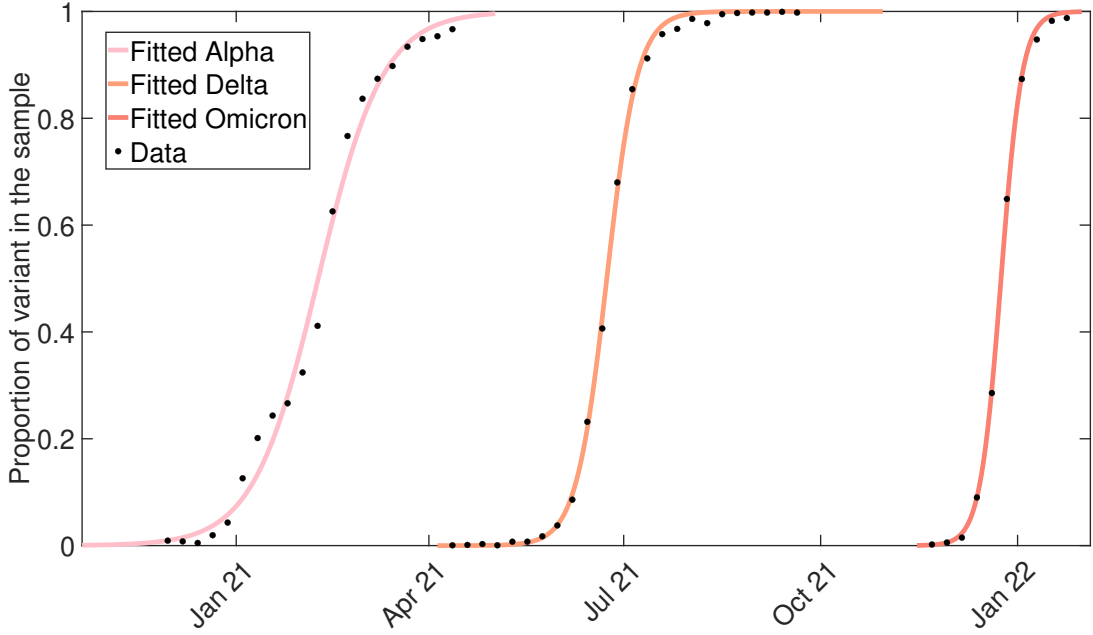
where $\ell \in \{\alpha, \delta, o\}$ denotes the Alpha, Delta and Omicron variants of concern, K_ℓ are the slope of the transition functions, and t_ℓ are the mid-times of transition when each new variant proportion in the sample reached 50%.

The nonlinear least squares estimates are in Table S2, and the fit used in the model is plotted in Figure S16.

Table S2: Parameter estimates for $g_\ell(t)$, where $\ell \in \{\alpha, \delta, o\}$ denotes Alpha, Delta, Omicron variants of concern.

K_α	t_α	K_δ	t_δ	K_o	t_o
0.06	February 8, 2021	0.14	June 23, 2021	0.20	December 24, 2021

Figure S16: Fitted versus data proportion of each variant of concern over time in random samples



1.9 Elementary and secondary school contact matrices $c_{ikk^*,ES}(t)$, $c_{ikk^*,SS}(t)$, all-setting contact matrix $c_{kk^*}^{(r)}$, and non-school contact matrix $c_{kk^*,NS}^{(r)}$ from surveys $r = 1, 2, 3$, among age categories $k, k^* = 1, 2, 3$

We first calculate from [7] daily the all-settings survey-based contact matrices, $c_{kk^*}^{(r)}$, defined as the average number of daily close contacts⁶ in all settings for one individual in age category k with all individuals in age category k^* in survey $r = 1, 2, 3$. Before the pandemic, the contact matrix is denoted with superscript $r = 1$ (February 2016 to October 2017); during the first lockdown in 2020 (April 2020 survey) it is denoted by superscript $r = 2$ and in summer 2020 (June 2020 survey) it is denoted by superscript $r = 3$. The contact matrices provided in [7] are among age categories of 10 years each, and we aggregate them into 3×3 contact matrices among young children, adolescents, and adults as follows. In the data in [7], for each of our age category k , there are G_k subcategories of pairwise contacts $cont_{k\ell\ell^*}^{(r)}$ with other G_{k^*} subcategories of age k^* , $\ell \in G_k$ and $\ell^* \in G_{k^*}$. The contact matrices are therefore calculated for each k by first summing over rows of the contacts with age group k^* , then by adding the columns within age k weighted by the fraction of population of each column in the total population of age category k :

$$c_{kk^*}^{(r)} = \sum_{\ell \in G_k} \frac{N_{\ell k}}{\sum_{\ell^* \in G_{k^*}} N_{\ell^* k}} \left[\sum_{j \in G_{k^*}} cont_{k\ell\ell^*}^{(r)} \right], \text{ where } r = 1, 2, 3. \quad (1)$$

⁶The definition of close contacts is according to [7]: hand-shakes, kissing, or other encounters that last more than 15 minutes and that occur at a close distance between individuals.

The resulting contact matrices for the three surveys, rounded to the nearest two digits, are given in Table S3.

Table S3: Survey-based contact matrices, $c_{kk^*}^{(r)}$, for ages $k, k^* = 1, 2, 3$ in survey $r = 1, 2, 3$.

Category	Survey 1			Survey 2			Survey 3		
	adults	adolescents	children	adults	adolescents	children	adults	adolescents	children
adults	11.18	1.50	1.05	4.15	0.50	0.45	6.85	0.98	0.92
adolescents	9.99	11.19	2.17	3.40	1.52	0.65	6.61	7.96	1.92
children	7.85	2.43	10.37	3.41	0.73	1.72	6.98	2.16	15.42

Next, we calculate elementary school (ES) and secondary school (SS) contact matrices $c_{ikk^*, ES}(t)$, $c_{ikk^*, SS}(t)$ over the entire sample used in fitting the model. We first calculate the school contact matrices before the pandemic and the all-setting contact matrices as in equation (1). For this, we use the synthetic Dutch population in one-year age categories provided in [15] and obtain the fraction of school contacts $f_{kk^*, S}^{(1)}$ when schools are fully open.^{7,8}

We further calculate the fraction of elementary school contacts $f_{kk^*, ES}^{(1)}$ and secondary school contacts $f_{kk^*, SS}^{(1)}$ in the total school contacts from [15], assuming they are additive since Dutch elementary and secondary schools are typically different institutions with different locations. Using the fact that in the Netherlands, roughly, children aged 4 to 11 years old are in elementary school, and adolescents aged 12 to 18 years old are in secondary school,⁹ we compute the elementary school contacts of one child with all other children, adolescents with adults, which are visible in the dataset in [15] due to the contact matrices being reported in one-year age categories, and find $f_{kk^*, ES}^{(1)}$ by dividing these by the total school contacts we calculated from [15].

However, the fraction of elementary school contacts of adults with adults in the total school contacts cannot be inferred directly from [15]. We, therefore, input these contacts by dividing the total personnel in elementary schools over that in all elementary and secondary schools.¹⁰ The fractions $f_{kk^*, ES}^{(1)}$ are then multiplied with the school contacts $c_{kk^*, S}^{(1)}$, calculated in the same way as the all-setting contacts $c_{kk^*}^{(1)}$, using equation (1), but from school contacts in [7] before the pandemic: $c_{kk^*, ES}^{(1)} = f_{kk^*, ES}^{(1)} \times c_{kk^*, S}^{(1)}$, and $c_{kk^*, SS}^{(1)} = (1 - f_{kk^*, ES}^{(1)}) \times c_{kk^*, S}^{(1)}$. These contacts are listed in Table S4, rounded to two digits (full digits are used in the model fitting).

Table S4: School contact matrices before pandemic, $c_{kk^*}^{(1)}$, for $k, k^* = 1, 2, 3$.

Age category	Elementary Schools			Secondary Schools		
	adults	adolescents	children	adults	adolescents	children
adults	0.68	0.05	0.11	0.31	0.47	0
adolescents	0.35	1.71	1.57	3.13	7.74	0
children	0.83	1.75	8.17	0	0	0

Note: Children aged 0-9 are not in secondary school, which explains the zero values. However, adolescents aged 10-11 still attend elementary school, which explains why the contacts of children with adolescents and adolescents with adolescents are non-zero.

During school closures due to the pandemic, for example, at the time of survey (2) in [7], we assume that the school contacts are zero: $c_{kk^*, S}^{(2)} = 0$.¹¹ The average school contacts are also time-varying due to vacations.

⁷We attempted to use directly the school contact matrices from [7] but this gave rise to negative school contacts.

⁸Note that school attendance is mandatory in the Netherlands and absences not motivated by illness are subject to serious fines.

⁹We assume the fraction of children of age 11 in secondary school is negligible. This is also present in the contact patterns in [15], where there are zero school contacts between 4 to 11 years old children and 12 to 18 years old children. We also assume that the fraction of elementary school contacts in the total school contacts when all schools are fully open is constant over time.

¹⁰Since a large part of the personnel works part-time, we obtained pre-processed personnel data from the company OpenInfo (www.openinfo.nl) on August 2, 2020 based on full-time equivalent jobs reported at the end of 2019. These are simple calculations and some extrapolations based on publicly available data on the full-time equivalent personnel reported by each school (www.duo.nl), which we henceforth assume constant when schools are fully open.

¹¹In reality, elementary schools were open for children whose parents were deemed “essential workers”. We used the first four waves

Based on news logs about coronavirus measures, we calculate a daily elementary and secondary school opening index, which is 1 if schools are fully open, 0 if they are closed due to vacations or measures, and between zero and one if schools were open at partial occupancy rate since the partial occupancy rate was typically announced: an occupancy of $1/2$ was implemented by most schools as children coming to school every other day; an occupancy of $1/3$ means every three days, and the occupancy $1/5$ for secondary schools was chosen to approximate the fact that secondary schools were closed part in the winter of 2021, except for students 17-18 years of age, who went to school normally. Since the vacation times differ across the North, South, and Central Netherlands, and these divisions do not completely overlap with the division by provinces, we assume, based on territory size and location, that provinces North Brabant, Limburg and Zeeland follow the South vacation schedule; Gelderland, Utrecht, and South Holland follow the Central schedule, and Groningen, Friesland, Drenthe, Flevoland, Overijssel, and North Holland follow the North schedule. A plot of constructed school opening indices is shown in Figures S17-S18.

Figure S17: Elementary School Opening Index

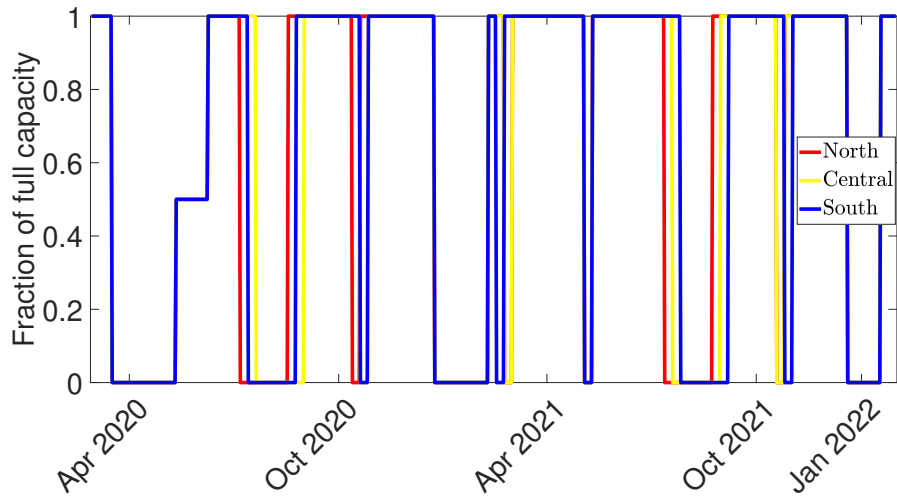
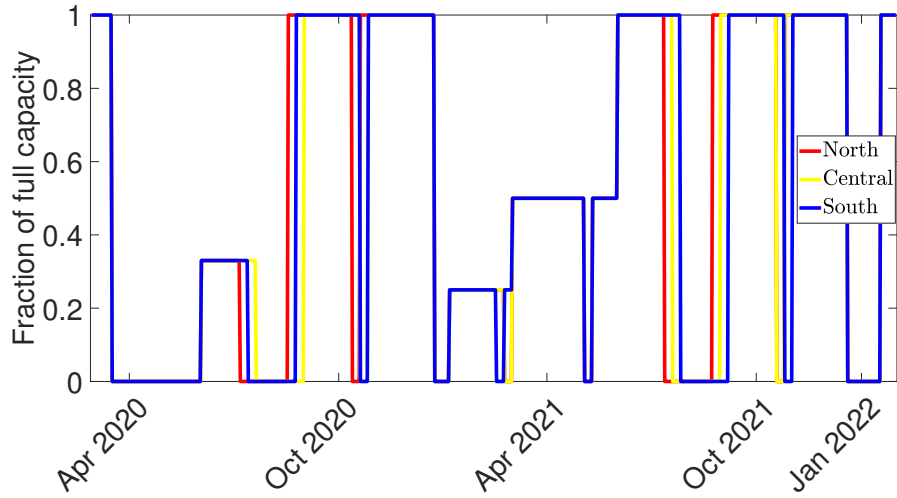


Figure S18: Secondary School Opening Index



Based on these elementary school indices es_{it} and secondary school indices ss_{it} for provinces $i = 1, \dots, 12$,

of the Tilburg University CenterER data random population survey LISS Panel on the effects of the COVID-19 outbreak and found that, depending on how questions are aggregated, elementary school attendance during the first lockdown was $3\% - 6\%$, therefore in the rest of the analysis we just assume that the contacts during school closures are zero. The LISS Panel is run by the CENTER Data Research Center, Tilburg University, and the COVID-19 study can be found at https://www.dataarchive.liSSdata.nl/study_units/view/927 and is available to researchers upon request.

we compute the time-varying school contacts over each province as $c_{ikk^*,ES}(t) = es_{it} c_{kk^*,ES}^{(1)}$ and $c_{ikk^*,SS}(t) = ss_{it} c_{kk^*,SS}^{(1)}$.

Note that the school index closure is the same across regions in all three surveys $r = 1, 2, 3$, so the school contacts are at the time of each three surveys constant across all provinces, i.e. $c_{ikk^*,S}^{(r)} = c_{kk^*,S}^{(r)}$. The non-school contacts before the pandemic, in the first lockdown and in the summer are simply calculated by subtracting school contacts from the total contacts given in Table S3: $c_{kk^*,NS}^{(1)} = c_{kk^*}^{(1)} - c_{kk^*,S}^{(1)}$, $c_{kk^*,NS}^{(2)} = c_{kk^*}^{(2)}$ (because all schools were closed at the time of survey (2)), and $c_{kk^*,NS}^{(3)} = c_{kk^*}^{(1)} - c_{kk^*,S}^{(3)}$, where $c_{kk^*,S}^{(3)}$ is evaluated at $t = 15$ June 2020, the assumed mid-time of survey (3). These contacts rounded to two digits are displayed in Table S5 (in the estimation, we use full digits).

Table S5: Constructed non-school contact matrices, $c_{kk^*,NS}^{(r)}$, for $k, k^* = 1, 2, 3$.

Category	Survey 1			Survey 2			Survey 3		
	adults	adolescents	children	adults	adolescents	children	adults	adolescents	children
adults	10.20	0.97	0.94	4.15	0.50	0.45	6.37	0.84	0.82
adolescents	6.51	1.75	0.60	3.40	1.52	0.65	5.69	4.93	0.53
children	7.02	0.68	2.20	3.41	0.73	1.72	6.25	0.60	3.27

2 Model

Figure 5 (main text) provides the diagram of the metapopulation transmission model. Section 2.1 explains the epidemiological model without vaccination. Section 2.2 adds vaccination to the model. Section 2.3 explains how we modeled time variation in the parameters of the epidemiological model. Section 2.4 explains how we modeled time variation in non-school contact matrices as a result of non-pharmaceutical interventions (NPIs).

2.1 Model without vaccination

We developed a new metapopulation SEIRHS model with mobility across regions. In the context of our study, regions are provinces in the Netherlands. As discussed in the main text, our model is equipped with additional dynamics for unreported infected compared to reported infected. Namely, we assume that unreported infected travel to other regions and infect others, and that susceptible individuals from one region can travel and get exposed in the other region, while reported infected do not travel. Because the case reporting rate is assumed the same across regions, this allows for identification of the unreported cases. Other studies [14, 16] also employ a metapopulation model and demonstrate identification by simulation. The study by Hortaçsu et al [11] provides a mathematical proof of identification, albeit in a simpler metapopulation model. Section 6 provides further identification checks.

Recall from the main text that S stands for susceptible, E for exposed, I^R for reported infected, I^U for unreported infected, H for hospitalized, R for recovered, and N is the population size. Also recall that a variable $X \in \{S, E, I^U, I^R, R, H, N\}$ with subscript ik denotes the number of individuals in compartment X in province i and age category k .

For simplicity, we assume that conditional on the state variable X at a particular point in time, individuals travel deterministically at the beginning of the day and return deterministically at the end of the day to their home province. Note that this is different than in [14], where the population can change as a result of traveling. In our case, the population is assumed not to change from one day to another because the vast majority of traveling

in the Netherlands is due to daily commutes. The model is formulated in terms of a variable $X \in \{S, E, I^U, R\}$ with subscript ijk that denotes the number of individuals of type X that travel from province j to province i and join the corresponding compartment X in province i and age k (if $i \neq j$; if $i = j$ then individuals do not travel). During the day, the population size of province i is changed, but at the end of the day all individuals return to their home province j .

A superscript $a = 1, 2$ of variable $X \in \{S, E, I^U, I^R, R, H, N\}$ refers to the set of compartments (see Figure 5 in the main text). The first set of compartments ($a = 1$) refers to individuals who have never been infected or who have had primary infection but the immunity conferred by this infection has not waned yet. The first set of compartments consists of individuals in the following states: fully susceptible/naive (S^1), latently infected after primary infection (E^1), reported primary infection ($I^{R,1}$), unreported primary infection ($I^{U,1}$), hospitalized after primary infection (H^1), and fully immune after primary infection (R^1). The second set of compartments ($a = 2$) refers to individuals who have lost immunity after primary infection. The second set of compartments consists of individuals in the following states: partially susceptible after waning of immunity after primary infection (S^2), latently re-infected (E^2), reported re-infection ($I^{R,2}$), unreported re-infection ($I^{U,2}$), hospitalized after re-infection (H^2) and fully immune after re-infection (R^2).

If time variation of a parameter is modeled explicitly, it appears as a function of t . Otherwise, its time variation is not modeled but approximated in the estimation step by filtering methods, including in some cases changing priors to accommodate changes in epidemiological features or government interventions. For example, because there is evidence that the incubation period for Omicron is lower than for other variants [1], we lower priors for this parameter at the end of the sample. Similarly, since the test capacity increased over the sample, we increase priors for the case detection rate parameters during the sample period (see Table S10). Furthermore, [16] demonstrated that the filtering technique we use can approximate well time variation in parameters even over shorter periods and without a change in prior. Section 6.2 further verifies this over shorter periods by simulation.

[Step 1: Beginning of day — travel to other provinces] At the beginning of each day t , we have compartments $X_{jk}^a(t_-)$, $a \in \{1, 2\}$, $X \in \{S, E, I^U, I^R, R, H\}$, where the beginning of the day, t_- , corresponds to the end of the previous day, $t_- = (t - 1)_+$. We assume that a fraction of individuals in province j who are not hospitalized or reported infected travel to another province i , and this fraction is proportional to their fraction in the total population that is eligible to travel from that province. So, for $i \neq j$,

$$m_{ijk}(t) = \frac{M_{ij}(t)}{\sum_{a=1}^2 S_{jk}^a(t_-) + E_{jk}^a(t_-) + I_{jk}^{U,a}(t_-) + R_{jk}^a(t_-)} \quad (2)$$

and the individuals who travel during day t are given by

$$X_{ijk}^a(t) = \theta_k m_{ijk}(t) X_{jk}^a(t_-), \quad i \neq j, \quad a \in \{1, 2\}, \quad X \in \{S, E, I^U, R\}. \quad (3)$$

Here θ_k is an age-specific mobility reporting error that we estimate and that accounts for the fact that people do not commute daily and that people may travel by other means (see the construction of data $M_{ij}(t)$ in Section 1). Since reported infected and hospitalized do not travel, $\forall i \neq j, I_{ijk}^{R,a}(t) = H_{ijk}^a(t) = 0$. For the rest of the compartments, the number of individuals who do not travel that day is calculated as the remainder:

$$X_{iik}^a(t) = X_{ik}^a(t_-) - \sum_{j \neq i} X_{jik}^a(t), \quad X \in \{S, E, I^U, R\}. \quad (4)$$

The population of each region is now the sum of the people who stayed and of those who moved there from other regions:

$$N_{ik}^a(t) = \sum_j [S_{ijk}^a(t) + E_{ijk}^a(t) + I_{ijk}^{R,a}(t) + I_{ijk}^{U,a}(t) + H_{ijk}^a(t) + R_{ijk}^a(t)]. \quad (5)$$

[Step 2: During the day — disease dynamics] Susceptibles get exposed at the rate $\beta_{ik}^a(t)$, and the exposed become infectious at the rate $1/Z$ (after Z days). A fraction of exposed, α_k , become reported infected, and the rest are unreported infected; we refer to this fraction as the “case detection rate” from now on. Both the reported infected (if not hospitalized) and the unreported infected are assumed to recover at the rate $1/D$ (after D days), after which they are no longer infectious. A proportion $\gamma_k^a(t)$ of reported infected are hospitalized, and they are discharged from the hospital at the rate $\delta_k(t)$; for simplicity, we assume that the hospitalized participate in the contact process but that they are not infectious; for example, they continue to have contacts with the personnel and visitors but cannot infect them due to use of protective measures. Note that the traveling exposed $E_{ijk}(t)$ can become reported or unreported infected during the day, so $I_{ijk}^{R,a}(t), i \neq j$ can become non-zero during the day, but there is no further evolution in the same day of these individuals towards other states. The recovered in the first and second set of compartments wane at the rate $\eta^1(t)$ and $\eta^2(t)$ and both enter the susceptibles in the second set of compartments. Let W_{ik} be the number of individuals in region i and age category k whose immunity from primary infection waned. We keep track of these individuals because they will also be vaccinated later. Let $\mathbf{1}[\mathbf{a} = \mathbf{1}]$ be the indicator function for the compartment set 1, and $\mathbf{1}[\mathbf{a} = \mathbf{2}]$ be the indicator function for compartment set 2. The model is given by

$$\frac{dS_{ijk}^a(t)}{dt} = -\beta_{ik}^a(t) S_{ijk}^a(t) + \mathbf{1}[\mathbf{a} = \mathbf{1}] \eta^1(t) R_{ijk}^1(t) + \mathbf{1}[\mathbf{a} = \mathbf{2}] \eta^2(t) R_{ijk}^2(t) \quad (6)$$

$$\frac{dE_{ijk}^a(t)}{dt} = \beta_{ik}^a(t) S_{ijk}^a(t) - \frac{E_{ijk}^a(t)}{Z} \quad (7)$$

$$\frac{dI_{iik}^{R,a}(t)}{dt} = \alpha_k \frac{E_{iik}^a(t)}{Z} - \gamma_k^a(t) I_{iik}^{R,a}(t) - \frac{1}{D} I_{iik}^{R,a}(t) \quad (8)$$

$$\frac{dI_{ijk}^{R,a}(t)}{dt} = \frac{\alpha_k}{Z} E_{ijk}^a(t), \quad \text{for } i \neq j \quad (9)$$

$$\frac{dI_{ijk}^{U,a}(t)}{dt} = \frac{(1 - \alpha_k)}{Z} E_{ijk}^a(t) - \frac{1}{D} I_{ijk}^{U,a}(t) \quad (10)$$

$$\frac{dH_{iik}^a(t)}{dt} = \gamma_k^a(t) I_{iik}^{R,a}(t) - \delta_k(t) H_{iik}^a(t) \quad (11)$$

$$\frac{dH_{ijk}^a(t)}{dt} = 0, \quad \text{for } i \neq j$$

$$\begin{aligned} \frac{dR_{ijk}^a(t)}{dt} &= \frac{1}{D} [I_{ijk}^{R,a}(t) + I_{ijk}^{U,a}(t)] + \delta_k(t) H_{ijk}^a(t) \\ &\quad - \mathbf{1}[\mathbf{a} = \mathbf{1}] \eta^1(t) R_{ijk}^1(t) - \mathbf{1}[\mathbf{a} = \mathbf{2}] \eta^2(t) R_{ijk}^2(t) \end{aligned} \quad (12)$$

$$W_{ik}(t) = \eta^1(t) \sum_j R_{ijk}^1(t) + W_{ik}(t_-), \quad (13)$$

where $W_{ik}(t_-)$ is the total number of individuals belonging to the first set of compartments that waned at the beginning of the day, and $\eta^1(t) \sum_j R_{ijk}^1(t)$, $\eta^2(t) \sum_j R_{ijk}^2(t)$ along with the other additive terms in the model will be subject to numerical integration in the estimation procedure described in Section 3.

[Step 3: End of day — travel back home] The day ends with all travelers going back to their province

of origin, into the compartment (disease state) they evolved to during the day.

$$\begin{aligned} X_{jk}^a(t_+) &= \sum_i X_{ijk}^a(t), \quad X \in \{S, E, I^R, I^U, R, H\} \\ N_{ik}^a(t_+) &= S_{ik}^a(t) + E_{ik}^a(t) + I_{ik}^{R,a}(t) + I_{ik}^{U,a}(t) + H_{ik}^a(t) + R_{ik}^a(t) \end{aligned}$$

Note that, by construction, $N_{ik}^1(t_+) + N_{ik}^2(t_+) = N_{ik}$, so the population of a given age in a province is constant at the end of each day, and only the distribution across disease states in the population has changed.

2.2 Model with vaccination

We add to the model Step 0, where individuals are vaccinated deterministically, after which Steps 1-3 occur as described in the previous section.

[Step 0: Vaccination] The day starts with vaccination. Recall that $V_{ik}(t)$ is the number of vaccinations on day t in age k and region i , and its construction was explained in Section 1. The fraction of daily vaccinated people is the number of daily vaccines over the eligible population, which excludes reported infected and hospitalized, but includes waned individuals that have not yet been vaccinated:

$$v_{ik}(t) = \frac{V_{ik}(t)}{S_{ik}^1(t_-) + E_{ik}^1(t_-) + I_{ik}^{U,1}(t_-) + R_{ik}^1(t_-) + W_{ik}^1(t_-)}.$$

The vaccination is assumed to be administered deterministically, before Step 1, and proportionally to the fraction of individuals in each disease state that is eligible for vaccination:

$$\begin{aligned} W_{ik}(t_-) &\leftarrow [1 - v_{ik}(t)] W_{ik}(t_-) \\ X_{ik}^1(t_-) &\leftarrow [1 - v_{ik}(t)] X_{ik}^1(t_-), \quad X \in \{S, E, I^U, R\} \\ X_{ik}^2(t_-) &\leftarrow X_{ik}^2(t_-) + v_{ik}(t) X_{ik}^1(t_-), \quad X \in \{S, E, I^U, R\}, \end{aligned}$$

where W now denotes the pool of waned people who are yet to be vaccinated.¹² Note that we have combined waned and vaccinated individuals into the second set of compartments, denoted by $a = 2$. Therefore, the implicit model assumption is that vaccinated or previously infected individuals whose immunity has waned before being vaccinated benefit from the same reduction in susceptibility, infectivity, and hospitalization rate.

2.3 Modelling time-varying parameters

Force of infection $\beta_{ik}^a(t)$. The time-dependent force of infection is age- and province-specific and depends on whether individuals are fully susceptible (before primary infection) or partially susceptible (after vaccination or waning of immunity after primary infection). We model the force of infection as a multiplicative function of constant probability of transmission per contact for the wild-type variant ϵ , susceptibility¹³ of age group $k = 2, 3$ ($k = 2$ — adolescents, $k = 3$ — children) relative to age group $k = 1$ (adults) $f_{\epsilon,k}$ (here $f_{\epsilon,1} = 1$), the increase in the probability of transmission per contact due to variants of concern $voc(t)$, the change in the probability of transmission per contact due to seasonality $season(t)$, and the time-dependent average number of contacts one individual in age group k and province i makes per day with all individuals in other age groups multiplied by

¹²For simplicity, we use \leftarrow and the same t_- to the left and the right to show the move across states induced by vaccination, but in the computation, vaccination occurs before Step 1.

¹³In the estimation procedure, the reference age group is $k = 1$ (adults), and $f_{\epsilon,1} = 1$.

the proportion of infectious individuals in those age groups $\lambda_{ik}^a(t)$ as follows:

$$\beta_{ik}^a(t) = \epsilon \times f_{\epsilon,k} \times voc(t) \times season(t) \times \lambda_{ik}^a(t). \quad (14)$$

Note that since ϵ is the probability of transmission per contact for the wild-type variant, and $\epsilon \times voc(t)$ is the probability of transmission per contact for the variants of concern, by multiplying $\epsilon \times voc(t)$ with $f_{\epsilon,k}$, and estimating $f_{\epsilon,k}$ over the entire sample, we allow the susceptibility of adolescents and children not only to be different than the susceptibility of adults for the wild-type variant but also to change with new variants (albeit without explicitly modeling this change).

The function $season(t)$ models the change in the probability of transmission per contact due to seasonality. For simplicity, we use a sinusoidal function with a period of one year and a maximum on 1 January as in [21] (i.e., Supplementary Material, page 44):

$$season(t) = 1 + 0.1 \cos \frac{2\pi(t - t^*)}{365.25}. \quad (15)$$

Due to many confounders, the amplitude of seasonality cannot be estimated in our study but is rather fixed at 0.1 as in [21].

To specify the $voc(t)$ function, we use the transition functions $g_{\ell,t}$, $\ell \in \{\alpha, \delta, o\}$ described in Section 1, which reflect the time-dependent proportion of the variant of concern with time, and define ρ_ℓ as the relative increase in the probability of transmission per contact due to the variants of concern, $\ell \in \{\alpha, \delta, o\}$:

$$\begin{aligned} voc(t) = & (1 - g_{\alpha,t}) + (1 + \rho_\alpha) g_{\alpha,t} (1 - g_{\delta,t}) + (1 + \rho_\alpha)(1 + \rho_\delta) g_{\delta,t} (1 - g_{o,t}) \\ & + (1 + \rho_\alpha)(1 + \rho_\delta)(1 + \rho_o) g_{o,t}. \end{aligned} \quad (16)$$

Since we do not model variants of concern separately using, e.g., multi-strain models, ρ_ℓ is best interpreted as the average increase in the probability of transmission per contact for the new variant of concern. Parameter ρ_ℓ will be calibrated in Section 3.1 because it enters multiplicatively with other parameters in $\lambda_{ik}^a(t)$ that will be estimated.

Let $0 \leq p_{I,k}(t) < 1$ be the reduction in susceptibility due to vaccination or previous infection for individuals in the second set of compartments relative to individuals in the first set of compartments; $0 \leq p_{TR,k}(t) < 1$ be the reduction in infectivity due to vaccination or previous infection of reported infected in the second set of compartments relative to reported infected in the first set of compartments; and $0 \leq p_{TU,k}(t) < 1$ be the reduction in infectivity due to vaccination or previous infection of unreported infected in the second set of compartments relative to unreported infected in the first set of compartments. For simplicity, we refer to these parameters as “protection levels” against infection and transmission due to vaccination or previous infection. Then:

$$\lambda_{ik}^1(t) = \sum_{k^*=1}^3 c_{i,kk^*}(t) \sum_j \left[\frac{I_{ijk^*}^{R,1}(t) + [1 - p_{TR,k^*}(t)] I_{ijk^*}^{R,2}(t)}{N_{ik^*}} + \mu \frac{I_{ijk^*}^{U,1}(t) + [1 - p_{TU,k^*}(t)] I_{ijk^*}^{U,2}(t)}{N_{ik^*}} \right] \quad (17)$$

$$\lambda_{ik}^2(t) = [1 - p_{I,k}(t)] \lambda_{ik}^1(t), \quad (18)$$

where $0 < \mu \leq 1$ is the relative infectivity of unreported infected compared to reported infected, typically lower due to asymptomatic or milder symptomatic cases, and $c_{i,kk^*}(t)$ are time-varying contact matrices described in

Section 2.4.

Hospitalization rate $\gamma_k^a(t)$. Let $0 \leq p_{H,k}(t) < 1$ be the reduction in hospitalization rate due to vaccination or previous infection, conditional on being infected, for individuals in the second set of compartments relative to individuals in the first set of compartments. We refer to this parameter as the “protection level” against hospitalization due to vaccination or previous infection. Therefore:

$$\gamma_k^2(t) = [1 - p_{H,k}(t)] \gamma_k^1(t), \quad \gamma_k^1(t) = \gamma_k^1. \quad (19)$$

We do not model the time-evolution of γ_k^1 but infer it during the estimation for different variants of concern. Parameters $p_{\ell,k}(t), \ell \in \{I, TR, TU, H\}$ are calibrated based on external data and previous studies as described in Section 3.1.

Immunity waning rate $\eta^a(t)$. There is evidence that Omicron variant was both more transmissible and provided partial immune escape from previous variants (see [10] and references therein). We, therefore, assume that the waning rate in the first set of compartments increases from η_A to η_B with the transition function for the Omicron variant $g_o(t)$:

$$\eta^1(t) = \eta_A (1 - g_o(t)) + \eta_B g_o(t). \quad (20)$$

The recovered in the second set of compartments have either been vaccinated before their immunity from primary infection waned, vaccinated and infected once or vaccinated and infected twice. Therefore, we assume that their immunity does not wane until Omicron, and then starts to wane at the same rate as for the recovered in the first set of compartments:

$$\eta^2(t) = \eta_B g_o(t).$$

2.4 Modelling time variation in non-school contact matrices as a result of NPIs

Denote by $c_{ikk^*}(t), k, k^* = 1, 2, 3$, the average number of contacts per day of one person in age group k with all people in age group k^* in region i at day t . We assume that contact matrix $c_{ikk^*}(t), k, k^* = 1, 2, 3$, is the sum of school (S) and non-school (NS) contact matrices: $c_{ikk^*}(t) = c_{ikk^*,S}(t) + c_{kk^*,NS}(t)$. The school contact matrix $c_{ikk^*,S}(t)$ is the sum of elementary and secondary school contact matrices: $c_{ikk^*,S}(t) = c_{ikk^*,ES}(t) + c_{ikk^*,SS}(t)$, which computation was explained in Section 1.9. The school contacts vary over provinces i due to different timing of school holidays in different provinces, while the non-school contacts are assumed constant across provinces.

We first model, via a logistic function, the transition of non-school contacts from those before the pandemic - survey (1) - to those in the first lockdown - survey (2) - to those in the summer, when some measures were relaxed - survey (3). After survey (3), survey data are either no longer available for some measures or are not consistent with the previous surveys.¹⁴ We therefore first define 11 additional regimes, each representing a major change in NPIs (semi-lockdowns, lockdowns, school openings, further relaxation of measures). The meaning and timings of each regime are carefully discussed in Section 3.1. The contacts in each of these regimes $r = 3, \dots, 13$ are assumed to transit from the level in the previous regime to new level in the current regime r (where note that the contacts in the current regime r are denoted by $c_{kk^*,NS}^{(r+1)}$ instead of $c_{kk^*,NS}^{(r)}$ to account for the use of three

¹⁴For example, in round 4 of the RIVM survey performed in Fall 2020, the contacts for children and adolescents are much higher than before the pandemic.

survey contact matrices for the first two regimes):

$$c_{kk^*,NS}^{(r+1)} = u_r \times c_{kk^*,NS}^{(1)} + \zeta_{kk^*} (1 - u_r) \times c_{kk^*,NS}^{(2)}. \quad (21)$$

This new level is a linear combination between pre-pandemic contacts $c_{kk^*,NS}^{(1)}$ and those in the first lockdown $c_{kk^*,NS}^{(2)}$, with u_r representing the probability that an average individual behaves as if there was no pandemic, and $(1 - u_r)$ representing the probability that an average individual behaves as in the first lockdown. Following [23], $u_r \in [0, 1]$ is estimated from fitting the model to the data. The parameter ζ_{kk^*} is a mitigation factor that comprises other measures such as masks and physical distancing measures that reduced the average number of close contacts of an adult with other adults (as children and adolescents were rarely required to social distance or wear masks in the Netherlands):

$$\zeta_{kk^*} = \begin{cases} \zeta \in (0, 1) & k = k^* = 1 \\ 1 & \text{otherwise.} \end{cases} \quad (22)$$

With this notation, the non-school contacts over the entire sample are:

$$\begin{aligned} c_{kk^*,NS}(t) &= c_{kk^*,NS}^{(1)} \times [1 - f_1(t)] + \zeta_{kk^*} c_{kk^*,NS}^{(2)} \times f_1(t) [1 - f_2(t)] \\ &\quad + \zeta_{kk^*} c_{kk^*,NS}^{(3)} \times f_2(t) \times [1 - f_3(t)] \\ &\quad + \sum_{r=3}^{12} c_{kk^*,NS}^{(r+1)} \times f_r(t) [1 - f_{r+1}(t)] + \zeta_{kk^*} c_{kk^*,NS}^{(14)} \times f_{13}(t), \\ f_r(t) &= \frac{1}{1 + \exp(-K_r(t - t_r))}. \end{aligned} \quad (23)$$

Here, $f_r(t)$ are logistic functions with estimated parameters K_r quantifying the speed of transition and calibrated parameters t_r indicating the time a NPI/government measure was taken up in the population. The use of logistic transitions in NPI regimes, as employed in [20] and [9], rather than change-points as in [3] and [21], allow contact patterns to incorporate a *behavioral* component.

First, when relaxation measures are announced, ahead of their implementation, people may already adjust their behavior. For example, when restaurants, workplaces, universities, and other locations are announced they can open, individuals have to prepare ahead of their opening, and therefore the number of average contacts per person increases ahead of the measure taking effect. Figure S19 compared against RIVM Dashboard data indicates that people do react to measures slightly ahead of their implementation, and in this case, the transition parameters K_r , which we estimate for all $r = 1, \dots, 13$, will capture a faster transition. Additionally, note that as in [20], we glued the transition functions in equation (23), to ensure only a particular regime is activated at each point in time while allowing us to fit the model in one go over the entire sample.¹⁵ Second, we estimate from the data the speed K_r of adjustment to new measures, and the size of the adjustment u_r .

Note that u_r enters multiplicatively with ϵ (probability of transmission per contact for the wild-type variant) and $f_{\epsilon,k}$, $k = 2, 3$ (susceptibility of adolescents and children relative to adults) in the specification of $\beta_{ik}^a(t)$, starting with the third regime, so one of these parameters cannot be separately identified if they were all estimated over the same sample. However, the parameter u_r does not enter the first two regimes, where we used the survey-based average contacts instead. Therefore, we estimate ϵ only over the first two regimes, fix it at its posterior

¹⁵For example, when $t - t_r \rightarrow -\infty$ for $r > 1$ because t is small, $f_r(t) \rightarrow 0$ for $r > 1$, and the contact rates are solely determined by the first regime: $c_{kk^*,NS}(t) = c_{kk^*,NS}^{(1)} \times [1 - f_1(t)] + \zeta_{kk^*} c_{kk^*,NS}^{(2)} \times f_1(t)$.

distribution, and continue estimating u_r along with $f_{\epsilon,k}$. We could estimate $f_{\epsilon,k}$ also over the first regimes only, and interpret it as the susceptibility of adolescents and children relative to adults to the wild-type variant, assuming that the same transition function $voc(t)$ applies to all age groups. However, as shown in Section 1, compared to adults, there are very few detected cases and hospitalizations in adolescents and children during those two regimes, weakening the identification of these parameters if only those two regimes were used. Therefore, we estimate these parameters over the entire sample. The advantage in doing so is that with new variants, $f_{\epsilon,k} \text{voc}(t)$ captures all changes in susceptibility of adolescents and children relative to adults, not only in the wild-type period but across all variant periods (so the estimate of $f_{\epsilon,k}$ may change with different variants).

3 Inference

Table S6 lists the estimated and calibrated parameters and the corresponding equations where they are defined. The additional calibrated transition functions for variants and boosters can be found in Section 1.

Table S6: Estimated and calibrated parameters

Parameter	Meaning	Equation	Estimated or calibrated
Assumed common across age categories			
μ	relative infectivity of unreported compared to reported infected	(17)	Estimated
Z	days from exposed to infectious state	(7)	Estimated
D	days from infectious to recovered state	(9)	Estimated
K_r	smoothness of non-school contact rates transition, $r = 1, \dots, 13$	(23)	Estimated
u_1	fraction of contacts, regime: School Holidays	(21)-(23)	Estimated
u_2	fraction of contacts, regime: Semi-lockdown 1 (SLD 1)	(21)-(23)	Estimated
u_3	fraction of contacts, regime: Lockdown 2 (LD 2)	(21)-(23)	Estimated
u_4	fraction of contacts, regime: Elementary Schools Open 2 (ES Open 2)	(21)-(23)	Estimated
u_5	fraction of contacts, regime: Further Relaxations (Relax 1)	(21)-(23)	Estimated
u_6	fraction of contacts, regime: Allowing Big Events (Big Ev)	(21)-(23)	Estimated
u_7	fraction of contacts, regime: Restriction on Big Events (Res Big Ev)	(21)-(23)	Estimated
u_8	fraction of contacts, regime: Further Relaxations (Relax 2)	(21)-(23)	Estimated
u_9	fraction of contacts, regime: Semi-lockdown 2 (SLD 2)	(21)-(23)	Estimated
u_{10}	fraction of contacts, regime: Lockdown 3 (LD 3)	(21)-(23)	Estimated
u_{11}	fraction of contacts, regime: Elementary Schools Open 3 (ES Open 3)	(21)-(23)	Estimated
Assumed different across age categories			
ϵ	probability of transmission per contact for the wild-type variant	(14)	Estimated
$f_{2,\epsilon}$	susceptibility of adolescents relative to adults ($f_{1,\epsilon} = 1$), all variants	(14)	Estimated
$f_{3,\epsilon}$	susceptibility of children relative to adults ($f_{1,\epsilon} = 1$), all variants	(14)	Estimated
α_1	adult case detection rate	(9)	Estimated
α_2	adolescent case detection rate	(9)	Estimated
α_3	child case detection rate	(9)	Estimated
θ_1	adult mobility reporting error	(3)	Estimated
$f_{2,\theta} = \theta_2/\theta_1$	adolescent mobility reporting error relative to adults	(3)	Estimated
$f_{3,\theta} = \theta_3/\theta_1$	child mobility reporting error relative to adults	(3)	Estimated
γ_1	adult hospitalization rate	(12)	Estimated
γ_2	adolescent hospitalization rate	(12)	Estimated
γ_3	children hospitalization rate	(12)	Estimated
ζ	reduction in close contacts due to protection measures for adults	(22)	Estimated
p_I^4	adult/adolesc. average reduction in probab. of infection due to boosters	(24)-(25)	Estimated
$\rho_\alpha, \rho_\delta, \rho_\omega$	relative increase in transmissibility of alpha, delta, omicron variants	(16)	calibrated, Table 3.1
$\text{season}(t)$	seasonality in transmission	(15)	calibrated,(15)
t_i	NPI regime mid-point	(23)	calibrated, Section 3.1
η_A	waning rate from primary infection before Omicron	(20)	calibrated, Section 3.1
η_B	waning rate after Omicron	(20)	calibrated, Section 3.1
$\delta_k(t)$	hospital discharge rate	(12)	calibrated, Section 3.1
$p_{I,k}(t)$	reduction in susceptibility, second compartment set	(18),(24)	partly calibrated, Section 3.1
$p_{TR,k}(t)$	reduction in infectivity for reported infected, second compartment set	(18),(24)	partly estimated based on p_I^4
$p_{TU,k}(t)$	reduction in infectivity for unreported infected, second compartment set	(18),(24)	calibrated, Section 3.1
$p_{H,k}(t)$	reduction in hospitalization rate for infected, second compartment set	(19),(24)	calibrated, Section 3.1

The rest of the section is structured as follows. First, we present an overview of estimated and calibrated parameters. Section 3.1 describes and motivates the calibrations based on previous studies or external data.

Section 3.2 presents and motivates the choice of parameter priors. Section 3.3 describes the estimation procedure and the initializations for the unobserved variables. Section 3.4 describes the estimation algorithm.

3.1 Calibrated parameters

Reduction in susceptibility, infectivity and hospitalization rate in the second compartment set ($p_{\ell,k}(t), \ell \in \{I, TR, TU, H\}, k = 1, 2, 3$). Because our model does not distinguish between the vaccinated and previously infected (and as mentioned before, this would be difficult as the vaccination data does not distinguish between these individuals either), we calibrate most of these parameters based on estimates of vaccine efficacies/effectiveness.

The vaccine efficacies are modeled as time-varying because they were found in the literature to differ across variants of concern and to wane over time. Let $p_{\ell}^b, \ell \in \{I, TR, TU, HUNC\}, b \in \{1, \dots, 4\}$ correspond to the vaccine efficacies against infection $\ell = I$, against transmission conditional on being reported infected $\ell = TR$, against transmission conditional on being unreported infected $\ell = TU$, and against hospitalization $\ell = HUNC$ (where the latter is now unconditionally on being infected, and therefore labeled “HUNC” rather than “H”). The superscript b refers to four time periods: $b = 1$ - before the Delta variant, $b = 2$ - when the Delta variant is 100% dominant (and a record number of vaccines were administered), $b = 3$ - when vaccine efficacies waned, assumed six months from the time the Delta is dominant (which coincides with the time most vaccines are administered in the Netherlands), and $b = 4$ - when most boosters have been administered (which coincides with the time Omicron became dominant), and the reduction in susceptibility, infectivity, and hospitalization rate get smaller again for an average individual in the second set of compartments.

The vaccine efficacies $\ell = I, TR, TU$ and $b = 1, 2$ are taken to be equal to those given for different vaccines in [17], Table 1, where we take $b = 1$ to correspond to the column “Alpha” (protection conferred by vaccines against Alpha variant), $b = 2$ to “Central Delta”, $\ell = I$ to correspond to protection against mild disease or infection, $\ell = TR$ against infectiousness if infected, and we take all the values for $\ell = TU$ to equal those for $\ell = TR$, as we already control for lower infectiousness of unreported cases in general through the parameter μ in equation (17). For $b = 3$, we assume due to waning of vaccine effectiveness without boosters, the reduction in probability of getting infected and the reduction in infectivity are equal to $p_{\ell}^b = 0.1$, for $\ell = \{I, TR, TU\}$.¹⁶ Next, we group the vaccines into two protection levels: mRNA (Pfizer and Moderna, PF-MO) and non-mRNA (Astra Zeneca and Janssen, AZ-JA). From the RIVM Coronavirus Dashboard vaccination data stratified by vaccine (taking into account that full vaccination refers to two doses of Astra Zeneca but one dose of Janssen), we calculated that 82% of fully vaccinated are with PF-MO, and 18% with AZ-JA. We used these weights to calculate a weighted average level of vaccine efficacies; the results are listed in Table S7, columns 3-4. The waned vaccine efficacies in Table S7, column 5, are assumed based on pessimistic scenarios in [17] for $p_I^3, p_{TR}^3, p_{TU}^3$, and based on a pessimistic estimate in [22] for p_{HUNC}^3 . The boosters were exclusively mRNA vaccines, so we assume p_{HUNC}^4 to be equal to the estimate in [2] for hospitalizations.

Note that the parameter p_I^4 is estimated within the model, and best interpreted as the reduction in the probability of being infected for the average individual adult/adolescent in the second set of compartments, as a result of administering boosters for some of these adult/adolescent individuals.

We now explain how we use the parameters in Table S7 to model $p_{\ell,k}(t)$. Recall that $g_{\delta}(t)$ is the transition

¹⁶This was chosen because vaccines alone seemed to protect very little against reinfection with Omicron; this contrasts with more optimistic estimates of approximately 40% after 200 days in [17], obtained for UK, before the arrival of Omicron.

Table S7: Reduction in susceptibility, infectivity and hospitalization rate in the second compartment set

Effectiveness	Vaccine	Source: Table 1 in [17]		$b = 3$ (waned)	$b = 4$ (booster)
		$b = 1$ (Alpha)	$b = 2$ (Delta)		
against infection p_I^b	PF-MO	0.93	0.86	-	-
	AZ-JA	0.74	0.58	-	-
	weighted	0.90	0.80	0.10 (assumed)	estimated
against transmission given infected $p_{TR}^b = p_{TU}^b$	PF-MO	0.45	0.40	-	-
	AZ-JA	0.74	0.58	-	-
	weighted	0.90	0.80	0.10 (assumed)	0 (assumed)
against hospitalization p_{HUNC}^b	PF-MO	0.95	0.95	-	-
	AZ-JA	0.90	0.90	-	-
	weighted	0.94	0.94	0.73 (assumed)	0.95

function for the Delta variant, and $g_{B,k}(t), k = 1, 2$ the transition functions for the boosters, whose computations are explained in Section 1. Let $g_{wane}(t)$ be the logistic transition function with which the vaccine efficacies wane from p_ℓ^2 to p_ℓ^3 in 6 months (chosen smoothness 0.05, and mid-point of transition 90 days). Then:

$$p_{\ell,k}(t) = p_\ell^1(1 - g_\delta(t)) + p_\ell^2 g_\delta(t) + (p_\ell^3 - p_\ell^2) g_{wane}(t) + (p_\ell^4 - p_\ell^3) g_{B,k}(t), \quad \ell \in \{I, TR, TU, HUNC\}, \quad (24)$$

Above, $p_{HUNC,k}(t)$ denotes the unconditional reduction in the hospitalization rate in the second set of compartments, but our model only features $p_{H,k}(t)$, the reduction in hospitalization rates conditional on being reported infected. Therefore, we follow [23] and calculate the conditional protection from hospitalization as:

$$p_{H,k}(t) = \frac{p_{HUNC,k}(t) - p_{I,k}(t) - (1 - p_{I,k}(t)) p_{TR,k}(t)}{(1 - p_{I,k}(t))(1 - p_{TR,k}(t))} \quad (25)$$

Also, note that we have modeled boosting differently than vaccinations: the boosted people are not moved for simplicity into a third set of compartments, but rather, with the booster transition function, the protection level in the second set of compartments rises to an average new level for everyone in that set (whether fully vaccinated, fully vaccinated and boosted, or non-vaccinated but with two previous infections).

Mid-points of transition of non-school contacts t_r . We found that the transition times are not separately identified from other parameters in the model. Because they indicate the time of NPI implementations, to which people react ahead of time, we fix them around the time of the most important NPIs, however, the smoothness of the transition K_r and the end-points u_r are estimated from the data.

Figure S19 gives a timeline of the most important measures and motivates our choice of t_r based on train transit and Google mobility data at transit stations, whose sources are explained in Section 1. The idea is that because the public transit network in the Netherlands is very much developed and used daily, trends in mobility data on trains or near transit stations should resemble trends in contact data between individuals: when mobility increases, so do the average contacts of an individual.

For Figure S19, just like for Figure S11, we first constructed the percentage change in $M_{ij}(t)$ for each day of the week relative to the average $M_{ij}(t)$ of those same weekdays in the two weeks February 1, 2020 - Feb 15, 2020 before the pandemic, to make it comparable to Google mobility data at transit stations, which is constructed in a similar fashion, but relative to the median mobility in the same weekday of the first 5 weeks of 2020.¹⁷ We then smoothed the transformed train mobility data, $n(t)$, and the Google mobility at transition stations, $g(t)$, with a Hodrick-Prescott filter, which is commonly used to extract trends from data that exhibits seasonality. The

¹⁷<https://www.google.com/covid19/mobility/>.

smoothed database on the Hodrick-Prescott filter is obtained from the penalized least-squares regression below:

$$\min_{sm_y(1), \dots, sm_y(T)} T^{-1} \sum_{t=1}^T (y(t) - sm_y(t))^2 + \omega \sum_{t=3}^T [(sm_y(t) - sm_y(t-1)) - (sm_y(t-1) - sm_y(t-2))]^2, \quad (26)$$

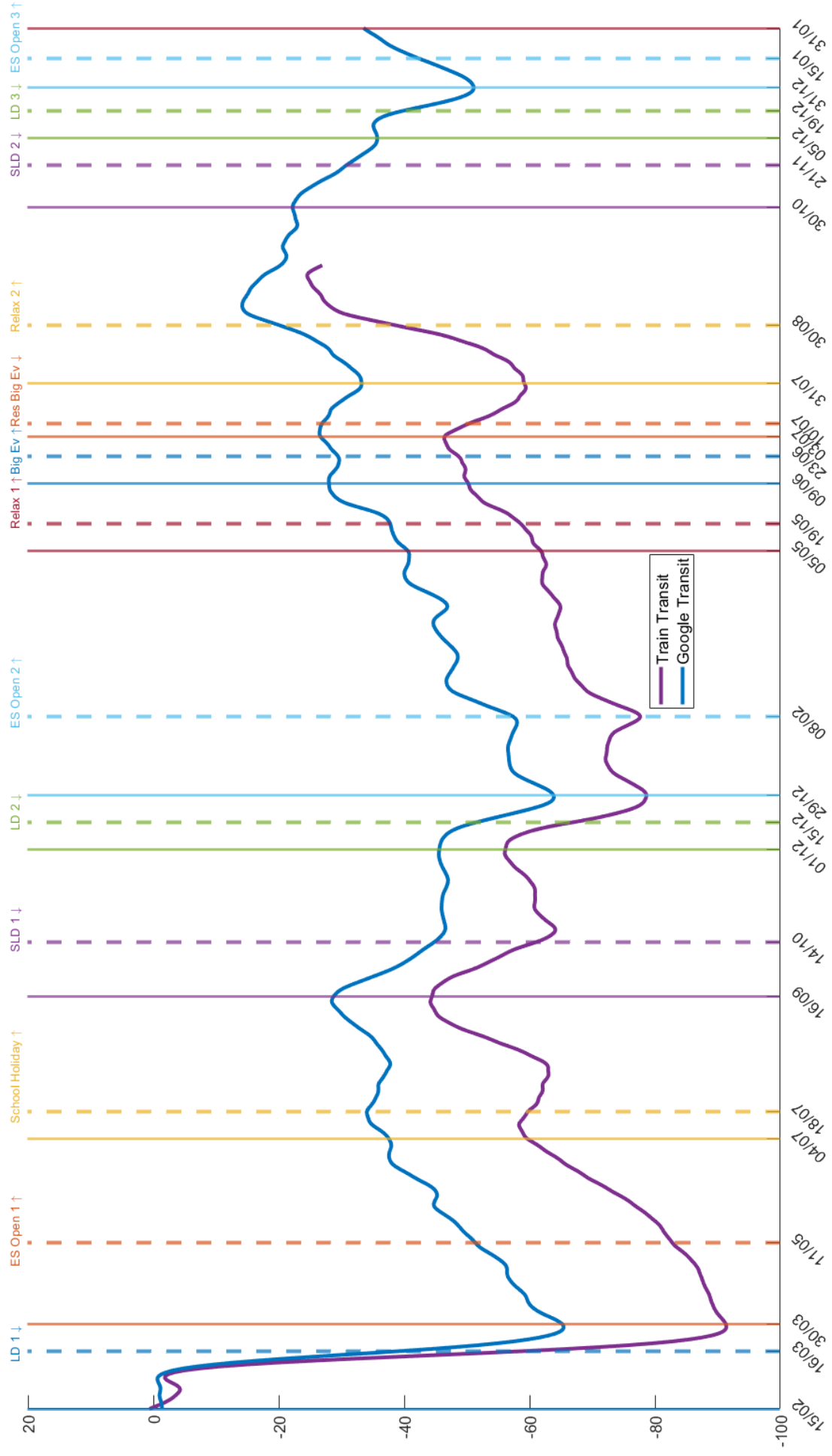
where T is the sample size available, $y \in \{g, n\}$, $sm_y(t)$ is the smoothed series, and ω is a tuning parameter set to 200 chosen to reflect the mid-term NPI change in patterns best and remove weekly seasonality.

Figure S19 shows the timing of most measures (also listed in Table S8). It can be seen that in each of the lockdowns, both train and transit mobility drop substantially. Checking the chosen transition mid-points against the timing of the measures on the RIVM dashboard reveals that adjustments in mobility mostly occur slightly ahead of the time measures are implemented. For each lockdown, we see that after 2 weeks (14 days), mobility rebounds, and this is shown by the solid lines after each lockdown measure t_r . The very first relaxation measure after each lockdown was invariably opening up elementary schools. We already model the effect of these school openings on school contacts, however, as can be seen from Figure S19, when elementary schools open, mobility increases further even though many elementary school children do not use public transportation, but are driven by parents or bike to school. Therefore, we introduce a regime that reflects an increase in non-school contacts for each of the elementary school openings after a lockdown. The other choices of regimes are motivated by either school holidays - when mobility and contacts typically increase as families go on vacation - or by further relaxation measures or by a restriction on big events, all of which are visible transitions both in Google and in the NS data. We note that the solid lines plotted in Figure S19 are typically chosen either two weeks before or after a mid-point, and are used in the estimation to stop updating a given regime and move to update a new regime - see Section 3.4 for more details.

Table S8: Choice of transition mid-points

Regime r	t_r	Symbol	Explanation
1	16/03/2020	LD 1	Lockdown 1, work from home, only essential stores open
2	11/05/2020	ES Open 1	First relaxation, elementary schools open at half capacity
3	18/07/2020	School Holidays	All schools entered summer holidays
4	14/10/2020	SLD 1	Semi-lockdown 1, restaurants and bars close, advice to work from home
5	15/12/2020	LD 2	Lockdown 2, work from home, only essential stores open
6	08/02/2021	ES Open 2	First relaxation, elementary schools open after lockdown 2
7	19/05/2021	Relax 1	Step 2 opening plan, further relaxations
8	23/06/2021	Big Ev	Allowed from June 26, chose June 23 to allow enough observations to the left and right of this regime
9	10/07/2021	Res Big Ev	Restrictions on big events
10	30/08/2021	Relax 2	Higher education opens with no distancing restrictions
11	21/11/2021	SLD 2	Semi-lockdown 2, mid-point between 13/11/2021 and 28/11/2021 when restrictions gradually increased, restaurants/bars close
12	19/12/2021	LD 3	Lockdown 3, work from home, only essential stores open
13	15/01/2022	ES Open 3	First relaxation, elementary schools open after lockdown 3

Figure S19: Choice of transition mid-points t_r



LD refers to lockdown, SLD to semi-lockdown, ES Open to elementary school openings, Relax to relaxation measures, Big Ev to big events, and Res Big Ev to restricting big events. The arrows next to them indicate whether the contact rate decreases or increases in that regime. The dashed lines are t_r , and the solid lines are end-points when we stop updating that regime. The meaning of t_r is also described in Table S8, and further information about the measures can be found on the RIVM Coronavirus Dashboard <https://coronadashboard.government.nl/>.

Other parameters such as $\rho_\alpha, \rho_\delta, \eta^1(t), \eta^2(t)$ **are calibrated at values from previous studies and are listed in Table S9.**

Table S9: Further calibrations

Parameter	Calibrated value	Source
ρ_α	0.3	[19]
ρ_δ	0.5	[18]
ρ_o	0.4	chosen to fit data best, see sensitivity analyses in Section 7
$\eta^1(t)$	$\frac{1}{365.5}(1 - g_o(t)) + \frac{4}{365.5}g_o(t)$	1 year waning period, transits to 3 months for Omicron see Section 7: 6 months and 2 years did not match seroprevalence data
$\eta^2(t)$	$\frac{4}{365.5}g_o(t)$	no waning before Omicron, transits to 3 months waning after Omicron see Section 7: results are similar for 2 and 4 months
$[\delta_1(t), \delta_2(t), \delta_3(t)]$	$[\frac{1}{8}, \frac{1}{3}, \frac{1}{3}]$; $[\frac{1}{3}, \frac{1}{2}, \frac{1}{2}]$	before Delta dominant (until June 1, 2021); after Delta dominant adults: based on values reported at https://covid-analytics.nl/ which were calculated from NICE (National Intensive Care Evaluation) data assumed for children based on NICE data, hospital occupancy per age

3.2 Estimated parameters and their priors

In this subsection, we list the estimated parameters along with their prior and motivations for it, as well as the regime in which they are updated, as some parameters like K_r, u_r are regime-specific.

Table S10: Parameter priors (all assumed uniformly distributed)

Parameter	Equation	Prior	Sample Updated	Explanation
Assumed common across age categories				
μ	(17)	[0.2 1]	Full Sample	wide prior
Z	(7)	[2 5] [2,3.5]	Regime 1 01/12/2021 - end	wide prior, [14] because of reduced incubation period Omicron
D	(9)	[3.5 5]	Full Sample	average estimates literature
K_r	(23)	[0.6 0.8]	Regime r	transition in $\sim 14 - 21$ days
u_1	(21)- (23)	[0.8 0.9]	Regime 3	most measures relaxed
u_2	(21)- (23)	[0.5 0.8]	Regime 4	work from home, other restrictions
u_3	(21)- (23)	[0.01 0.3]	Regime 5	lockdown, non-essential stores closed
u_4	(21)- (23)	[0.3 0.5]	Regime 6	gradual relaxations
u_5	(21)- (23)	[0.5 0.8]	Regime 7	further relaxations
u_6	(21)- (23)	[0.8 1]	Regime 8	all measures relaxed, big events allowed
u_7	(21)- (23)	[0.75 0.9]	Regime 9	restrictions on large events
u_8	(21)- (23)	[0.8 1]	Regime 10	further relaxations (for vaccinated)
u_9	(21)- (23)	[0.6 0.8]	Regime 11	semi-lockdown, work from home
u_{10}	(21)- (23)	[0.01 0.3]	Regime 12	lockdown
u_{11}	(21)- (23)	[0.3 0.8]	Regime 13	relaxations
Assumed different across age categories				
ϵ	(14)	[0.02 0.08]	Regimes 1-2	[0.25 1]/11.18; 11.18 =adult contacts with adults, and [0.25 1] ~ force of infection
$f_{2,\epsilon}$	(14)	[0.5 1.25]	Full Sample	adults w/out variants, seasonality, NPIs
$f_{3,\epsilon}$	(14)	[0.5 1]	Full Sample	wide prior
α_1	(9)	[0.02 0.1] [0.2 0.5]	27/02/20 - 30/04/20 01/05/20 - 31/05/21	relatively wide prior test only by severe symptoms
		[0.3 0.8]	01/06/21 - end	test capacity expanded test by mild symptoms
α_2	(9)	same as for α_1	Full Sample	test capacity further expanded
α_3	(9)	same as for α_1		test without symptoms
θ_1	(3)	[0.2 1]		
$f_{2,\theta} = \frac{\theta_2}{\theta_1}$	(3)	[0.02 0.5]	Full Sample	unlikely to commute every day
$f_{3,\theta} = \frac{\theta_3}{\theta_1}$	(3)	[0.02 0.5]	Full Sample	traveling across provinces costly
γ_1	(12)	[0.001 0.1]	Full Sample	adolescents travel less than adults
γ_2	(12)	[0.00005 0.1]	Full sample	children travel less than adults
γ_3	(12)	[0.00005 0.1]	Full sample	wide prior, γ_1 is cond. on rep. infection
ζ	(22)	[0.85 1]	Full Sample	wide prior
p_I^4	(24)-(25)	[0.3 0.7]	31/12/21 - end	social distancing 1.5m most of sample masks compulsory only for limited periods of time boosters only administered end of sample

As previously mentioned, ϵ is updated only in regimes 1-2, to avoid identification problems due to it entering in the model multiplicatively with u_r . Similarly, parameters $K_r, u_r, r = 3, \dots, 13$ are updated only in the particular regime, due to the fact it is unlikely that the effect of government measures or holidays in the past can be identified from information much later on, in a new regime. Additionally, some priors change over the sample

to reflect increased PCR testing or a lower incubation period for Omicron. Since the incubation period was well identified at the beginning of the sample (see Section 4), we fixed it after the first regime to reduce the number of parameters. Thus, the maximum number of parameters estimated in each regime is 17, with most regimes having 15 – 16 parameters, while the total number of spatial series fitted is 50 per day (36 reported case series, 12 hospitalization series for adults, and 2 hospitalization series for children and adolescents, see Section 3.3), and our sample consists of 705 days, while the shortest regime is the first, containing 33 days.

3.3 Estimation via the ensemble adjustment Kalman filter

The model in Steps 0-3, Section 2.1-2.2, represents the transition equations for a state-space model. Let \mathbf{Y}, \mathbf{X} be the vector of observed, respectively unobserved state variables, with typical elements $Y(t)$ and $X(t)$ stacked in order, and Θ the vector of estimated parameters listed in Table S10. Then the transition equations from one day $(t-1)_+$ to another t_+ (where, unless indicated otherwise, we substituted t_+ with t for simplicity, but it should be noted that in the updating, t_+ variables are updated, after completing all the transition equation steps):

$$\begin{bmatrix} \mathbf{Y}(t) \\ \mathbf{X}(t) \end{bmatrix} = \mathbf{F}_t \left(\begin{bmatrix} \mathbf{Y}(t-1) \\ \mathbf{X}(t-1) \end{bmatrix}, \Theta \right), \quad (27)$$

with \mathbf{F}_t a non-linear vector-valued function representing the SEIRHS model. Step 0-1 and Step 3 are deterministic, but Step 2 employs a stochastic version, where, as in [14], \mathcal{E} Poisson random variables are drawn for each unique term in the model equations (6)-(13), and a Runge-Kutta RK4 method is employed for numerical integration for each ensemble member $e = 1, \dots, \mathcal{E}$. As a result, we obtain ensemble members with typical elements $X^e(t), Y^e(t)$. The measurement equations are:

$$Y^{obs}(t) = Y(t) + \epsilon_Y(t), \quad (28)$$

where the observed variables $Y(t)$ are:

- new reported cases:

$$I_{newik}(t) = \frac{\alpha}{Z} (E_{ik}^1(t) + E_{ik}^2(t)), k = 1, 2, 3, i = 1, \dots, 12,$$

- regional hospitalizations for adults, where $s = 1, 2$ refer to hospitalization datasets 1 and 2 described in Section 1:

$$H_{newi1,(s)}(t) = \gamma_1^1 I_{i1}^{R,1}(t) + \gamma_1^2(t) I_{i1}^{R,2}(t), i = 1, \dots, 12, s = 1, 2$$

- due to many zeros, only national hospitalizations in children and adolescents, where $s = 1, 3$ refer hospitalization datasets 1 and 3 in Section 1:

$$H_{newk,(s)}(t) = \sum_{i=1}^{12} \left[\gamma_k^1 I_{ik}^{R,1}(t) + \gamma_k^2(t) I_{ik}^{R,2}(t) \right], k = 2, 3, s = 1, 3$$

Therefore, in total, in each period, we fit 50 data series.

The term $\epsilon_Y(t)$ is a mean-zero an additive observation or perturbation error ([13],[14]), assumed independent across provinces, time, and age categories. We chose the variance to be proportional to the mean so that the transition and the measurement stochasticity are roughly of similar order, i.e., $\epsilon_Y(t) \sim i.i.d.(0, \sigma_Y^2(t))$,

where $\sigma_Y^2(t) = \max(4, Y^{obs}(t))$, and $Y^{obs} \in \{Inew_{ik}^{obs}, Hnew_{i1,(1)}^{obs}, \sum_{i=1}^{12} Hnew_{ik}^{obs}, k = 2, 3\}$ until September 30, 2021, and $Y^{obs} \in \{Inew_{ik}^{obs}, Hnew_{i,(2)}^{obs}, Hnew_{k,(3)}^{obs}, k = 2, 3\}$ starting October 1, 2021. For the latter series, $Y^{obs} \in \{Hnew_{k,(3)}^{obs}, k = 2, 3\}$, we used $\sigma_Y^2(t) = \max(2, Y^{obs}(t))$ instead.

We updated the system via the ensemble adjustment Kalman filter (EAKF). This filtering method was introduced in [4] as an extension to the ensemble Kalman filter to model high dimensional state variables that are partially unobserved in atmospheric science and was subsequently used in [14], [16] and [24], among others, for modeling COVID-19 infections, hospitalizations, and deaths within SEIR-type models.¹⁸ In the updates, \mathcal{E} ensembles draws are individually propagated forward by means of closed-form updates, based on the normal distribution approximation. The observable ensemble members are updated based on their own observations, sequentially for each time period, using a square-root correction to both adjust for small samples and dampen the variance inflation needed to keep the ensemble from collapsing - [13]. Let $\mathcal{Z}^{e,post}(t-1)$ be an ensemble member posterior from the last period, where $e \in \{1, \dots, \mathcal{E}\}$, and where $\mathcal{Z} \in \{Y, X\}$ can be an unobservable or an observable variable. Each member is variance inflated by a factor $\lambda > 1$:

$$\mathcal{Z}^e(t) = \bar{\mathcal{Z}}^{post}(t-1) + (\lambda - 1)(\mathcal{Z}^{e,post}(t-1) - \bar{\mathcal{Z}}^{post}(t-1)), \quad (29)$$

where $\bar{\mathcal{Z}}^{post}(t-1)$ is the mean over ensemble members $\mathcal{Z}^{e,post}(t-1)$. Then $\mathcal{Z}^e(t)$ completes the transition equation (SEIRHS model) and yields the prior $\mathcal{Z}^{e,prior}(t)$, $\mathcal{Z} \in \{Y, X\}$. Let $r_Y(t) = \sigma_Y^2(t)/(\sigma_Y^2(t) + \hat{\sigma}_{Y,prior}^2(t))$, where $\hat{\sigma}_{Y,prior}^2(t) = \widehat{Var}(Y^{e,prior}(t))$ is the sample variance of $Y^{e,prior}(t)$, and $\bar{Y}^{prior}(t)$ is the sample mean over $Y^{e,prior}(t)$. The observable state updates are:

$$Y^{e,post}(t) = r_Y(t)\bar{Y}^{prior}(t) + [1 - r_Y(t)]Y^{obs}(t) + \sqrt{r_Y(t)}[Y^{e,prior}(t) - \bar{Y}^{prior}(t)]. \quad (30)$$

Those variables X that are defined as “neighbors” of the variable Y are then sequentially based on their ensemble covariance with Y , where the neighbors are defined below. Let n_Y be the index of a neighbor of state variable Y , and X_{n_Y} a corresponding unobserved neighboring state variable. Let $\sigma_{X_{n_Y}}^2(t) = \widehat{Var}(X_{n_Y}^{e,prior}(t))$ and $\bar{X}_{n_Y}^{prior}(t)$ be the variance and the mean over ensemble members $X_{n_Y}^{e,prior}(t)$. Then, for all neighboring state variables,

$$X_{n_Y}^{e,post}(t) = X_{n_Y}^{e,prior}(t) + \frac{\widehat{Cov}(X_{n_Y}^{e,prior}(t), Y^{e,prior}(t))}{\sigma_{X_{n_X}}^2(t)}[Y^{e,post}(t) - Y^{e,prior}(t)]. \quad (31)$$

Next, we explain which unobserved state variables X will be updated. While we have 14 unobserved state variables per age/province ($S_{ik}^a, E_{ik}^a, I_{ik}^{R,a}, I_{ik}^{U,a}, H_{ik}^a, R_{ik}^a, N_{ik}^a, a = 1, 2$), we effectively have only 11 degrees of freedom, because of three equalities. One is explicit, the sum of the population in the two sets of compartments is constant. The other two are implicit: the newly recovered, $Rnew_{ik}^a(t) = \frac{1}{D}(I_{ijk}^{R,a}(t) + I_{ijk}^{U,a}(t)) + \delta_k(t)H_{ijk}^a(t)$, plus the newly waned individuals from the first set of compartments, $Wnew_{ik}(t) = \eta^1(t)R_{ik}^1(t)$, fully define the evolution of recovered on both compartment sets, as well as the susceptibles in both compartment sets given the other states. Therefore, the unobserved state variables we update based on observed state variables are $Y \in \{E^a, I^{R,a}, I^{U,a}, H^a, Rnew^a, a \in \{1, 2\}, Wnew\}$.

After updating these 11 variables per region and age category, we calculate the posterior updates for suscepti-

¹⁸It is well known that the particle filter and other sequential Monte Carlo methods collapse in high dimensions because it requires the number of particles to grow exponentially with the number of states to avoid degeneracy of importance sampling weights [8]. The EAKF avoids this pitfall by not resampling and can be viewed as a method in-between a Kalman filter (which requires normality and linearity of the system) and other filters, which do not require it. Recently, [13] showed that despite nonlinearity, the method converges in mean square error to the true process that drives the observations, for fixed ensemble size, uniformly in finite time.

bles and recovered using the following formula, where recall that $R_{ik}^a(t_-)$ refer to total recovered after vaccination (so after Step 0 is performed):

$$R_{ik}^{a,post}(t) = R_{ik}^a(t_-) + Rnew_{ik}^{a,post}(t) - \mathbf{1}[\mathbf{a} = \mathbf{1}] Wnew_{ik}^{post}(t) \quad (32)$$

$$N_{ik}^{1,post}(t) = N_{ik}^{1,post}(t-1)_+ - V_{ik}(t) - Wnew_{ik}^{post}(t) \quad (33)$$

$$N_{ik}^{2,post}(t) = N_{ik} - N_{ik}^{1,post}(t) \quad (34)$$

$$S_{ik}^{a,post}(t) = N_{ik}^{a,post}(t) - \sum_{X \in \{E, I^R, I^U, H, R\}} X_{ik}^{a,post}(t) \quad (35)$$

To estimate the parameters, we simply augment the state space with the set of parameters, which are treated exactly as unobserved state variables, but with a constant transition equation. Therefore, their update is based on a random walk where the mean and variance change in the update, allowing the filter to capture parameter changes over a longer period of time, as demonstrated by simulation in [16]. The number of initially infected people is assumed in a range $[r_{low}, r_{up}] = [500, 1500]$, approximately based on the posterior 95% credible intervals (CrI henceforth) from [20]. The second set of compartments is initialized at zero for all state variables. For the first set of compartments, we assume no epicenter, as in [20], because shortly after the first case was announced in the province North Brabant, multiple cases were found ex-post in other provinces, so we assume the unobserved and exposed cases are proportional to population in that region/age: $I_{ik,b}^{U,1}(0) = E_{ik,b}^1(0) = r_b \frac{N_{ik}}{\sum_i \sum_k N_{ik}}$, $b \in \{low, up\}$, and $I_{ik,b}^{R,1}(0) = R_{ik}^1(0) = H_{ik}^1(0) = Wnew_{ik}(0) = Rnew_{ik}^1(0) = 0$. Note that new reported cases at the beginning of the sample are set to zero because: (1) there were initially no cases reported before February 27, 2020; (2) the ex-post updated cases are few and we found them uninformative for estimation; (3) the established timing of these cases as symptomatic is questionable.

3.4 Algorithm

We added to the EAKF the four rounds of external observed seroprevalence data described in Section 1. This was done by adding a likelihood at $t = t_h^{ser}$, $h \in \{1, \dots, 4\}$ for each age category, where t_h^{ser} was defined in Section 1. Within the EAKF, this just means that we augment the observed state variables - at days t_h^{ser} only, $h = 1, \dots, 4$ - with $Z_k(t_h^{ser}) = \frac{n_{hk}}{N_k}(N_k - S_k^1(t_h^{ser}) - S_k^2(t_h^{ser}))$, where $N_k = \sum_{i=1}^{12} N_{ik}$, and where we assume $Z_k(t_h^{ser}) \sim i.i.d. BIN[n_{hk}ser_{hk}, n_{hk}ser_{hk}(1 - ser_{hk})]$. Then, on those days, all unobserved variables and parameters are updated with their covariance with all the $Z_k(t_h^{ser})$.

Additionally, for each location i and observable variable per age-region, its neighbors are defined as unobservables of: (1) same age-region; (2) same age and neighboring regions, defined as the union of the three provinces for which inward and outward mobility ($w_{ij}^{(1)}, w_{ij}^{(2)}$) defined in Section 1.5 are the largest; (3) all other ages and same region if the observables are for adults, as the adult data has the highest signal value over all periods. For each national observation per age (hospitalizations in children and adolescents), the neighbors are all unobservables of types (1) and (2). For each seroprevalence round, the neighbors are simply all the variables in the system, including parameters.

For $t = 0$, the priors are obtained by drawing $\mathcal{E} = 300$ ensemble uniformly on a Latin Hypercube for all the estimated parameters and state variables in range, to visit all areas of the joint parameter and unobservable space. For $t \geq 1$, the posteriors at $t - 1$ become the priors at t , after being variance inflated and completing the transition equation. Then, we proceed as follows. For each $t = 1, \dots, T$ ($T = 705$ days):

1. retrieve posteriors at time $t - 1$
2. variance inflate each ensemble member according to equation (29), but only referring to states and parameters that are updated (recall that some parameters are only updated in particular regimes)
3. check whether priors need to be changed (at later dates, due to for example increases in test capacity)
4. run the stochastic version of the SEIR model (Steps 0-3) and obtain the priors for each variable
5. update observable state variables according to equation (30)
6. for each observed variable Y , update neighboring unobservable states based on their covariance with observables (equation (31))
7. for each observed variable Y , update all parameters that should be updated in a particular regime based on covariance with observables (equation (31))
8. do so for infection data, hospitalization data, and seroprevalence data
9. update other states via equalities (32)-(35)
10. if parameter posteriors are out of their prior bounds, redistribute them with a small variance (0.001) inside the bounds
11. $t = t + 1$; stop if $t = T$.

4 Parameter Estimates

4.1 Time Evolution of Posterior Distributions

This section presents the time evolution of all parameter posteriors (means and 95% CrI) over the entire sample, plotted against their prior range, and provides a discussion of parameter time-variation and identifiability.

We first focus on age-specific parameters. Figure A1 shows the smoothed evolution of key parameters, where the smoothing of both the means and the credible intervals over time was done with the Hodrick-Prescott filter and a chosen smoothing parameter $\omega = 20,000$. See equation 26 for the Hodrick-Prescott filter formula.

Susceptibility. Figure A1 shows that the posterior mean of susceptibility of adolescents and children relative to adults ($f_{2,\epsilon}$ and $f_{3,\epsilon}$), even when controlling for the average rise in transmission due to variants, increased over time. But it also shows that the credible intervals are wide for the wild-type period and less so for other variant periods, consistent with the notion that the true relative susceptibility of children and adolescents is harder to identify in periods when schools are closed and children and adolescents have few contacts, as was the case at the beginning of the pandemic. Note that we allowed the relative susceptibility of adolescents to be larger than that of adults because lowering the upper bound of this prior did not fit the data well. The estimate of the susceptibility of children relative to adults, $f_{3,\epsilon}$, decreases in times of school holidays or school closures, while that for adolescents, $f_{2,\epsilon}$, does not decrease. This can be explained by the fact that even though we model school contacts, we do not model day-care and after-school-care contacts; both of these are attended by children, and much fewer adolescents attend after-school care. During school closures, day-cares and after-school-care facilities were also closed. During school holidays, some are not, however, this is usually the time that parents can take holidays, as school is compulsory in the Netherlands. Therefore, during both elementary school

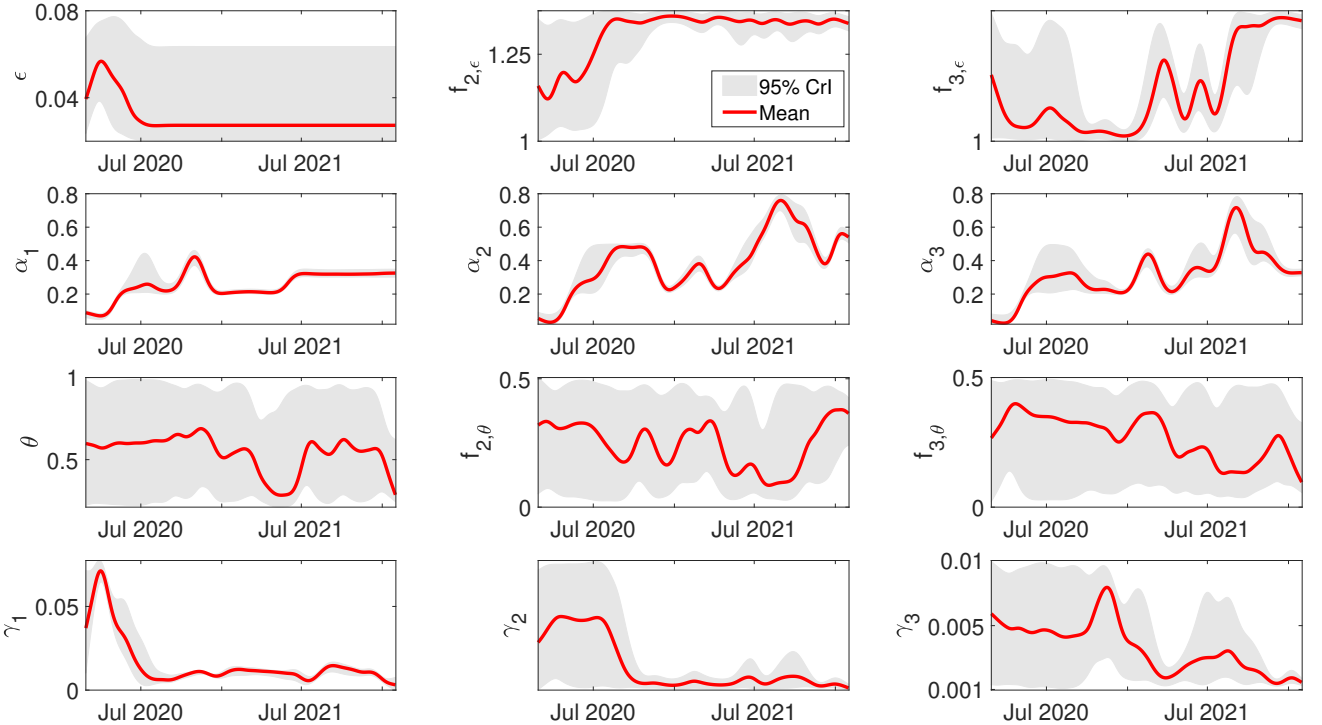
closures and holidays, the average number of unmodeled contacts of children decreases by much more than those of adolescents.

Case detection rate. The estimated case detection rates are initially very small: the posterior means on March 30, 2020 (during the first lockdown) are 6% for adults and 3% for adolescents and children. This makes sense, as only severe cases in adults were tested, and children and adolescents were rarely tested. Figure A1 also shows that the estimated case detection rates increase over time, in line with higher testing capacity and contact tracing measures that lead to testing in schools. The estimated case detection rate for adults fluctuates around 1/3, close to the lower bound of the prior, for most of the sample after July 2021. This may reflect a ceiling in the official PCR test capacity.

Mobility reporting errors. The estimates are relatively constant over the entire sample, and the uncertainty around them is relatively large, however the prior around them is relatively tight.

Hospitalization rates. Despite very wide priors, the posterior credible intervals for the hospitalization rate are very tight during most periods, and the identification analysis in Section 6.2 demonstrates by simulation that these parameters are robustly recovered from generated data even at the beginning of the sample, where the uncertainty in other parameter estimates is large. We find that hospitalization rates dropped substantially over time, in line with better treatment and vaccination mitigating the hospitalization burden.

Figure A1: Smoothed evolution of parameter posteriors over time (x -axis) plotted against prior range (y -axis): I

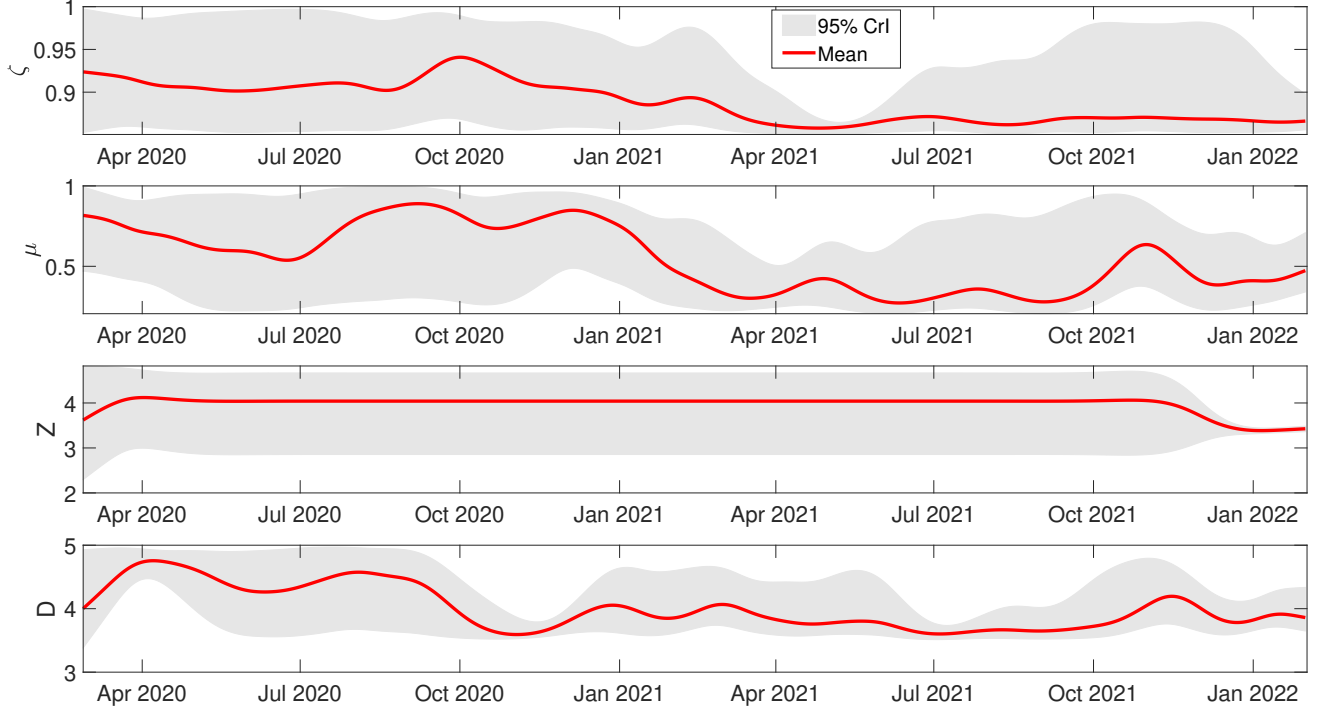


Note: Parameter ϵ is not updated over the entire sample. For some parameters, the priors change over the sample, see Table S10.

Figure A2 shows the smoothed time evolution of other key parameter estimates. The estimated mitigation factor ζ decreased over the sample, in line with more prevention measures, and mask use (masks were introduced outside public transportation only in December 2020, and were required only for parts of the year 2021, in specific indoor settings). The relative infectiousness of unreported infected μ over the sample also decreased, suggesting that cases became milder with repeated infections and vaccination. The estimates of incubation period Z are

deliberately estimated to be lower for Omicron, by setting lower priors. The estimates of the infectious period D are around 4.5 days at the beginning of the pandemic and lower later on, likely due to other prevention measures such as quarantine and isolation that were possible due to increased testing. These estimates are in line with previous studies -[20, 14], and their posteriors tighten as we move away from the beginning of the pandemic.

Figure A2: Smoothed evolution of parameter posteriors over time (x -axis) plotted against prior range (y -axis): II



Note: Parameter Z is only updated in regimes 1 and regime 13 (described in Table S10 and Figure S19). For some parameters, the priors change over the sample, see Table S10.

As the rest of the parameters (p_I^4, K_r, u_r) are regime-specific and were estimated over relatively shorter subsamples (see Table S10), Figures A3-A4 plot only their unsmoothed posterior evolution. The transition smoothness parameters K_r - except for the last regime - seem less well identified than the other parameters, however, their priors are also tight to ensure fast enough transitions so that the regimes do not overlap. The identification of the u_r and p_I^4 parameters seems stronger, with posteriors tighter than the priors in general. The estimated posteriors of p_I^4 suggest that the average reduction in the probability of infection conferred by the booster in the mixed population of boosted and non-boosted individuals is around 30%.

Concluding this section, for most parameters, the posterior distributions tighten as the testing capacity increases, indicating that the data is informative for these parameters. However, these distributions are wide for several parameters, especially in the first two regimes (lockdown and slow lifting of lockdown). Therefore, in Section 6.2, we verify identification of the parameters in these regimes via simulating 100 synthetic breaks in several scenarios.

Figure A3: Unsmoothed evolution of parameter posteriors over time (x -axis) plotted against prior range (y -axis): I

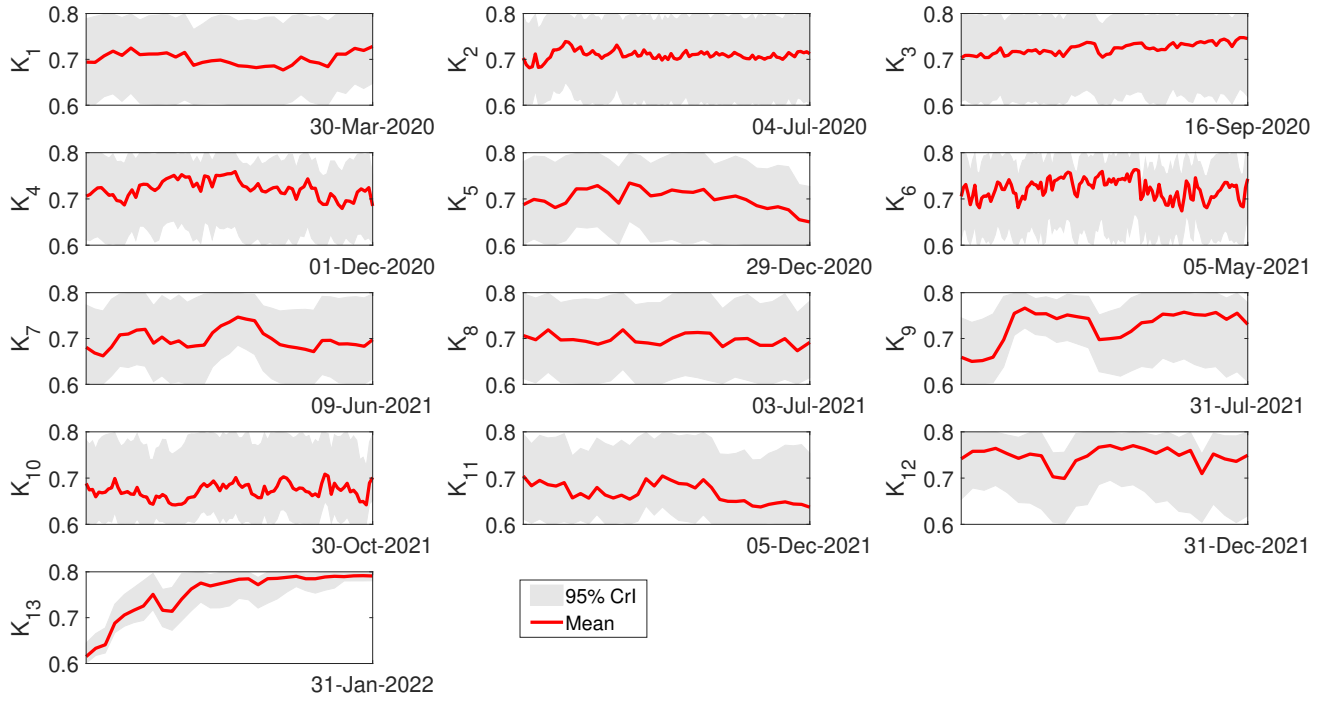
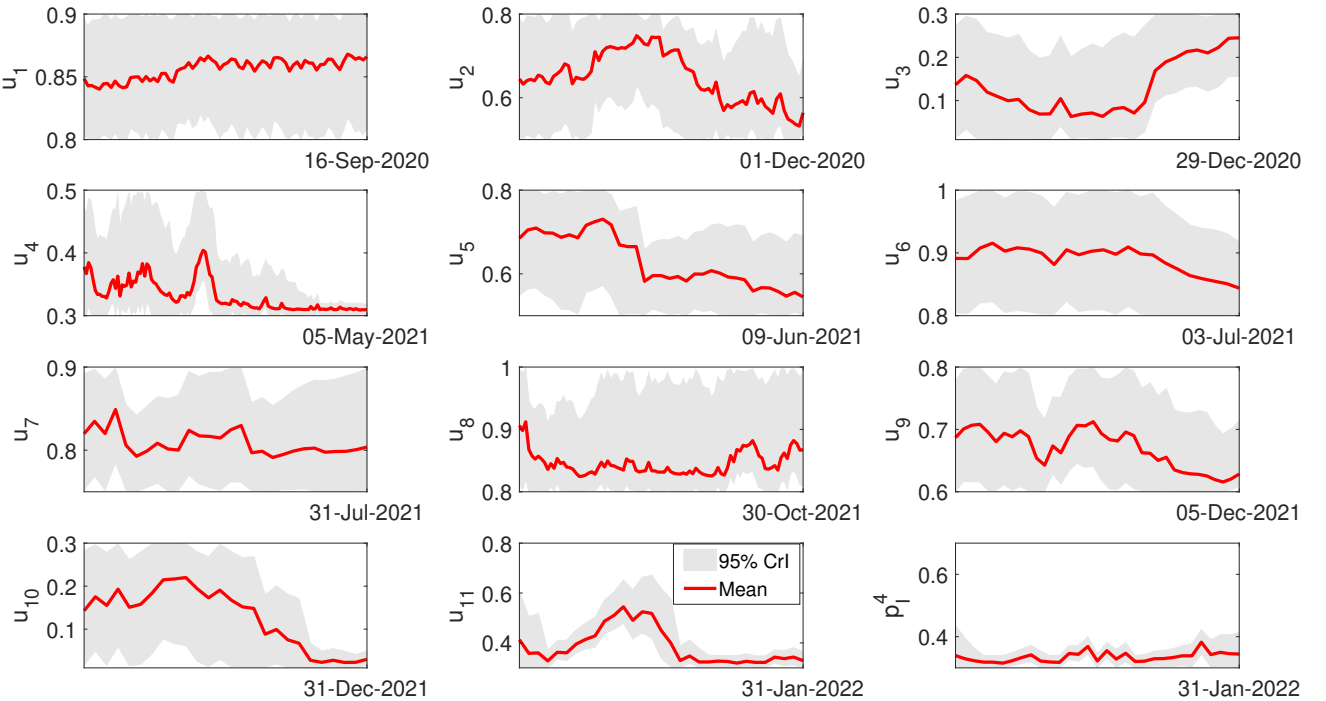


Figure A4: Unsmoothed evolution of parameter posteriors over time (x -axis) plotted against prior range (y -axis): II



4.2 Parameter estimates over variant periods

Table A1 defines 4 periods, each when a new variant makes up (approximately to) 5% of the total random samples in the data detailed in Section 1.8 (beginning of sub-sample for the new variant), along with the dates a new variant became dominant (50%) (solid and dotted lines in Figures 1-2 (main text)). The sub-samples defined in Table A1 are the “variant periods” used in the main text and all subsequent tables when referring to a variant.

Below, we provide for each variant period the end-of-sample and the average across the variant sample parameter estimates along with their 95% CrI (Tables A2 - A6).

Table A1: Sub-samples allocated to each variant

Variant	Beginning sub-sample	End sub-sample	Date 50% dominant
wild-type	February 27, 2020	December 28, 2020	-
Alpha	December 29, 2020	May 31, 2021	February 8, 2021
Delta	June 1, 2021	December 9, 2021	June 23, 2021
Omicron	December 10, 2021	January 31, 2021	December 24, 2021

Table A2: Parameter estimates I: end of sub-sample for each variant

Name	Wild-type			Alpha			Delta			Omicron		
	Mean	95% CrI		Mean	95% CrI		Mean	95% CrI		Mean	95% CrI	
ϵ	0.03	0.02	0.06	0.03	0.02	0.06	0.03	0.02	0.06	0.03	0.02	0.06
$f_{2,\epsilon}$	1.22	1.18	1.25	1.17	1.00	1.25	1.18	1.14	1.22	1.14	1.09	1.18
$f_{3,\epsilon}$	0.52	0.50	0.55	0.66	0.60	0.84	0.97	0.95	1.00	0.98	0.95	1.00
α_1	0.21	0.20	0.23	0.21	0.20	0.23	0.32	0.30	0.35	0.32	0.30	0.35
α_2	0.23	0.22	0.25	0.38	0.32	0.45	0.32	0.30	0.34	0.45	0.42	0.48
α_3	0.21	0.20	0.23	0.38	0.30	0.48	0.34	0.31	0.36	0.33	0.30	0.35
θ	0.41	0.20	0.80	0.31	0.21	0.94	0.54	0.24	0.95	0.41	0.33	0.91
$f_{2,\theta}$	0.12	0.02	0.40	0.10	0.02	0.43	0.41	0.16	0.50	0.24	0.04	0.35
$f_{3,\theta}$	0.22	0.03	0.44	0.19	0.03	0.49	0.33	0.16	0.44	0.10	0.02	0.42
γ_1	0.00797	0.00649	0.00943	0.00747	0.00445	0.00867	0.01285	0.01068	0.01500	0.00238	0.00126	0.00569
γ_2	0.00034	0.00006	0.00086	0.00087	0.00034	0.00159	0.00040	0.00026	0.00061	0.00019	0.00014	0.00029
γ_3	0.00377	0.00155	0.00608	0.00210	0.00048	0.00427	0.00052	0.00035	0.00081	0.00042	0.00027	0.00061

Note: Parameter subscripts 1, 2, 3 refer to adults, adolescents and children respectively. If parameter estimates and credible intervals are identical across variant periods, it means they were not updated in those sub-samples.

Table A3: Parameter estimates I: average over the sub-sample for each variant

Name	Wild-type			Alpha			Delta			Omicron		
	Mean	95% CrI		Mean	95% CrI		Mean	95% CrI		Mean	95% CrI	
ϵ	0.03	0.02	0.06	0.03	0.02	0.06	0.03	0.02	0.06	0.03	0.02	0.06
$f_{2,\epsilon}$	1.04	0.88	1.15	1.20	1.18	1.22	1.19	1.15	1.21	1.20	1.18	1.21
$f_{3,\epsilon}$	0.57	0.53	0.68	0.64	0.59	0.71	0.84	0.72	0.88	0.97	0.96	0.98
α_1	0.23	0.21	0.27	0.21	0.21	0.21	0.32	0.32	0.32	0.32	0.32	0.33
α_2	0.29	0.27	0.34	0.30	0.28	0.32	0.57	0.53	0.62	0.50	0.48	0.52
α_3	0.21	0.18	0.28	0.31	0.28	0.34	0.48	0.42	0.54	0.33	0.32	0.34
θ	0.61	0.29	0.92	0.44	0.29	0.83	0.53	0.31	0.87	0.47	0.32	0.75
$f_{2,\theta}$	0.27	0.07	0.43	0.25	0.11	0.39	0.17	0.09	0.41	0.37	0.19	0.43
$f_{3,\theta}$	0.33	0.08	0.45	0.29	0.10	0.42	0.18	0.09	0.44	0.19	0.10	0.37
γ_1	0.02259	0.01941	0.02675	0.01122	0.00977	0.01199	0.01074	0.00933	0.01172	0.00644	0.00513	0.00714
γ_2	0.00338	0.00073	0.00614	0.00054	0.00041	0.00072	0.00081	0.00046	0.00149	0.00045	0.00033	0.00062
γ_3	0.00510	0.00145	0.00864	0.00216	0.00113	0.00406	0.00201	0.00102	0.00453	0.00084	0.00055	0.00128

Note: Parameter subscripts 1, 2, 3 refer to adults, adolescents and children respectively. If parameter estimates and credible intervals are identical across variant periods, it means they were not updated in those sub-samples.

Table A4: Parameter estimates II: end of sub-sample for each variant

Name	Wild-type			Alpha			Delta			Omicron		
	Mean	95% CrI		Mean	95% CrI		Mean	95% CrI		Mean	95% CrI	
μ	0.63	0.34	0.85	0.29	0.24	0.50	0.27	0.20	0.52	0.50	0.26	0.80
Z	4.04	2.85	4.67	4.04	2.85	4.67	3.43	3.33	3.49	3.45	3.36	3.50
D	4.32	3.72	4.97	4.09	3.72	4.76	3.70	3.58	3.99	3.62	3.51	4.11
ζ	0.91	0.85	0.99	0.87	0.85	0.88	0.87	0.85	0.99	0.89	0.88	0.95

Note: If parameter estimates and credible intervals are identical across variant periods, it means they were not updated in those sub-samples.

Table A5: Parameter estimates II: average over the sub-sample for each variant

Name	Wild-type			Alpha			Delta			Omicron		
	Mean	95% CrI		Mean	95% CrI		Mean	95% CrI		Mean	95% CrI	
μ	0.73	0.43	0.89	0.43	0.30	0.60	0.38	0.30	0.77	0.43	0.30	0.60
Z	4.03	2.90	4.63	4.04	2.85	4.67	4.01	2.89	4.61	3.41	3.36	3.44
D	4.25	4.01	4.48	3.89	3.74	4.23	3.78	3.67	4.03	3.82	3.71	4.02
ζ	0.91	0.87	0.98	0.87	0.86	0.91	0.87	0.86	0.95	0.87	0.86	0.94

Note: If parameter estimates and credible intervals are identical across variant periods, it means they were not updated in those sub-samples.

Table A6: Parameter estimates III - end of sub-sample in which they were updated

Name	Mean	95% CrI	
K_1	0.73	0.65	0.80
K_2	0.71	0.60	0.80
K_3	0.75	0.62	0.80
K_4	0.68	0.60	0.75
K_5	0.65	0.60	0.73
K_6	0.74	0.66	0.80
K_7	0.70	0.61	0.80
K_8	0.69	0.61	0.78
K_9	0.73	0.61	0.78
K_{10}	0.70	0.65	0.80
K_{11}	0.64	0.60	0.75
K_{12}	0.75	0.62	0.80
K_{13}	0.79	0.78	0.80
u_1	0.87	0.81	0.90
u_2	0.56	0.53	0.68
u_3	0.25	0.16	0.30
u_4	0.31	0.30	0.32
u_5	0.54	0.50	0.69
u_6	0.84	0.80	0.92
u_7	0.80	0.75	0.90
u_8	0.87	0.81	0.99
u_9	0.63	0.61	0.71
u_{10}	0.03	0.02	0.05
u_{11}	0.33	0.30	0.37
p_I^4	0.34	0.30	0.41

Note: see Table S10 and Figure S19 for a list of regimes (sub-samples) in which these parameters were updated.

5 Supplement to Main Text, Section “Results”

This section provides computation details for Figures 1-4 (main text), and further results cited in the main text: tables that detail the data in Figures 1-4 (main text) or additional results cited in the main text.

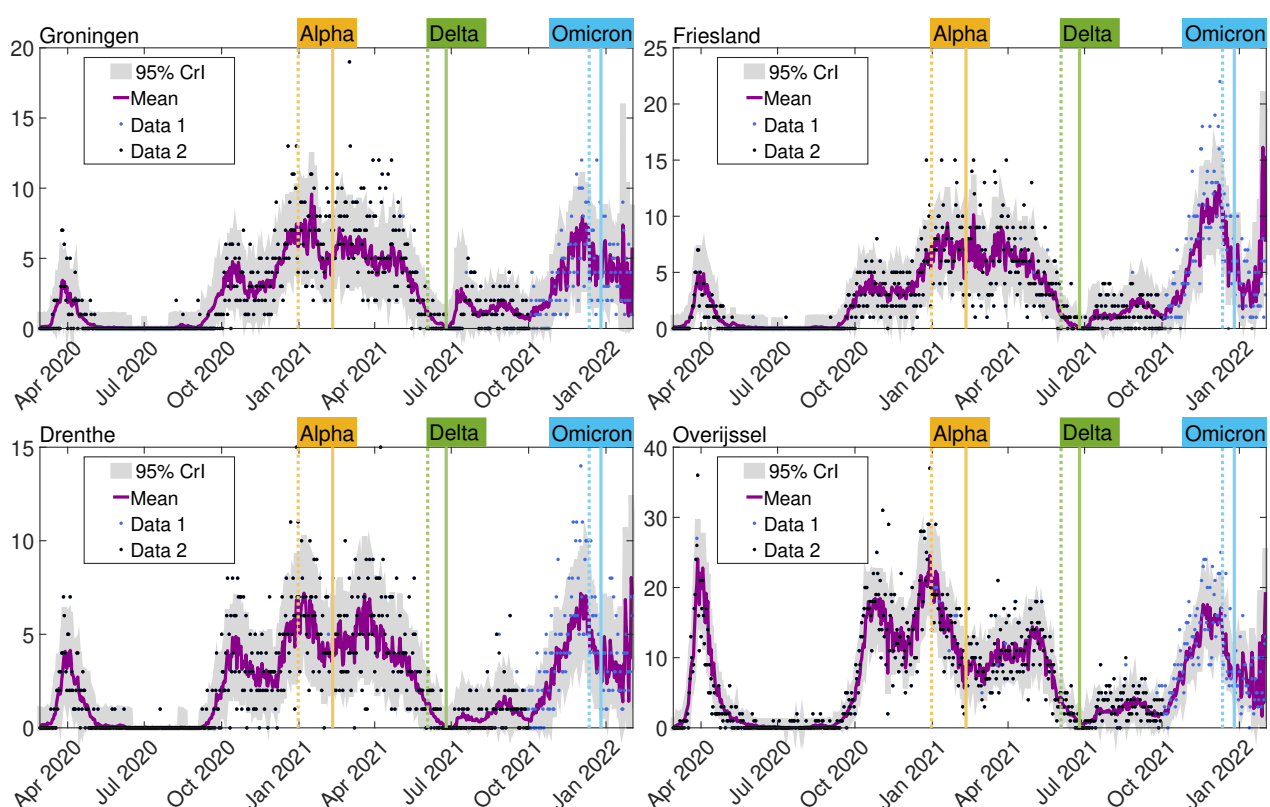
5.1 Time-dependent burden of hospital admissions

Computations for Figure 1. Recall that subscripts $i = 1, \dots, 12$ stand for provinces, and $k = 1, \dots, 3$ for age groups, while superscripts $a = 1, 2$ refer to the two-compartment sets. Figure 1 (main text) displayed a good fit of the model to the three hospitalization datasets at the national level. The data in these figures are described in Section 1, and correspond to: (1) Data 1: $\sum_{i=1}^{12} \sum_{k=1}^3 Hnew_{ik,(1)}^{obs}(t)$ and Data 2: $\sum_{i=1}^{12} Hnew_{i,(2)}^{obs}(t)$ over the entire sample in Figure 1 **A**, and (2) Data 1: $\sum_{i=1}^{12} Hnew_{ik,(1)}^{obs}(t)$ until September 30, 2021, and Data 3: $Hnew_{k,(3)}^{obs}(t)$, $k = 1, 2, 3$ afterwards, in Figure 1 **B-D**, where $Hnew_{1,(3)}^{obs}(t) = \sum_{i=1}^{12} Hnew_{i,(1)}^{obs}(t) - \sum_{k=2}^3 Hnew_{k,(1)}^{obs}(t)$ (the difference between all hospitalizations in Data 2 and hospitalizations in children and adolescents in Data 3) was not used in the estimation. The corresponding model estimates for (1) and (2) are the posterior means and 2.5% and 97.5% quantiles over the 300 ensemble members. The posteriors for each ensemble member e are computed as: (1) $\sum_{a=1}^2 \sum_{i=1}^{12} \sum_{k=1}^3 Hnew_{ik}^{a,e,post}(t)$ in Figure 1 **A**; (2) $\sum_{a=1}^2 \sum_{i=1}^{12} Hnew_{ik}^{a,e,post}(t)$ in Figure 1 **B-D**, with $Hnew_{ik}^{a,e,post}(t) = \gamma_k^{e,post}(t) I_{ik}^{R,a,e,post}(t)$, and with $I_{ik}^{R,a,e,post}(t)$ and $\gamma_k^{e,post}(t)$ calculated according to equation (31), as explained in the algorithm in Section 3.4.

Below, we display the model fit to regional hospitalizations (Datasets 1 and 2 described in Section 1). Even though our model was fitted to the data on regional hospitalizations only for adults, there are very few hospitalizations per province in children and adolescents, often zero. Therefore, we only plot the model fit for hospitalizations across all ages. The black and blue dots, corresponding to Datasets 1 and 2 respectively, are computed as $\sum_{k=1}^3 Hnew_{ik,(1)}^{obs}(t)$ until September 30, 2021, and as $Hnew_{i,(2)}^{obs}(t)$ afterwards. The corresponding model estimates are the posterior means and 2.5% and 97.5% quantiles over the 300 ensemble members, where the posteriors for each ensemble member e are $\sum_{a=1}^2 \sum_{k=1}^3 Hnew_{ik}^{a,e,post}(t)$.

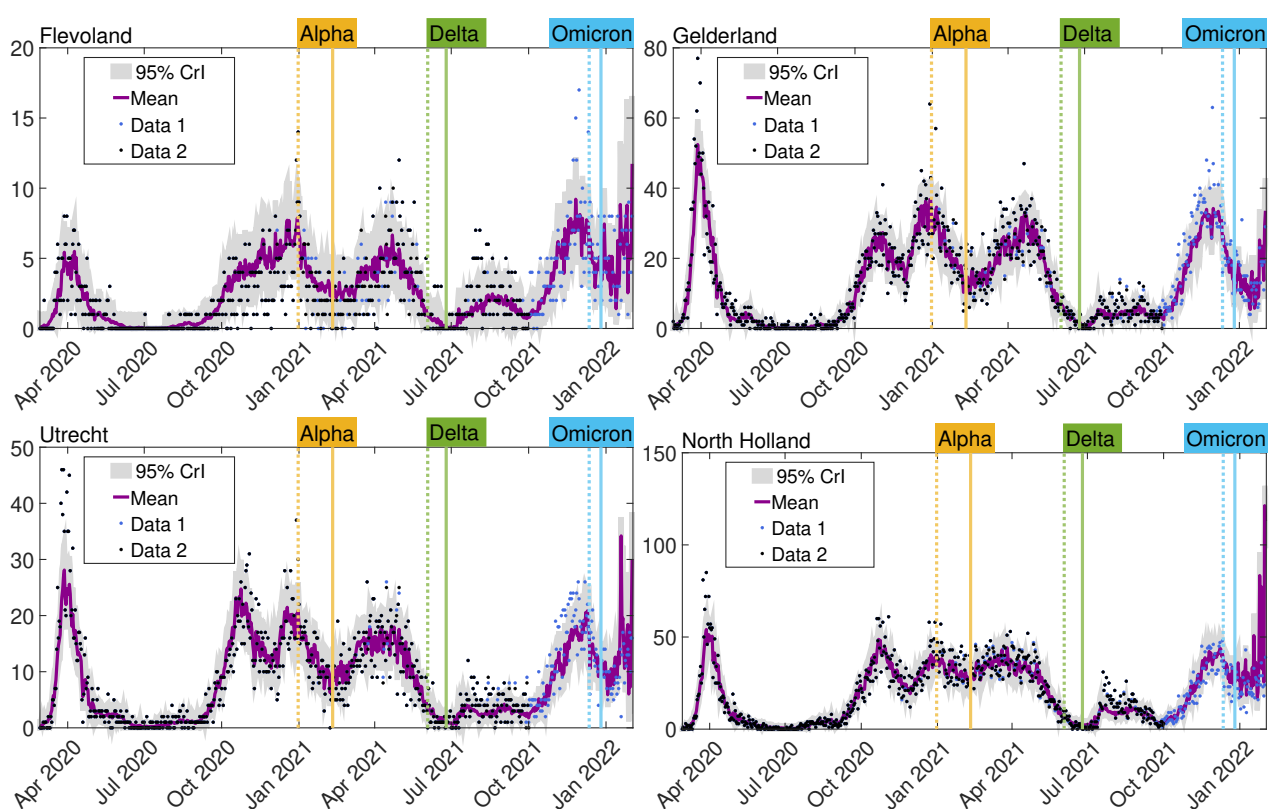
Figures A5-A7 demonstrate a good fit, with the exception of a short period at the beginning of August 2021, after big events were allowed, then restricted again, and the Delta variant took over. The underfitting during this short period can be explained by the fact that our model does not capture transmission from younger to older adults separately. Yet this is likely the explanation for the steep temporary rise in hospitalizations during that period: most of this rise is due to hospitalizations in individuals age 90 or above (see RIVM <https://coronashboard.government.nl/landelijk/ziekenhuis-opnames>, Figure: Hospital admissions per age group over time), but big events before this rise were attended in mass by younger adults, and it took longer for the infection in young adults to spread to older adults than in other periods.

Figure A5: Regional daily hospitalizations for all ages I



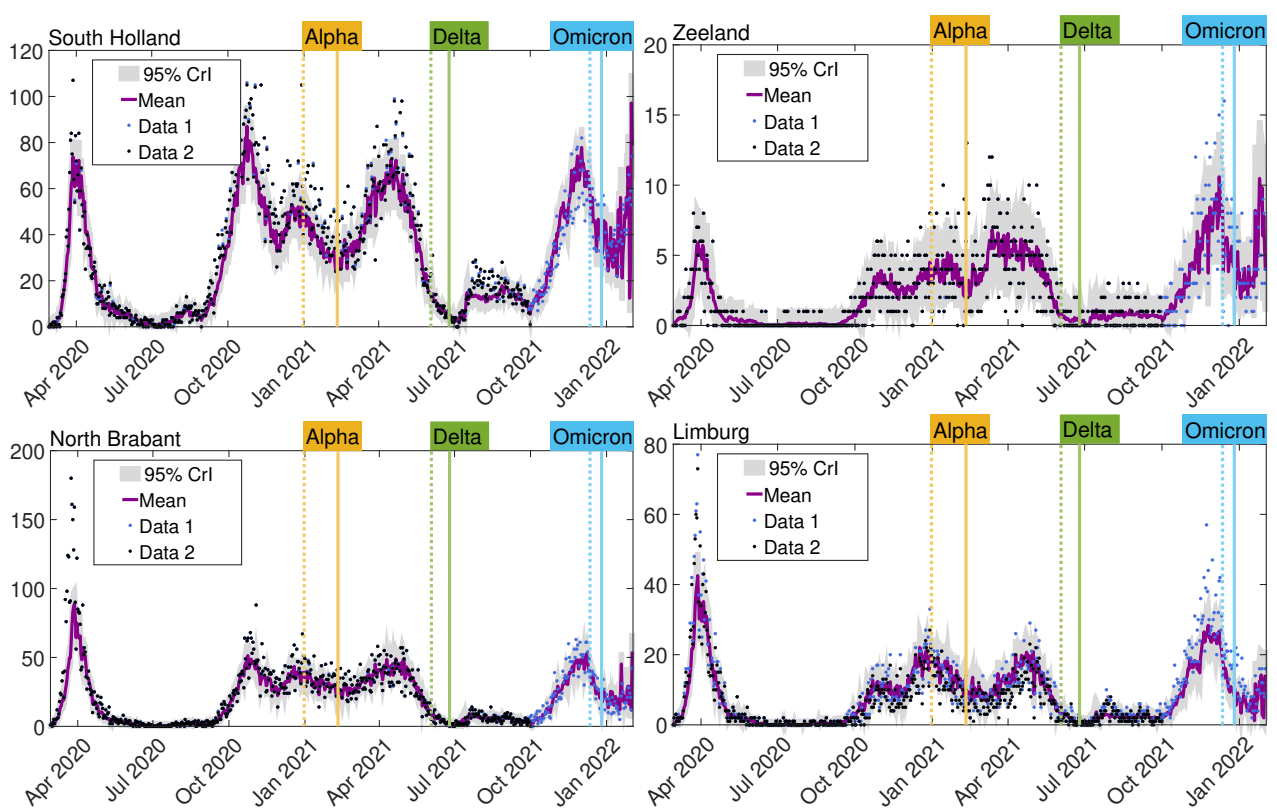
Note: The plots show daily hospital admissions per province (RIVM datasets described in Table 1 (main text) and Section 1), and model fit. Dashed and solid lines indicate when each variant corresponded to 5%, respectively 50% of cases in the RIVM variant data described in Section 1.

Figure A6: Regional daily hospitalizations for all ages II



Note: The plots show daily hospital admissions per province (RIVM datasets described in Table 1 (main text) and Section 1), and model fit. Dashed and solid lines indicate when each variant corresponded to 5%, respectively 50% of cases in the RIVM variant data described in Section 1.

Figure A7: Regional daily hospitalizations for all ages III



Note: The plots show daily hospital admissions per province (RIVM datasets described in Table 1 (main text) and Section 1), and model fit. Dashed and solid lines indicate when each variant corresponded to 5%, respectively 50% of cases in the RIVM variant data described in Section 1.

Table A7 provides the cumulative posterior mean and 95% CrI estimates of the hospitalizations per variant and in total, per age and across ages. To calculate these quantities, the posteriors $\sum_{a=1}^2 H_{new}^{(a),e,post}(t)$ were summed over different regions, then over variant periods and or/age, for each ensemble member, then the mean and the 2.5% and 97.5% quantiles over ensemble members were calculated.

Table A7: Cumulative hospitalizations per variant and in total

Wild-type			
Age	Adults	Adolescents	Children
Mean	30099	210	139
2.5%	29126	118	41
97.5%	30784	357	191
Alpha			
Age	Adults	Adolescents	Children
Mean	28249	200	258
2.5%	27450	145	132
97.5%	28920	271	461
Delta			
Age	Adults	Adolescents	Children
Mean	15789	266	388
2.5%	14986	173	258
97.5%	16308	453	693
Omicron			
Age	Adults	Adolescents	Children
Mean	8352	292	433
2.5%	7895	239	333
97.5%	8816	346	586
All ages, per variant (row 1: mean, row 2-3: 95%CrI)			
Wild-type	Alpha	Delta	Omicron
30448	28707	16443	9076
29482	27851	15600	8646
31191	29392	16988	9507
All variants			
Age	All ages	All age/population × 1,000	
Mean	84674	4.86	
2.5%	82729	4.75	
97.5%	86151	4.95	

Note: 2.5% and 97.5% refer to the lower and upper bounds of the 95% CrI.

5.2 Time-dependent burden of confirmed cases and seroprevalence

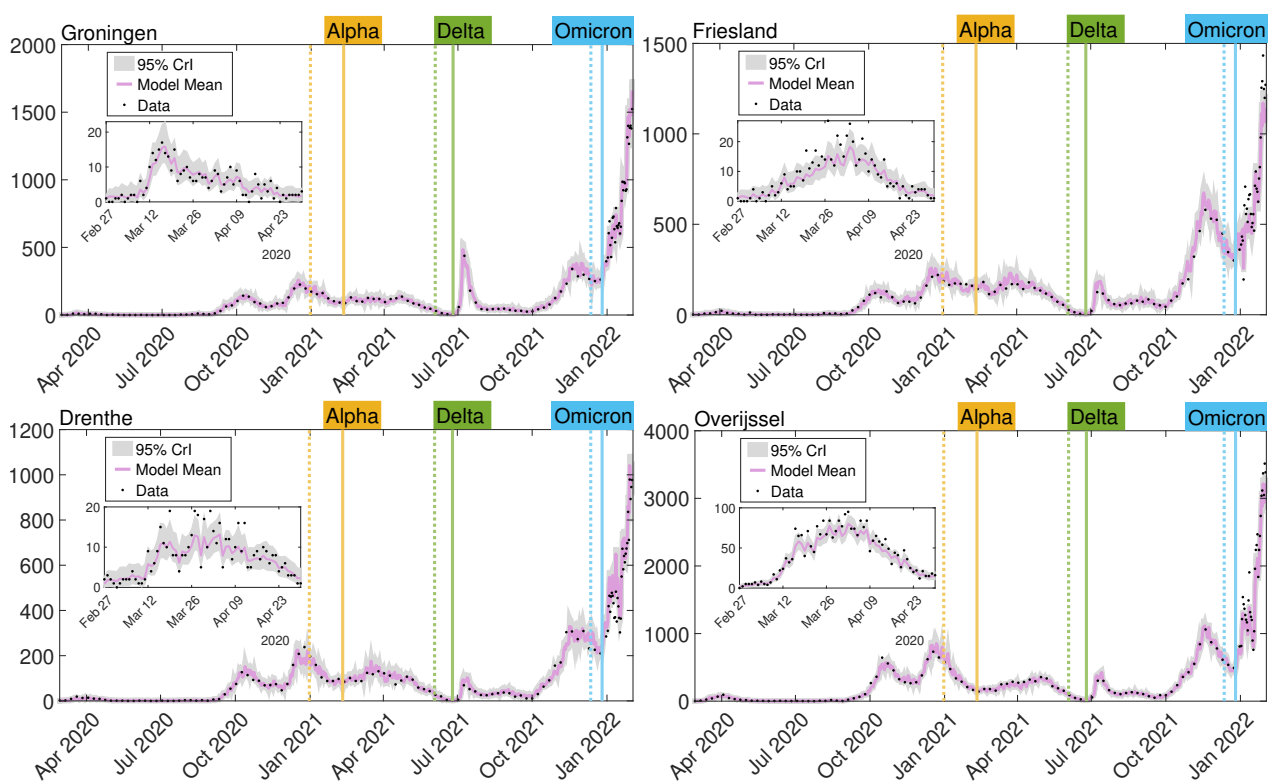
Computations in Figure 2 A. The posterior mean fraction of seropositive adults, adolescents, and children in their own population, along with their 95% CrI and means from the 4 PICO serosurveys are shown in Figure 2 A, main text. The data dots in Figure 2 A are ser_{hk} , described in Section 1, for the 4 seroprevalence rounds $h = 1, \dots, 4$, plotted at the assumed median times of seroconversion $n_{hk}, h = 1, \dots, 4, k = 1, 2, 3$. The mean and credible intervals of the estimated seroprevalence rounds are calculated from the posteriors over 300 ensemble members. The posterior over each ensemble member is computed as $1 - \frac{\sum_{a=1}^2 \sum_{i=1}^{12} S_{ik}^{a,e,post}(t)}{\sum_{i=1}^{12} N_{ik}}$, where $S_{ik}^{a,e,post}(t)$ was computed using (35) as explained in the algorithm in Section 3.4. The posterior means and 95% CrI in Figure 2 A at the end of each variant period are also listed in Table A8 below.

Table A8: Cumulative seroprevalence estimates at the end of each variant period: means and 95% CrI - Fitted data in Figure 2 **A**, main text

Variant	Wild-type	Alpha	Delta	Omicron
Adults				
Mean	0.19	0.32	0.48	0.84
2.5%	0.17	0.31	0.46	0.82
97.5%	0.20	0.34	0.50	0.86
Adolescents				
Mean	0.16	0.29	0.40	0.90
2.5%	0.15	0.27	0.38	0.87
97.5%	0.17	0.31	0.43	0.93
Children				
Mean	0.023	0.11	0.23	0.64
2.5%	0.019	0.09	0.20	0.60
97.5%	0.027	0.12	0.25	0.68
All ages				
Mean	0.17	0.30	0.45	0.83
2.5%	0.15	0.28	0.43	0.81
97.5%	0.18	0.31	0.46	0.85

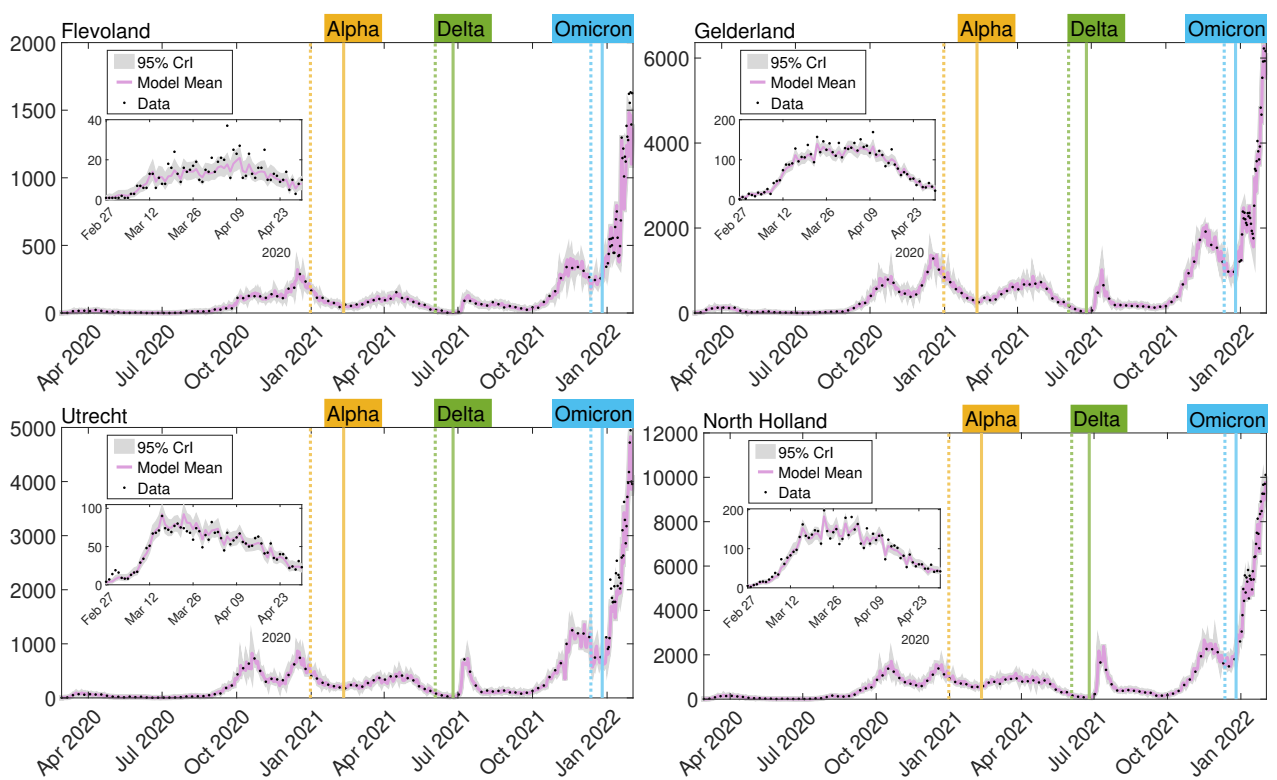
Computation in Figures 2 B-D. The national reported cases in each age group in their own population ($\times 1,000$), were calculated as $\frac{\sum_{i=1}^{12} I_{newik}^{obs}(t)}{\sum_{i=1}^{12} N_{ik}} \times 1,000, k = 1, 2, 3$, where $I_{newik}^{obs}(t)$ was defined in Section 1. The corresponding mean and 95% CrI were computed over the 300 ensemble members, where estimates per ensemble member e were computed as: $\frac{\sum_{a=1}^2 \sum_{i=1}^{12} I_{newik}^{a,e,post}(t)}{\sum_{i=1}^{12} N_{ik}} \times 1,000, k = 1, 2, 3$, where $I_{newik}^{a,e,post}(t) = \frac{\alpha_k^{e,post}(t)}{Z^{e,post}(t)} E_{ik}^{a,e,post}$, and where $E_{ik}^{a,e,post}(t)$, $\alpha_k^{e,post}(t)$ and $Z^{e,post}(t)$ were calculated according to (30) as explained in Sections 3.3-3.4. These figures demonstrated a good model fit nationally. Figures A8-A16 demonstrate that our model also fits well all 36 reported case series, regionally and per age. In these figures, the data is $I_{newik}^{obs}(t)$, and the model mean and 95% CrI are over ensemble members e , with each ensemble member computed as $\sum_{a=1}^2 I_{newik}^{a,e,post}(t)$.

Figure A8: ADULTS: Regional daily reported cases I



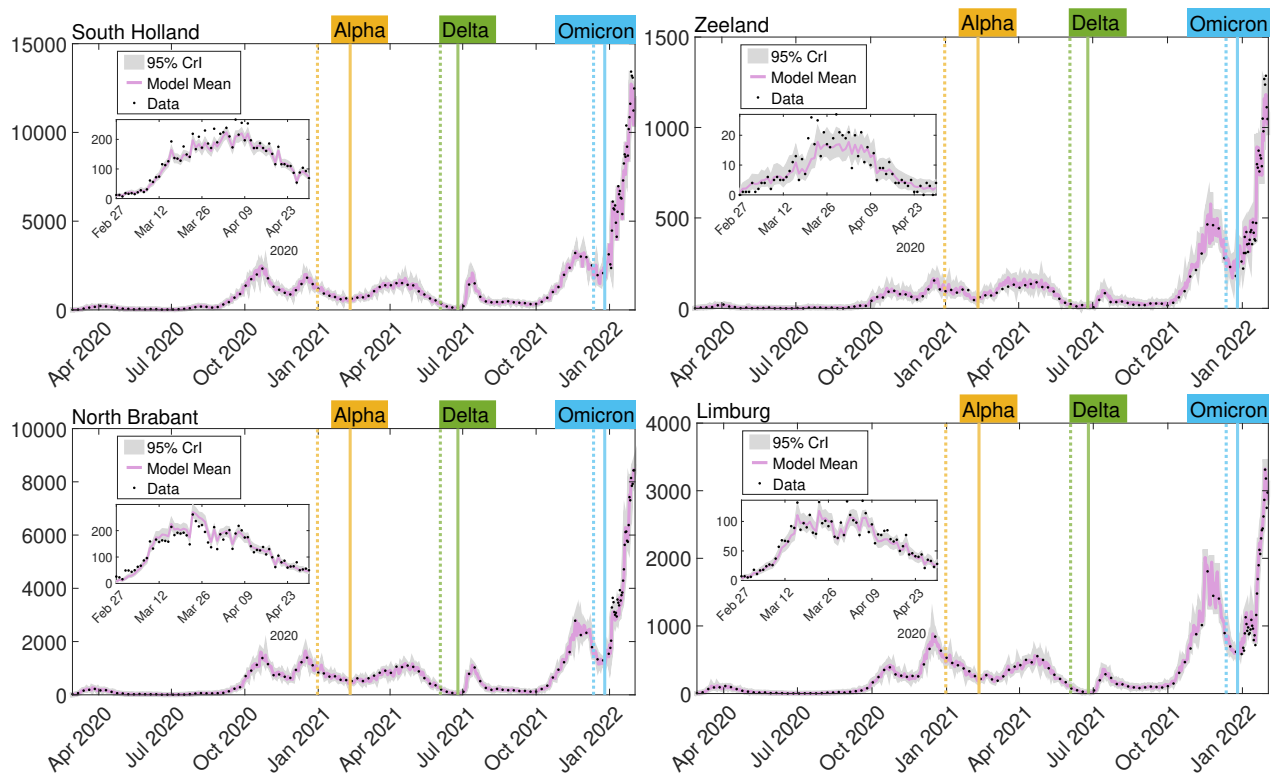
Note: The plots show daily reported cases per province (RIVM Dashboard reported case data described in Section 1), and model fit. Dashed and solid lines indicate when each variant corresponded to 5%, respectively 50% of cases in the RIVM variant data described in Table 1 (main text).

Figure A9: ADULTS: Regional daily reported cases II



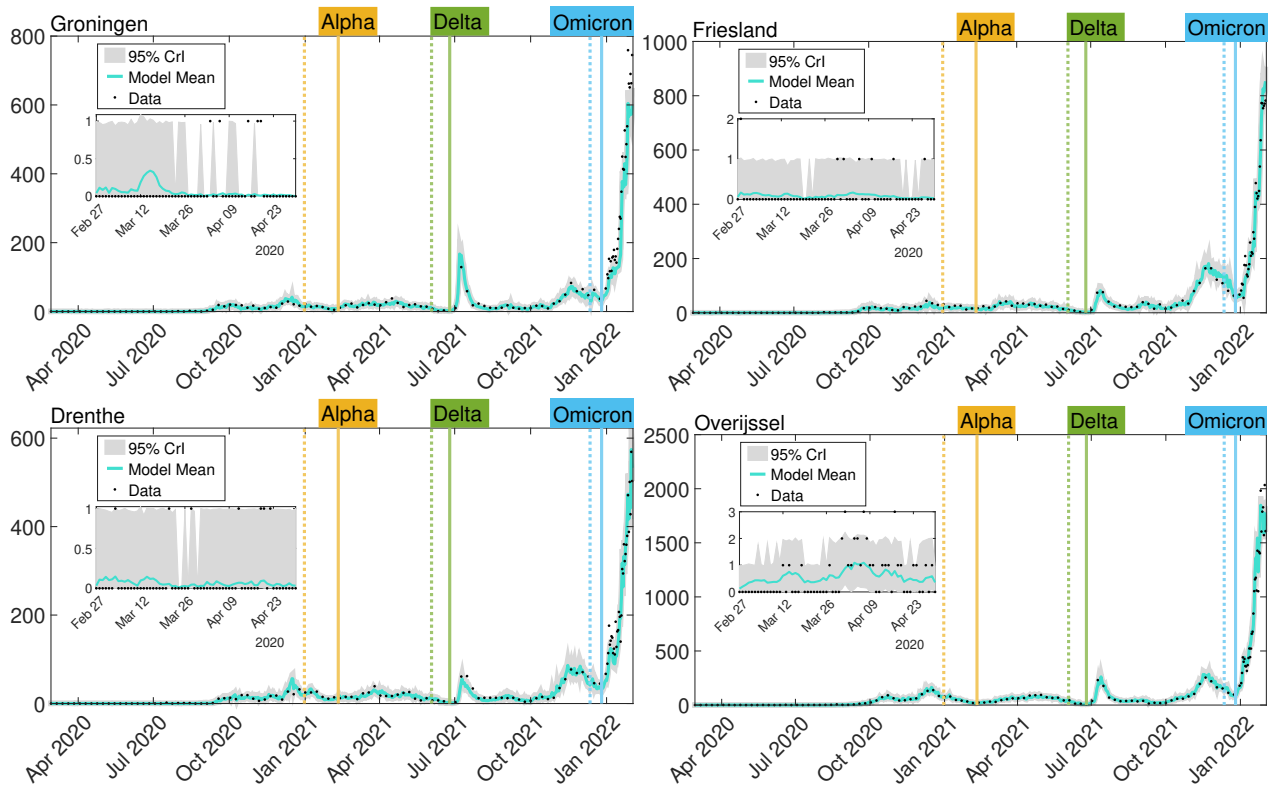
Note: The plots show daily reported cases per province (RIVM Dashboard reported case data described in Section 1), and model fit. Dashed and solid lines indicate when each variant corresponded to 5%, respectively 50% of cases in the RIVM variant data described in Table 1 (main text).

Figure A10: ADULTS: Regional daily reported cases III



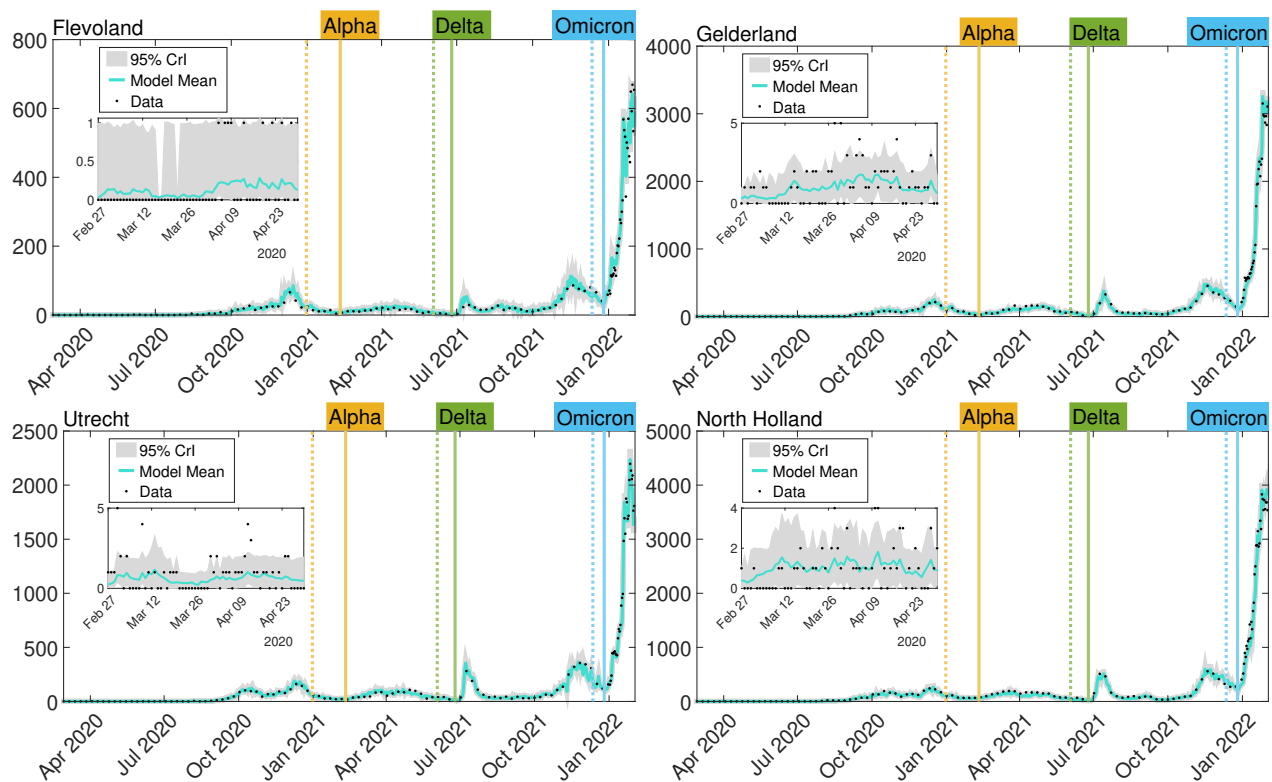
Note: The plots show daily reported cases per province (RIVM Dashboard reported case data described in Section 1), and model fit. Dashed and solid lines indicate when each variant corresponded to 5%, respectively 50% of cases in the RIVM variant data described in Table 1 (main text).

Figure A11: ADOLESCENTS: Regional daily reported cases I



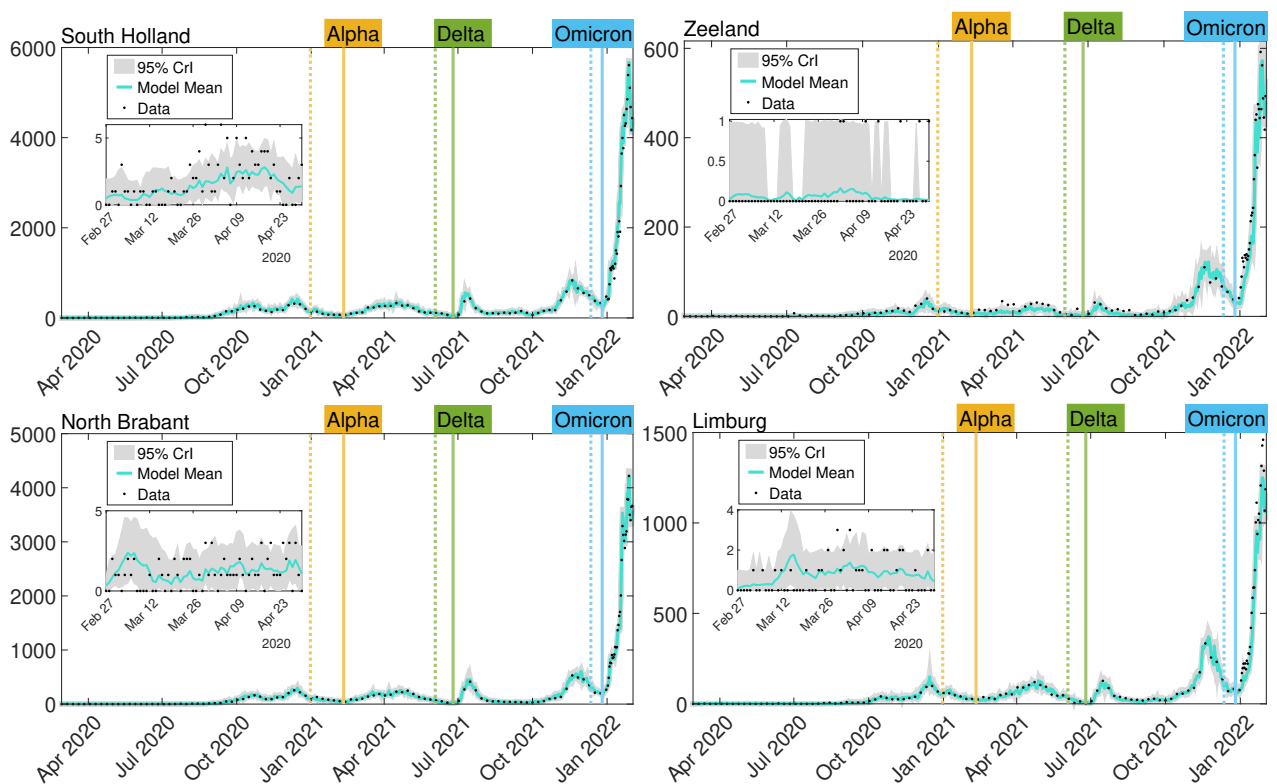
Note: The plots show daily reported cases per province (RIVM Dashboard reported case data described in Section 1), and model fit. Dashed and solid lines indicate when each variant corresponded to 5%, respectively 50% of cases in the RIVM variant data described in Table 1 (main text).

Figure A12: ADOLESCENTS: Regional daily reported cases II



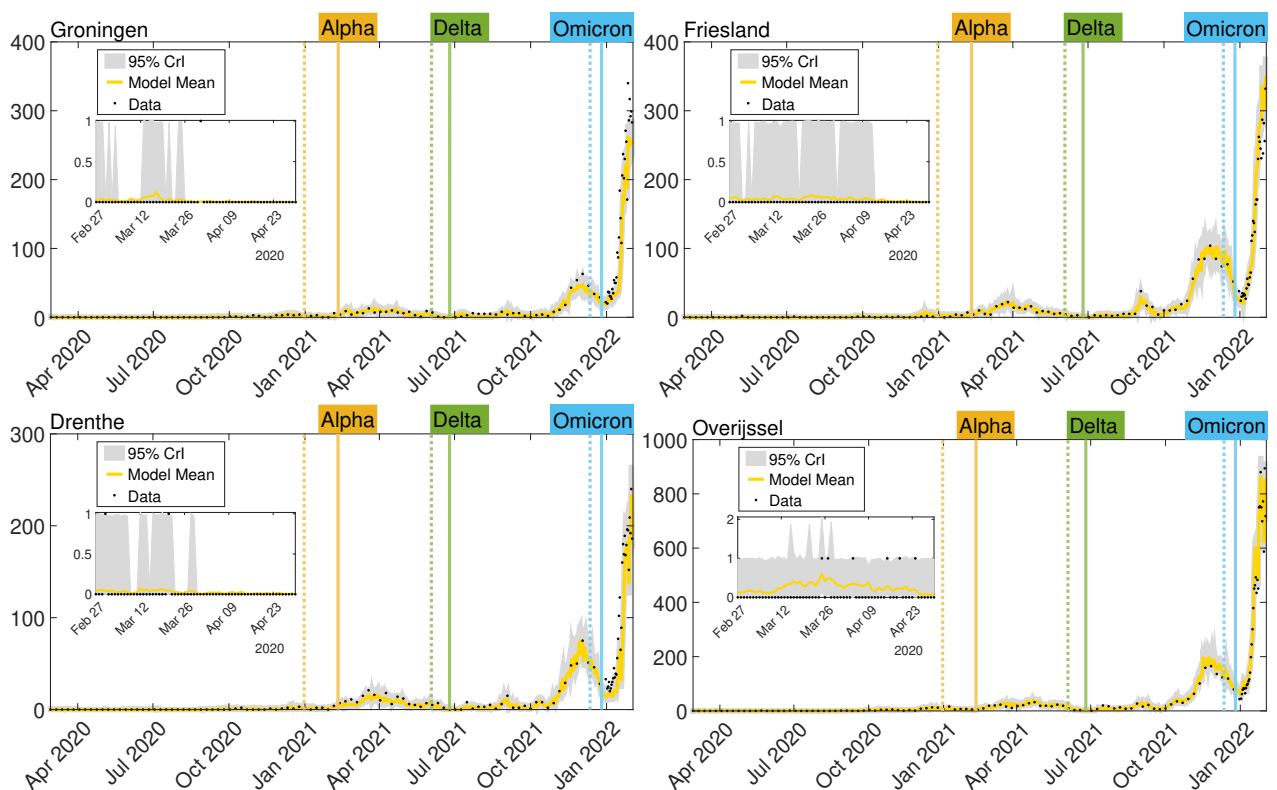
Note: The plots show daily reported cases per province (RIVM Dashboard reported case data described in Section 1), and model fit. Dashed and solid lines indicate when each variant corresponded to 5%, respectively 50% of cases in the RIVM variant data described in Table 1 (main text).

Figure A13: ADOLESCENTS: Regional daily reported cases III



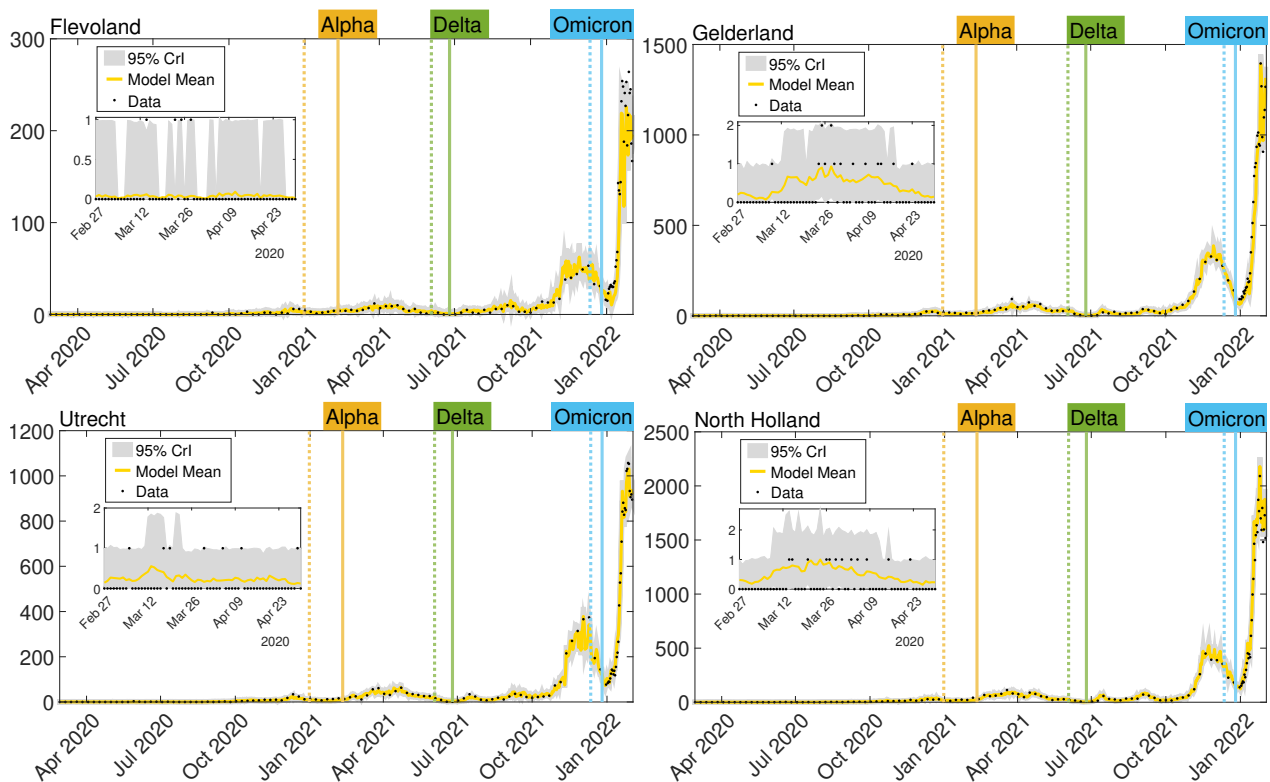
Note: The plots show daily reported cases per province (RIVM Dashboard reported case data described in Section 1), and model fit. Dashed and solid lines indicate when each variant corresponded to 5%, respectively 50% of cases in the RIVM variant data described in Table 1 (main text).

Figure A14: CHILDREN: Regional daily reported cases I



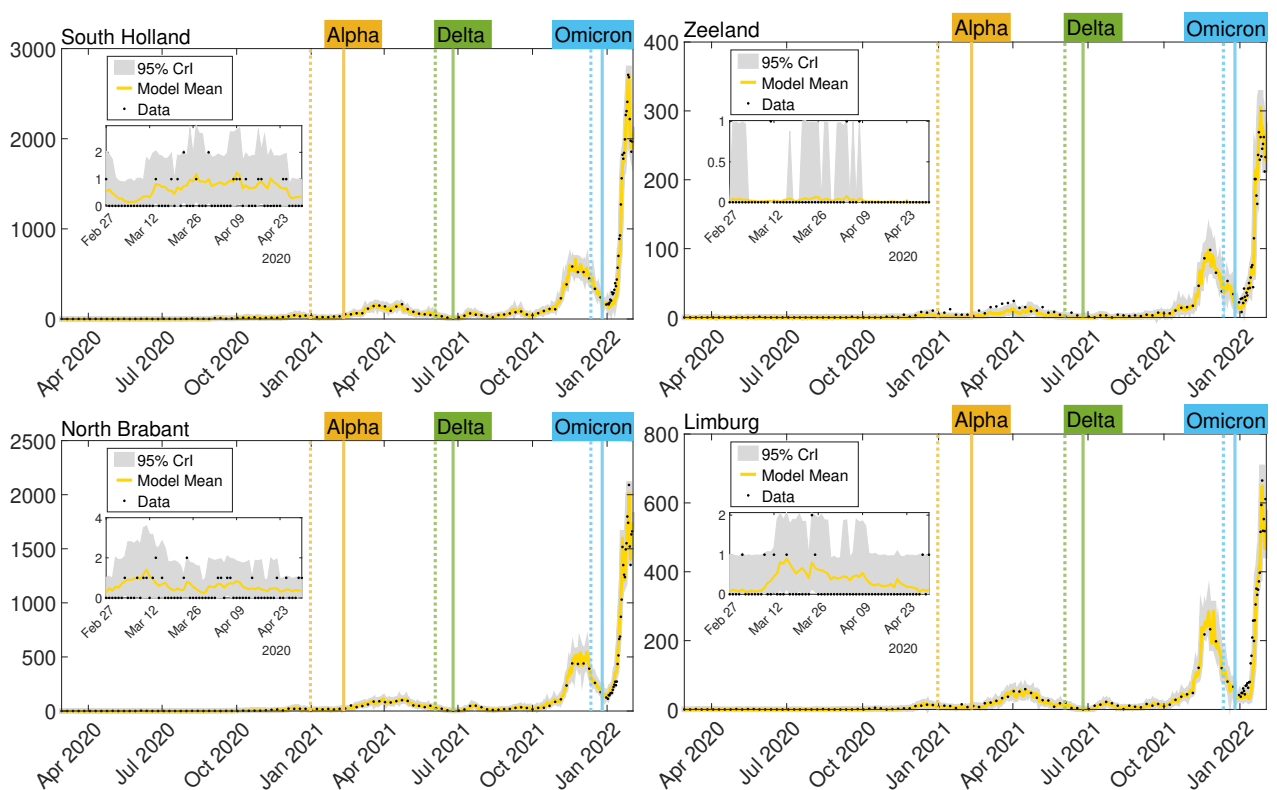
Note: The plots show daily reported cases per province (RIVM Dashboard reported case data described in Section 1), and model fit. Dashed and solid lines indicate when each variant corresponded to 5%, respectively 50% of cases in the RIVM variant data described in Table 1 (main text).

Figure A15: CHILDREN: Regional daily reported cases II



Note: The plots show daily reported cases per province (RIVM Dashboard reported case data described in Section 1), and model fit. Dashed and solid lines indicate when each variant corresponded to 5%, respectively 50% of cases in the RIVM variant data described in Table 1 (main text).

Figure A16: CHILDREN:: Regional daily reported cases III



Note: The plots show daily reported cases per province (RIVM Dashboard reported case data described in Section 1), and model fit. Dashed and solid lines indicate when each variant corresponded to 5%, respectively 50% of cases in the RIVM variant data described in Table 1 (main text).

5.3 Age distribution of total infections and hospital admissions by VoC

Computation in Figure 3 A. Figure 3 A displays the estimated fractions of unreported and reported cases in total cases, each per age and per variant period, in *the total reported and unreported infections across all ages for the same variant period*. For each ensemble member, the number of reported cases at time t is $\sum_{a=1}^2 \sum_{i=1}^{12} I_{new}^{a,e,post}(t)$, and the total cases over all ages are $\sum_{k=1}^3 \sum_{a=1}^2 \sum_{i=1}^{12} \frac{I_{new}^{a,e,post}(t)}{\alpha_k^{e,post}(t)}$. Each of these quantities is summed separately over each variant period defined in Table A1, and their ratio (fraction) is obtained by dividing the former by the latter. This is the estimated fraction of reported cases in that variant period for a given age category k for a given ensemble member e . The fraction of unreported cases per ensemble member e is calculated in the same way, but we substitute - in the numerator only - $I_{new}^{a,e,post}(t)$ with $\frac{1-\alpha_k^{e,post}(t)}{\alpha_k^{e,post}(t)} I_{new}^{a,e,post}(t)$. From these fractions for each ensemble member, the mean and 95% CrI are calculated.

The data behind Figure 3 A is in Table A9 below.

Table A9: Posterior fraction of new infections (reported and unreported) in total cumulative new infections per variant: Data in Figure 3 A, main text

	Rep. Adults	Unrep. Adults	Rep. Adolesc.	Unrep. Adolesc.	Rep. Children	Unrep. Children
Wild-Type						
Mean	0.208	0.677	0.030	0.071	0.003	0.011
2.5%	0.192	0.656	0.027	0.066	0.002	0.009
97.5%	0.220	0.701	0.033	0.078	0.003	0.014
Alpha						
Mean	0.179	0.667	0.030	0.078	0.012	0.034
2.5%	0.177	0.657	0.029	0.073	0.012	0.029
97.5%	0.181	0.673	0.031	0.084	0.013	0.038
Delta						
Mean	0.253	0.541	0.061	0.063	0.034	0.047
2.5%	0.249	0.533	0.060	0.056	0.034	0.036
97.5%	0.257	0.552	0.063	0.071	0.036	0.053
Omicron						
Mean	0.217	0.451	0.092	0.112	0.042	0.087
2.5%	0.205	0.424	0.087	0.098	0.039	0.077
97.5%	0.228	0.479	0.098	0.125	0.044	0.097

Note: The means and quantiles are based on the distribution of the ratio over ensemble members (and not the ratio of the distributions). Some rows for the mean may not add up to 1 due to rounding error. The ratios of total infections (reported and unreported) per age in a given variant period, reported in the main text, below Figure 3, are calculated by adding the mean percentages of reported and unreported cases in this table.

In Table A10, we list the cumulative posterior infections per variant and age (reported and unreported), from which some percentages of total unreported and total infections per age-variant period in the total infections over the sample were calculated based on the means in this table and reported in Section “Age distribution of total infections and hospital admissions per VoC” (main text).

Table A10: Cumulative posterior infections per variant and in total, broken down by reported and unreported cases

Wild-type						
Age	Rep Adults	Unrep Adults	Rep. Adolesc.	Unrep Adolesc.	Rep Children	Unrep. Children
Mean	687291	2245669	98862	235814	8883	36757
2.5%	677124	2050121	95282	221640	8154	30284
97.5%	716426	2537442	109526	262342	11179	46253
Alpha						
Mean	678891	2524969	113770	296111	45538	128719
2.5%	670466	2478203	110710	274070	43723	110042
97.5%	706436	2627743	125072	334552	52075	149815
Delta						
Mean	878861	1875982	212141	220064	119430	164615
2.5%	869781	1836206	207930	191430	116459	123955
97.5%	917356	1959297	230597	250604	133275	190244
Omicron						
Mean	1189614	2484510	438759	434905	199020	402471
2.5%	1183602	2436933	434460	392841	196630	381351
97.5%	1210400	2548445	451366	476198	208153	423849

Note: Some percentages of total unreported and total infections per age-variant period in the total infections over the sample were calculated based on the means in this table and reported in Section “Age distribution of total infections and hospital admissions per VoC” (main text).

Computation in Figure 3 B. Figure 3 B displays the fraction of hospitalizations for each age category in the total hospitalizations, in each variant period separately, multiplied by 1,000. For each ensemble member, we calculated $\sum_{a=1}^2 \sum_{i=1}^{12} H_{new}^{a,e,post}(t)$ and $\sum_{k=1}^3 \sum_{a=1}^2 \sum_{i=1}^{12} H_{new}^{a,e,post}(t)$. We then summed each of these quantities over variant periods separately, calculated their ratio for each $k = 1, 2, 3$ separately, and multiplied them by 1,000. The mean and the 95% CrI displayed in Figure 3B are calculated over the 300 ensemble values of these ratios (fractions). The data behind Figure 3 B is in Table A11 below.

Table A11: Mean of the fraction of new age-specific hospitalizations in total cumulative new hospitalizations for all ages per variant: Data in Figure 3 B, main text

	Adults	Adolescents	Children
Wild-Type			
Mean	0.989	0.007	0.005
2.5%	0.983	0.004	0.001
97.5%	0.993	0.012	0.006
Alpha			
Mean	0.984	0.007	0.009
2.5%	0.977	0.005	0.005
97.5%	0.989	0.010	0.016
Delta			
Mean	0.960	0.016	0.024
2.5%	0.938	0.011	0.015
97.5%	0.972	0.028	0.042
Omicron			
Mean	0.920	0.032	0.048
2.5%	0.901	0.026	0.036
97.5%	0.933	0.038	0.065

Note: The means and quantiles are based on the distribution of the ratios over ensemble members (and not the ratio of the distributions). Some rows for the mean may not add up to 1 due to rounding error.

5.4 Age-specific burden stratification by immune status and VoC

Computation in Figure 4 A-B. Figure 4 A displays the estimated fractions of age-specific primary and respectively breakthrough or re-infection cases in total cases, per variant period, where “primary infections” were modeled by the first compartment set ($a = 1$), and “breakthrough or re-infections” by the second compartment set ($a = 2$). For each ensemble member, and each compartment set $a = 1, 2$, the number of infections in that compartment set at time t is $\sum_{i=1}^{12} \frac{I_{newik}^{a,e,post}(t)}{\alpha_k^{e,post}(t)}$, and fractions are relative to the population in each age category, $\sum_{i=1}^{12} N_{ik}$. Each of these fractions is summed separately over each variant period defined in Table A1. The fraction of hospital admissions per ensemble member, after primary or breakthrough/re-infections is calculated in the same way, but substituting $\frac{I_{newik}^{a,e,post}(t)}{\alpha_k^{e,post}(t)}$ with $H_{newik}^{a,e,post}(t) \times 1,000$. Figure 4 A-B reports the mean and the 95% CrI over the 300 ensemble values of these fractions. The data behind Figures 4 A-B are presented in Tables A12-A13.

Table A12: Primary infections versus breakthrough or re-infections as a fraction of population per variant: Data in Figure 4 A, main text

	Adults		Adolescents		Children	
	Prim	Break/Re-	Prim	Break/Re-	Prim	Re-
Wild-Type						
Mean	0.211	0.004	0.166	0.001	0.026	0.00003
2.5%	0.197	0.003	0.157	0.001	0.022	0.00001
97.5%	0.230	0.006	0.184	0.002	0.032	0.00010
Alpha						
Mean	0.206	0.029	0.191	0.014	0.097	0.0013
2.5%	0.202	0.027	0.180	0.012	0.086	0.0010
97.5%	0.214	0.032	0.213	0.016	0.111	0.0019
Delta						
Mean	0.042	0.160	0.137	0.078	0.149	0.0116
2.5%	0.041	0.157	0.127	0.072	0.128	0.0087
97.5%	0.043	0.167	0.152	0.088	0.166	0.0146
Omicron						
Mean	0.039	0.231	0.226	0.210	0.305	0.0343
2.5%	0.038	0.227	0.215	0.199	0.294	0.0314
97.5%	0.040	0.236	0.239	0.221	0.318	0.0373

Note: "Prim" and "Break/Re-" refer to primary and breakthrough/re-infections. The fractions of total primary and breakthrough or re-infections per age, reported in the main text, Section “Age-specific burden stratification by immune status and VoC”, are calculated by adding the mean percentages in this table across primary and breakthrough/re-infections.

Table A13: Hospitalizations among primary infections versus breakthrough or re-infections as a fraction of population, per variant, multiplied by 1,000: Data in Figure 4 **B**, main text

	Adults		Adolescents		Children	
	Prim	Break/Re-	Prim	Break/Re-	Prim	Re-
Wild-Type						
Mean	2.18	0.03	0.11	0	0.07837	0
2.5%	2.11	0.01	0.06	0	0.02311	0
97.5%	2.24	0.05	0.18	0	0.10786	0
Alpha						
Mean	1.83	0.24	0.10	0	0.1453	0.0002
2.5%	1.77	0.22	0.07	0	0.0744	0.0001
97.5%	1.89	0.27	0.13	0	0.2602	0.0007
Delta						
Mean	0.42	0.73	0.12	0.02	0.2172	0.0015
2.5%	0.40	0.69	0.08	0.01	0.1436	0.0007
97.5%	0.44	0.76	0.20	0.03	0.3871	0.0039
Omicron						
Mean	0.15	0.46	0.10	0.04	0.2372	0.0070
2.5%	0.14	0.43	0.08	0.03	0.1807	0.0047
97.5%	0.17	0.49	0.12	0.05	0.3249	0.0106

Note: "Prim" and "Break/Re-" refer to hospitalization after primary and breakthrough/re-infections.

6 Parameter and system identifiability

6.1 Simulated model fit

We limit the sample period to the first regime (lockdown, Feb 27, 2020 to March 30, 2020), where the parameters can reasonably be assumed to be constant. We fix the parameters at their posterior means from the original sample, and call them "true" parameters; these parameters, rounded to two digits (except for hospitalization rate, rounded to three digits) are given in Table A14. We simulate one synthetic outbreak, and from this, we also generate seroprevalence data on March 23 ($= t_1^{ser}$), and use the synthetic reported case data, hospitalizations, and seroprevalence data to refit the model. All other calibrations and estimation are as for the original data. Note that we initialize the estimation as described in Section 3.3, not assuming that the initial state variables are known.

Table A14: Parameters fixed in synthetic outbreak

ϵ_1	$f_{2,\epsilon}$	$f_{3,\epsilon}$	α_1	α_2	α_3	θ_1	$f_{2,\theta}$	$f_{3,\theta}$	γ_1	γ_2	γ_3	ζ	μ	Z	D	K_1
0.06	0.65	0.56	0.06	0.03	0.03	0.50	0.38	0.36	0.096	0.004	0.004	0.92	0.66	4.04	4.92	0.73

The synthetic seroprevalence fit on March 23, when the synthetic serosurvey is assumed to be collected, is very similar to the synthetic data and given in Table A15.

Table A15: Seroprevalence: synthetic data versus model fit

Age category	Synthetic Data	Mean	95% CrI	
Adults	0.0144	0.0086	0.0050	0.0156
Adolescents	0.0028	0.0024	0.0006	0.0052
Children	0.0019	0.0014	0.0004	0.0036

Figure A17-A20 show a very good fit to the synthetic hospitalization reported case data across all regions. These figures also show that the simulated pattern of infections and hospitalizations largely reproduces the patterns in the original data: fewer reported cases in children and adolescents, and more reported cases and hospitalizations in larger regions. The number of confirmed cases and hospitalizations is relatively smaller than in the real data, likely because the parameters are fixed at their posteriors and as such do not represent the full

uncertainty in the original data.

Figure A17: Regional daily hospitalizations for all ages

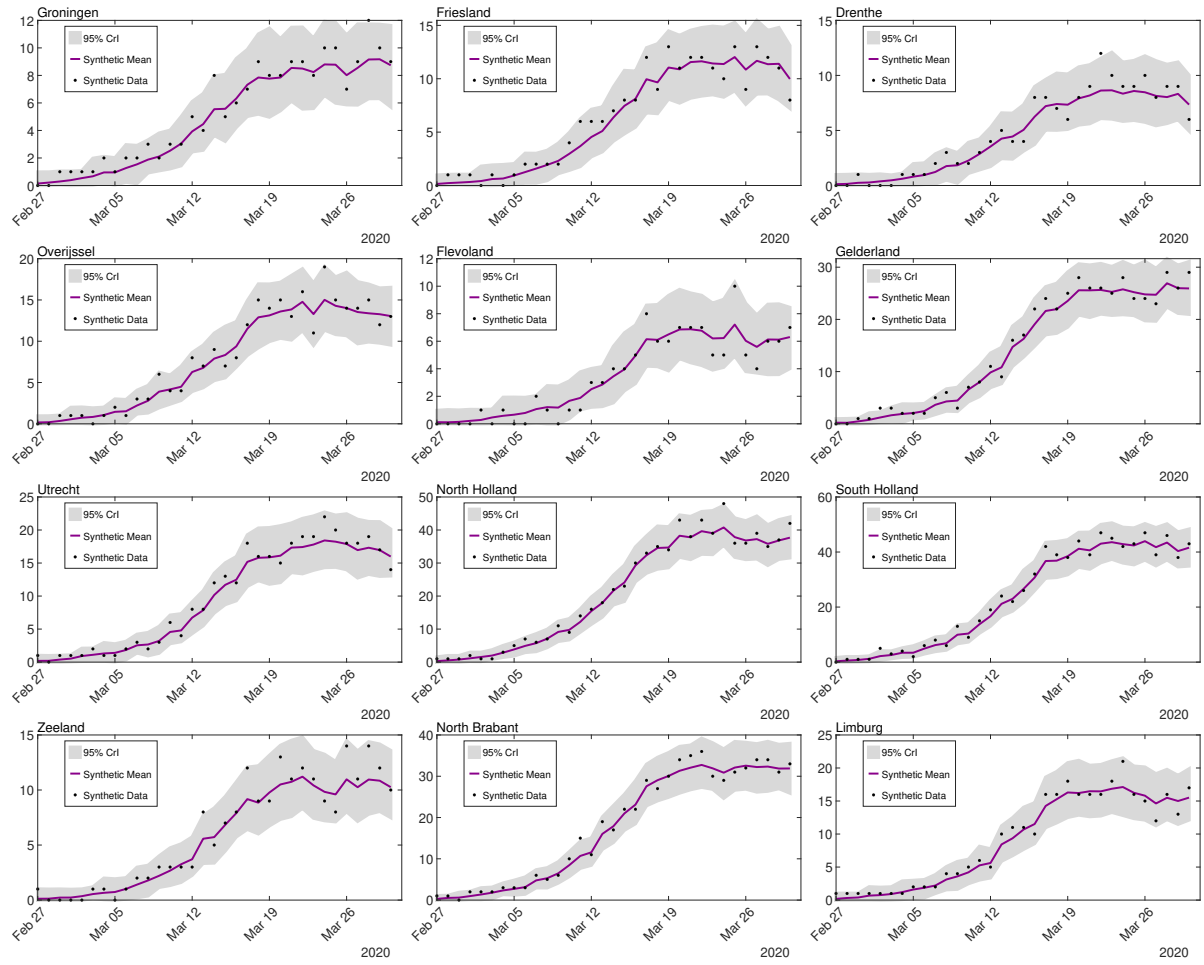


Figure A18: ADULTS: Regional daily reported cases

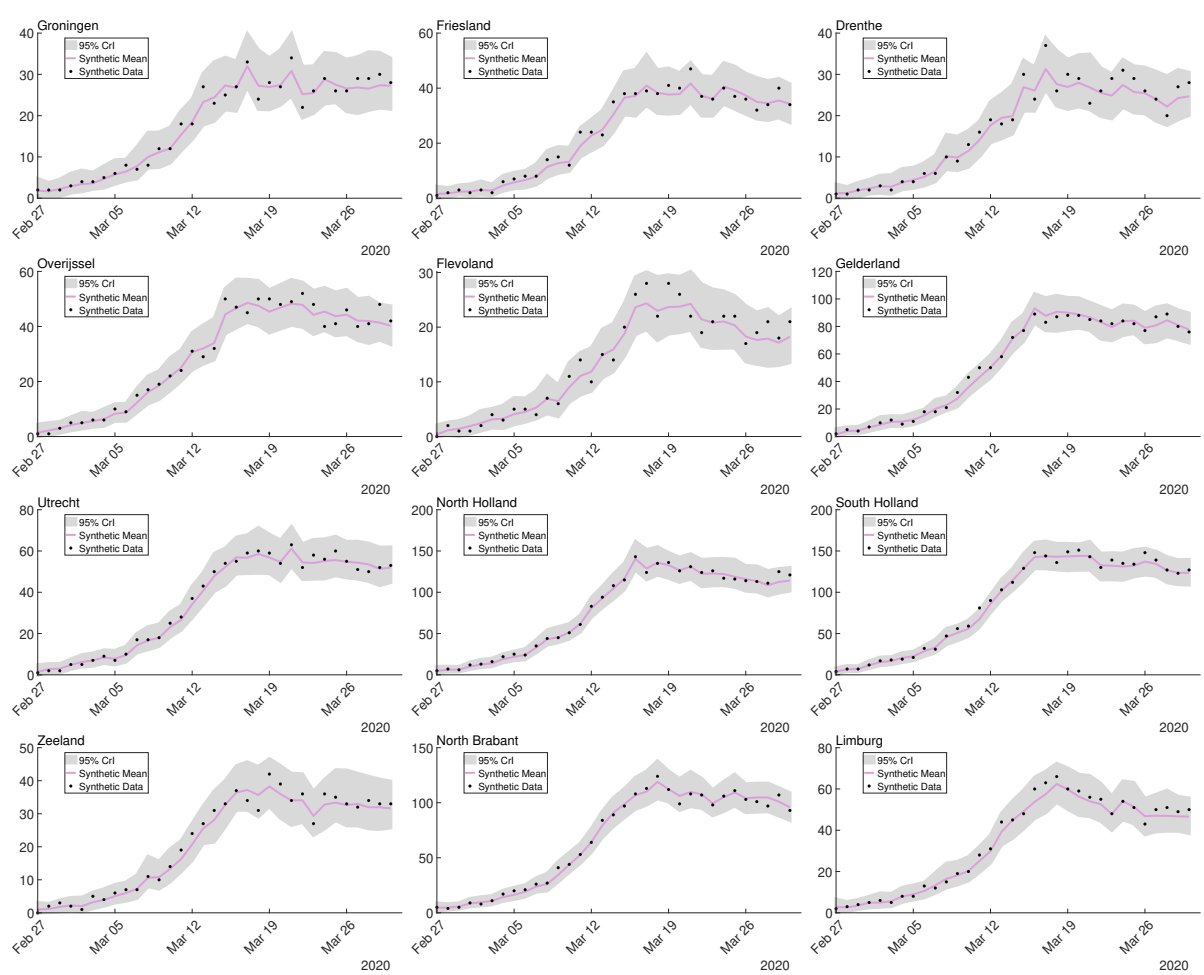


Figure A19: ADOLESCENTS: Regional daily reported cases

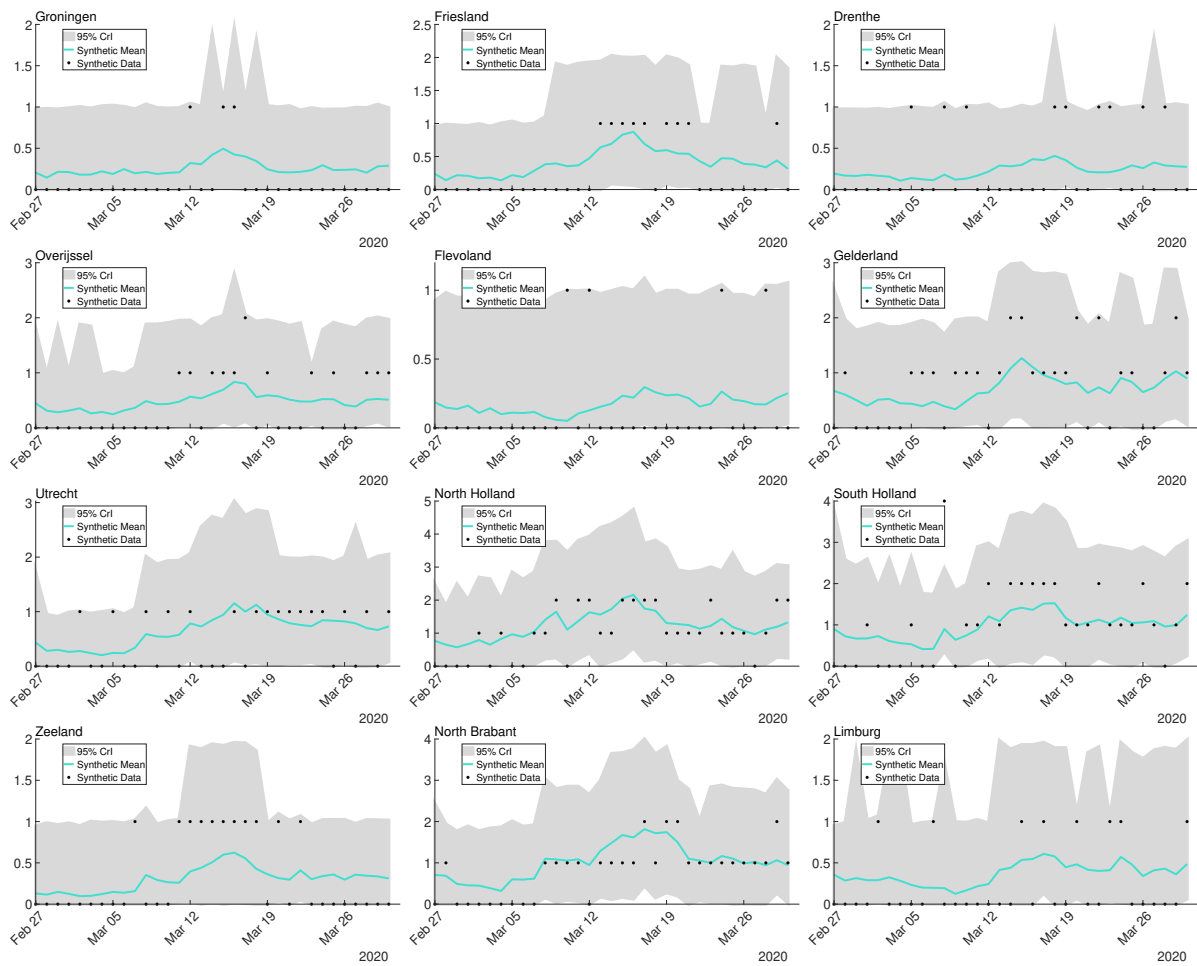
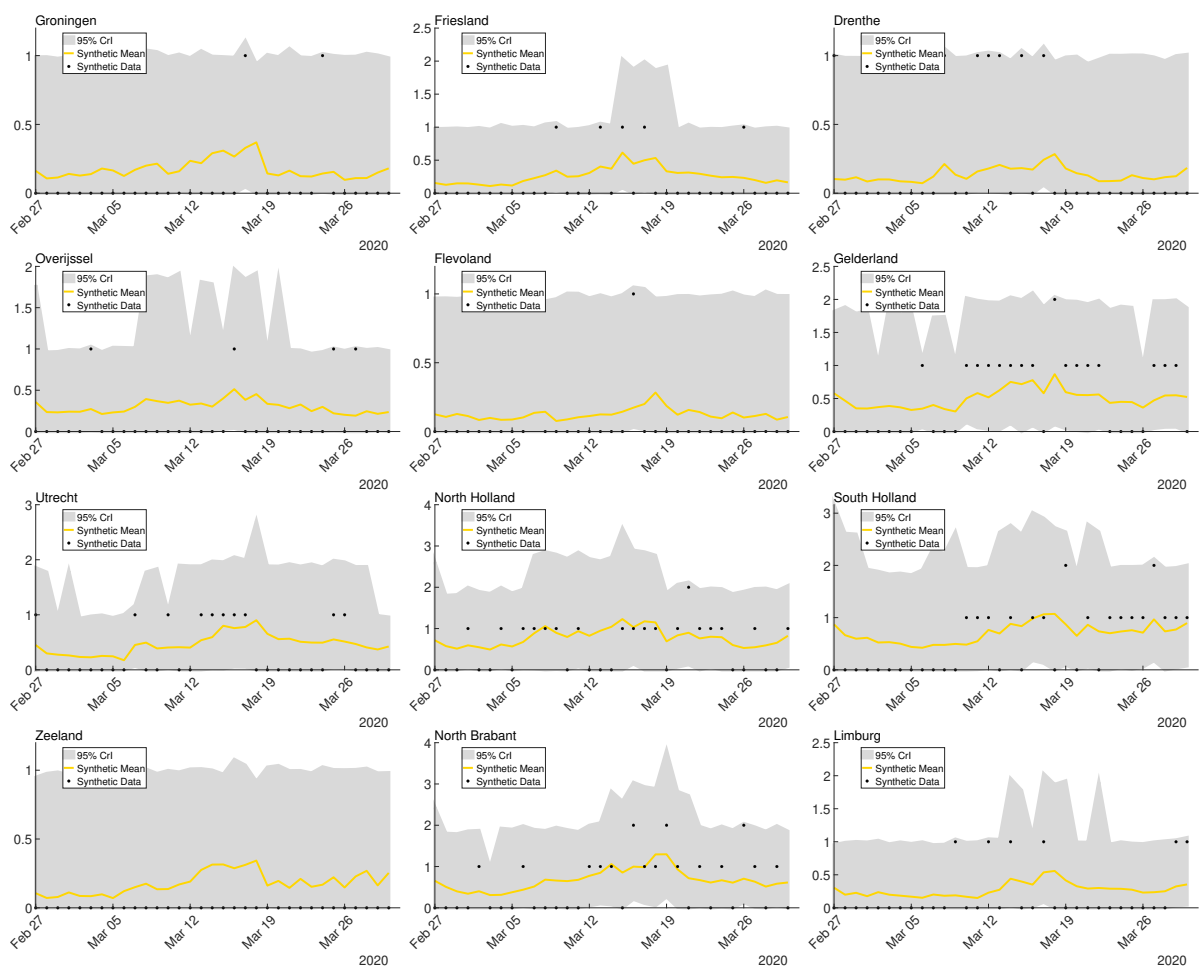


Figure A20: CHILDREN: Regional daily reported cases I



6.2 Parameter identification

In Section 4, we showed that the posteriors for most parameters tighten over the sample, and are most uncertain at the beginning of the sample. Therefore, this section provides simulations to check parameter identification at the beginning of the sample (first wave, February 27, 2020 - April 30, 2020).

Note that EAKF does not in general deliver fully Bayesian posterior credible intervals, as it does not take into account the full joint uncertainty in parameters and unobservables ([5], published in [6]), and it inflates credible intervals to prevent the filter from collapsing, widening posterior credible intervals.¹⁹ At the same time, the EAKF does not deliver classical (frequentist) confidence intervals because informative priors shrink these, while variance inflation widens them to keep some of the information in the priors to safeguard against the possibility that the data signal is weak relative to previous updates.

Hence, there is no established framework to check identification in our setting. Also, due to large uncertainty at the beginning of the sample, with few regions per period compared to [14], one cannot expect a single synthetic outbreak (one dataset) to recover the true parameters. Therefore, we proceed as follows. We generate 100 synthetic outbreaks with parameters fixed at some “true” values. We draw the initial values of the unobserved state variables once and keep them fixed in each of the 100 generated synthetic outbreaks. For each of these, we re-estimate the model using the same parameter priors, initializations, and estimation technique described in Section 3 and obtain 100 simulated posterior means.²⁰ We then plot the smoothed density of these means against the true parameters to check if the true parameter falls within the range of this distribution, or alternatively, to assess how close the simulated means are to the true means.

We consider three simulation designs. Design A is as in Section 6.1, but 100 synthetic outbreaks are generated as explained above. Design B is as Design A, but the case detection rates are increased to $\alpha_1 = 0.10$ and $\alpha_2 = \alpha_3 = 0.08$. As changes in parameters such as case detection rates are not modeled, we verify via simulation that the filtering technique can recover these changes. To that end, we introduce Design C, where the number of observations is increased within one month to 64 observations (Feb 27, 2020 - April 30, 2020), and the case detection rates are the same as in Design A, but increase after 33 observations (on March 31, 2022) to the values in Design B. For Design C, we also maintain the first (lockdown) regime, so that K_2 is not learned in the same short sub-sample where changes in the case detection rates occur.

Figures A21 - Figures A23 show that the true mean falls within the range of the distribution of means for most parameters. Figure A24 also shows that the filter can learn a change in the case detection rate relatively quickly, adjusting to this almost immediately.

The hospitalization rates seem well identified across the simulations, especially for adults, despite their wide prior. The case detection rates are often (but not always) over-estimated in Design A, and under-estimated in Designs B-C, but Figure A24 shows that this is solely due to large uncertainty at the beginning of the sample, and slow learning of the true parameters, compared to [14] and [16], where the number of regions is large. We also find that the mobility reporting error rates $\theta, f_{2,\theta}, f_{3,\theta}$ and the smoothness of NPI transition K_1 are the least well identified, centering around the mid-point of the prior. On the other hand, the prior on these parameters are tight, and in the model fitting, their uncertainty is maintained throughout, so changes in these parameters within the prior range will not qualitatively affect the results of this study.

¹⁹Note that the filtering cannot be iterated as in [14] to remove the variance inflation, because doing so would not approximate well the time-varying path of some parameters like the case detection rate.

²⁰We widened the priors on the case detection rates to $[0.02, 0.3]$ to accommodate larger case detection rates in some synthetic designs

Figure A21: Design A: Smoothed density of posterior means versus true parameters

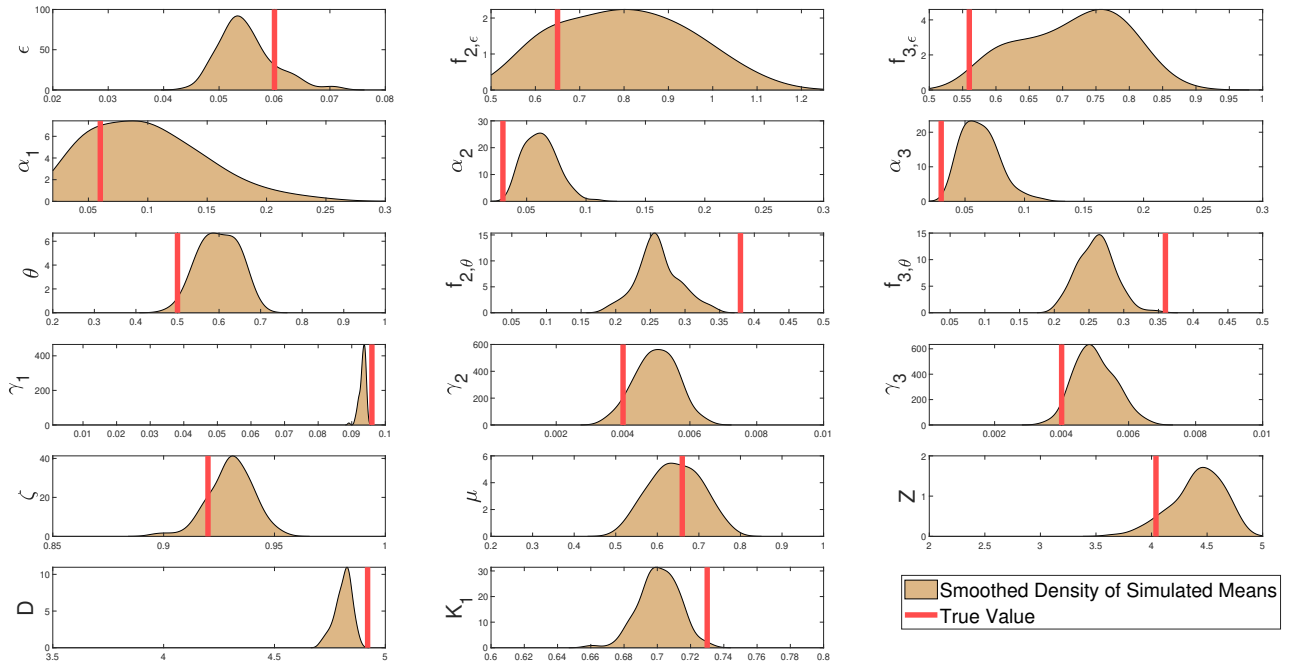


Figure A22: Design B: Smoothed density of posterior means versus true parameters

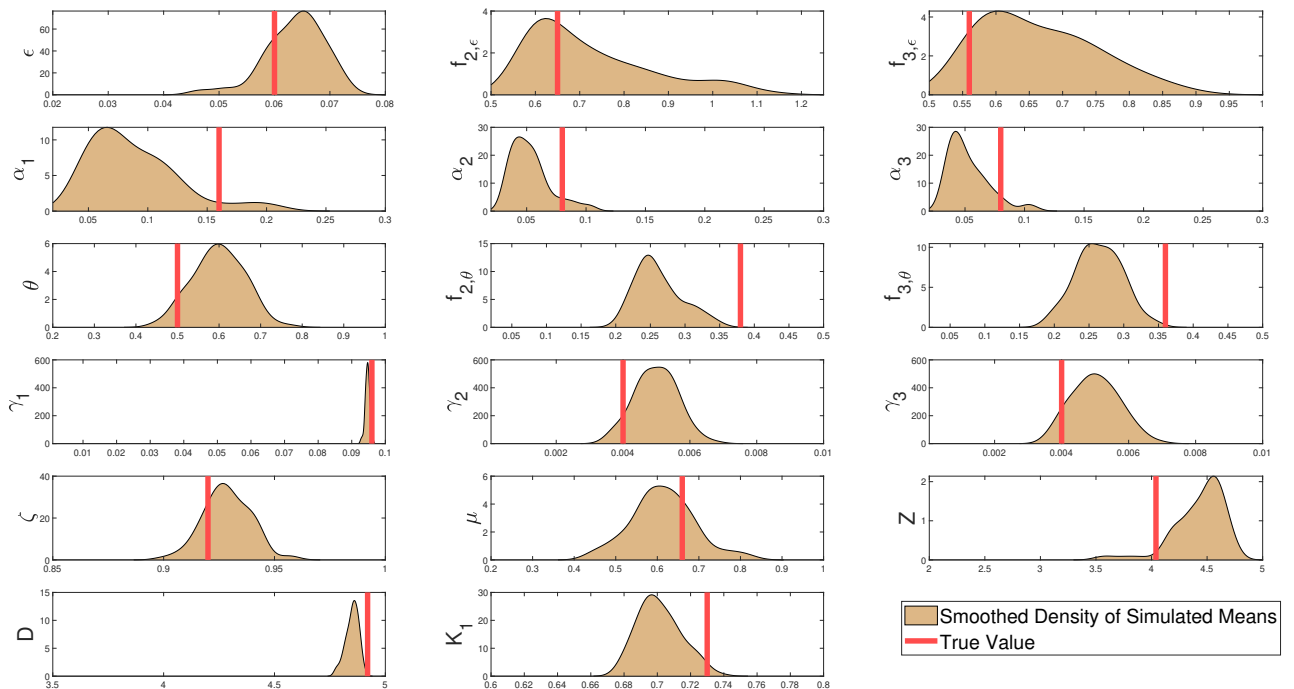


Figure A23: Design C: Smoothed density of posterior means versus true parameters

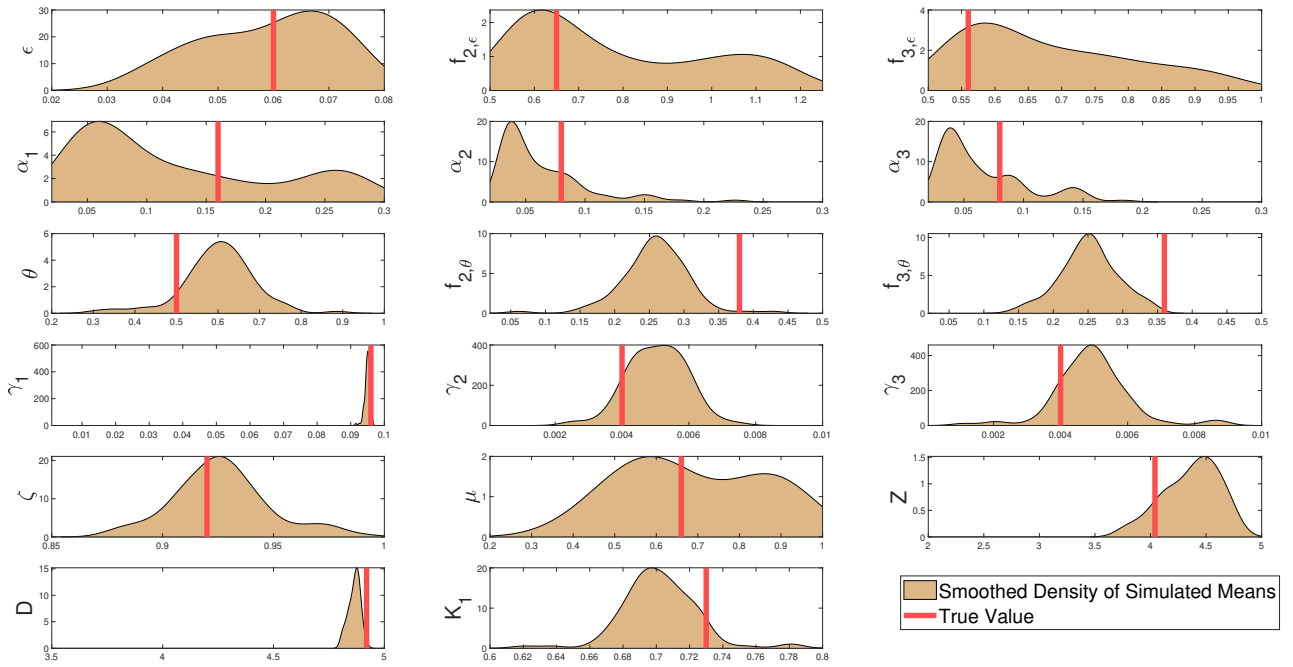
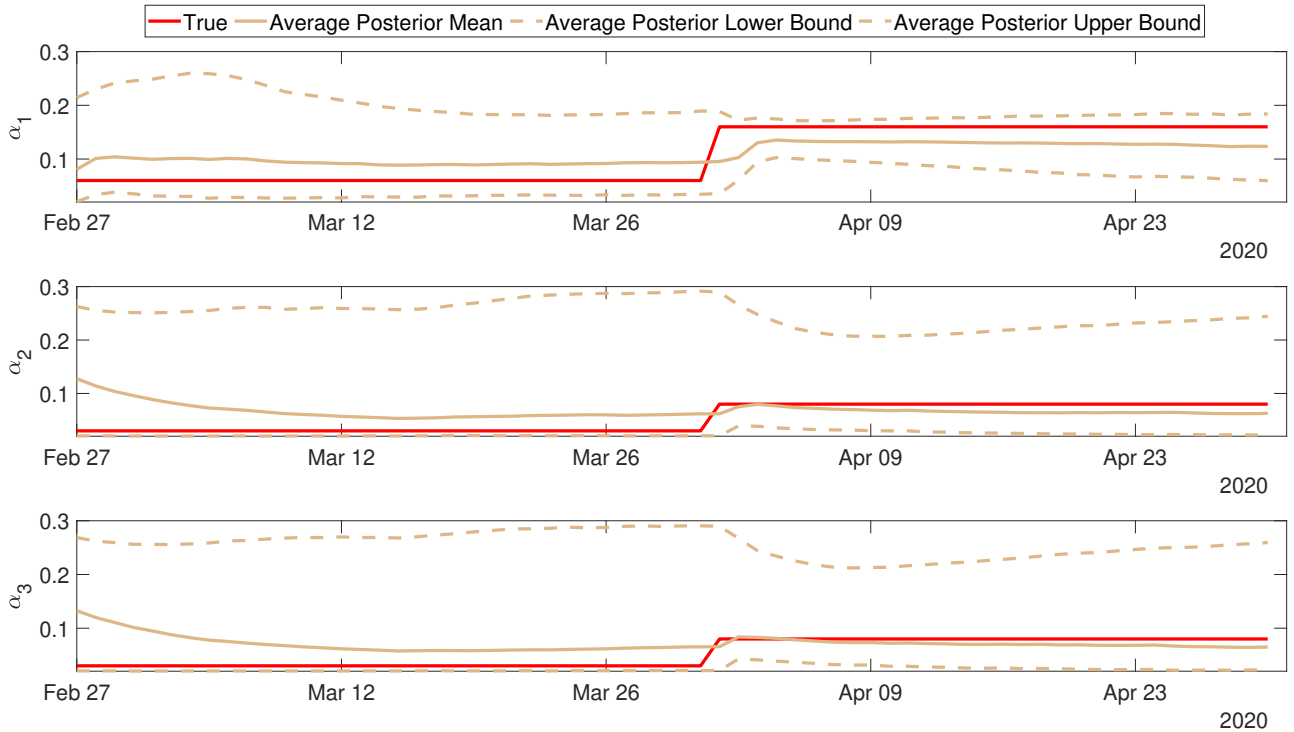


Figure A24: Design C - Posterior evolution of means, lower and upper CrI bounds, averaged over simulations, versus true evolution of α_k



7 Sensitivity analysis

In this section, we evaluate the sensitivity of model fit and parameter estimates to seroprevalence dates, use of seroprevalence data on top of mobility, and to calibrated parameters such as waning rates, relative increase of transmissibility of Omicron, and seasonality.

7.1 Sensitivity to seroprevalence

The four seroprevalence surveys are implemented at the median time of collection minus 14 days to allow for seroconversion. We shortened the time allowed for seroconversion to 10 days, and we also tried not using the seroprevalence data at all in the estimation. The model fit to the data, the parameter estimates, and the estimated seroprevalence over the whole sample are virtually unchanged in both cases, and therefore not shown: Table A8 is identical in both cases because the results are identical when rounded to the first two digits. This underlines the fact that in a model where infections are stochastic and fitted to infection data at high frequency (as opposed to a deterministic model of infections, where infection data is not used, and parameters are calibrated to match observed seroprevalence), a few seroprevalence rounds are not very informative for identifying unreported cases on top of identification through mobility.

7.2 Sensitivity to waning rates

The waning period was calibrated at $1/\eta_A = 1$ year before Omicron and then assumed to rise with the transition function for Omicron to $1/\eta_B = 3$ months. We reran the estimation with $1/\eta_A = 6$ months and $1/\eta_A = 2$ years respectively. A waning period $1/\eta_A$ of 6 months results in the model output in individuals getting infected quicker, but at the same time moving faster into the second compartment set where they are only partially susceptible. While the data fit is not very different than for $1/\eta_A = 1$ year, Table A16 shows that the implied seroprevalence is much lower, only 36% (95% CrI [35%, 38%]) for the entire population before Omicron, and 75% (95% CrI: [73%, 77%]) at the end of the sample, compared to 45% (95% CrI: [43%, 46%]) and 83% (95% CrI: [81%, 85%]). Note that the implied seroprevalence in adults is also substantially lower than the estimates from RIVM Pienter Corona²¹ in the November /December Survey, whose lower credible intervals are around 80% for adults. On the other hand, a waning period $1/\eta_A = 2$ years before Omicron means that individuals lose immunity much slower, so more of them have to be infected at the beginning of the sample to fit the data. The implied seroprevalence is therefore substantially larger at the beginning of the sample, with 25% of adults seropositive for the wild-type period (CrI: [23%, 26%]), which is approximately twice as high as that implied by the fourth seroprevalence round from RIVM in February, despite this round being used in fitting the model. The analysis, therefore, suggests that a waning period of one year is more plausible.

²¹<https://www.rivm.nl/en/pienter-corona-study/results>

Table A16: Cumulative seroprevalence at the end of each variant period: means and 95% CI. Different waning periods before Omicron

Variant	waning period $1/\eta_A = 6$ months				waning period $1/\eta_A = 2$ years			
	Wild-type	Alpha	Delta	Omicron	Wild-type	Alpha	Delta	Omicron
Adults								
Mean	0.17	0.25	0.40	0.76	0.25	0.41	0.58	0.88
2.5%	0.16	0.24	0.38	0.73	0.23	0.39	0.56	0.86
97.5%	0.19	0.26	0.41	0.78	0.26	0.42	0.60	0.90
Adolescents								
Mean	0.15	0.24	0.28	0.87	0.19	0.38	0.48	0.92
2.5%	0.14	0.22	0.26	0.84	0.17	0.35	0.45	0.90
97.5%	0.16	0.25	0.31	0.91	0.21	0.40	0.51	0.94
Children								
Mean	0.02	0.06	0.18	0.55	0.03	0.13	0.30	0.71
2.5%	0.02	0.05	0.14	0.51	0.02	0.11	0.27	0.68
97.5%	0.02	0.07	0.20	0.58	0.03	0.14	0.32	0.74
All ages								
Mean	0.16	0.23	0.36	0.75	0.22	0.38	0.54	0.87
2.5%	0.14	0.22	0.35	0.73	0.21	0.36	0.52	0.85
97.5%	0.17	0.24	0.38	0.77	0.23	0.39	0.55	0.89

Next, we vary the waning period after Omicron $1/\eta_B$ to 2 and 4 months respectively. The fit to the data is very similar to the original model which assumed $1/\eta_B = 3$ months. The resulting seroprevalence estimates are shown in Table A17. Note that the slower waning period does not necessarily imply a smaller seroprevalence because some parameter estimates slightly change. However, there are no substantial changes in both the parameter estimates, model fit, or seroprevalence. Therefore, the analysis is robust to setting the waning period to 2 or 4 months for Omicron, instead of 3 months.

Table A17: Cumulative seroprevalence over the full sample: means and 95% CI. Different waning periods after Omicron

waning period $1/\eta_B$	3 months	2 months	4 months
Adults			
Mean	0.84	0.84	0.85
2.5%	0.82	0.83	0.83
97.5%	0.86	0.87	0.87
Adolescents			
Mean	0.90	0.93	0.93
2.5%	0.87	0.89	0.91
97.5%	0.93	0.95	0.95
Children			
Mean	0.64	0.64	0.64
2.5%	0.60	0.60	0.60
97.5%	0.68	0.67	0.67
All ages			
Mean	0.83	0.83	0.84
2.5%	0.81	0.81	0.82
97.5%	0.85	0.85	0.86

7.3 Sensitivity to higher transmissibility of Omicron

In the sample, the transmissibility of Omicron relative to the Delta variant, ρ_o , was calibrated to 40%. We rerun the estimation with $\rho_o = 60\%$ and obtained very similar results in terms of fit and seroprevalence (see Table

A18). All parameter estimates are also very similar, except for p_I^4 , the parameter that measures the average reduction in transmissibility due to boosters. This parameter doubled, with end of sample posterior mean now estimating a 66% reduction (95% CrI: [63%, 69%] in transmissibility as compared to a 34% reduction (95% CrI: [30%, 41%]) when $\rho_o = 0.40$, explaining the slight reduction in the seroprevalence estimates. This indicates that both transmission increases are plausible, depending on how effective boosters would be in reducing average transmissibility in a mixed population of boosted and non-boosted individuals, with little change in the results.

Table A18: Cumulative seroprevalence at the end of the Omicron sample period: means and 95% CI. Different transmissibility of Omicron relative to Delta

Increase transmissibility Omicron	$\rho_o = 0.4$	$\rho_o = 0.6$
Adults		
Mean	0.84	0.83
2.5%	0.82	0.80
97.5%	0.86	0.85
Adolescents		
Mean	0.90	0.90
2.5%	0.87	0.87
97.5%	0.93	0.93
Children		
Mean	0.64	0.63
2.5%	0.60	0.59
97.5%	0.68	0.66
All ages		
Mean	0.83	0.81
2.5%	0.81	0.79
97.5%	0.85	0.84

7.4 Sensitivity to seasonality factor

The seasonality factor was calibrated at $season(t) = 1 + 0.1 \cos \frac{2\pi(t-t^*)}{365.25}$. We re-estimated the model with no seasonality $season(t) = 1$; the fit to the data is similar, but the parameter estimates change to accommodate this new calibration. The new seroprevalence estimates are shown in Table A19 side-by-side with the original model estimates in Table A8. With no seasonality, the disease burden across age categories changes, but the changes are only substantially different during Omicron, where the estimated reduction in probability of infection in the average population due to boosters (p_I^4) rises again to 66% (95% CrI: [0.63%, 0.69%]) to accommodate more infections in the absence of seasonality. Note that the implied seroprevalence in adults is, as in the case of slower waning rates, relatively lower than the estimates from RIVM study ²² in the November /December Survey, suggesting that either seasonality or a richer model capturing nonlinearities in transmission during colder seasons may be needed to capture the transmission pattern of SARS-CoV-2 more accurately.

²²<https://www.rivm.nl/en/pienter-corona-study/results>

Table A19: Cumulative seroprevalence at the end of each variant period: means and 95% CI. Original model seasonality versus no seasonality

Variant	Seasonality				No seasonality			
	Wild-type	Alpha	Delta	Omicron	Wild-type	Alpha	Delta	Omicron
Adults								
Mean	0.19	0.32	0.48	0.84	0.21	0.33	0.48	0.82
2.5%	0.17	0.31	0.46	0.82	0.17	0.30	0.44	0.78
97.5%	0.20	0.34	0.50	0.86	0.24	0.36	0.52	0.86
Adolescents								
Mean	0.16	0.29	0.40	0.90	0.12	0.27	0.35	0.85
2.5%	0.15	0.27	0.38	0.87	0.10	0.25	0.33	0.81
97.5%	0.17	0.31	0.43	0.93	0.14	0.30	0.40	0.90
Children								
Mean	0.02	0.11	0.23	0.64	0.02	0.08	0.20	0.55
2.5%	0.02	0.09	0.20	0.60	0.02	0.06	0.17	0.50
97.5%	0.03	0.12	0.25	0.68	0.03	0.09	0.23	0.58
All ages								
Mean	0.17	0.30	0.45	0.83	0.18	0.30	0.44	0.79
2.5%	0.15	0.28	0.43	0.81	0.15	0.28	0.40	0.76
97.5%	0.18	0.31	0.46	0.85	0.21	0.32	0.47	0.83

References

- [1] Sam Abbott, Katharine Sherratt, Moritz Gerstung, and Sebastian Funk. Estimation of the test to test distribution as a proxy for generation interval distribution for the Omicron variant in England. 2022. <https://www.medrxiv.org/content/10.1101/2022.01.08.22268920v1.full.pdf>.
- [2] Laith J. Abu-Raddad, Hiam Chemaitelly, Houssein H. Ayoub, Sawsan AlMukdad, Hadi M. Yassine, Hebah A. Al-Khatib, Maria K. Smatti, Patrick Tang, Mohammad R. Hasan, Peter Coyle, Zaina Al-Kanaani, Einas Al-Kuwari, Andrew Jeremijenko, Anvar H. Kaleeckal, Ali N. Latif, Riyazuddin M. Shaik, Hanan F. Abdul-Rahim, Gheyath K. Nasrallah, Mohamed Ghaith Al-Kuwari, Adeel A. Butt, Hamad Eid Al-Romaihi, Mohamed H. Al-Thani, Abdullatif Al-Khal, and Roberto Bertolini. Effect of mRNA vaccine boosters against SARS-CoV-2 Omicron infection in Qatar. *The New England Journal of Medicine*, 398:1825–1835, 2022.
- [3] Kylie E. C. Ainslie, Jantien Backer, Pieter de Boer, Albert Jan van Hoek, Don Klinkenberg, Hester Korthals Altes, Ka Yin Leung, Hester de Melker, Fuminari Miura, and Jacco Wallinga. The impact of vaccinating adolescents and children on COVID-19 disease outcomes. *Medrxiv*, 2021. <https://doi.org/10.1101/2021.10.21.21265318>.
- [4] Jeffrey L. Anderson. An Ensemble Adjustment Kalman Filter for data assimilation. *Monthly Weather Review*, 129:2884–2903, 2001. [https://doi.org/10.1175/1520-0493\(2001\)129<2884:AEAKFF>2.0.CO;2](https://doi.org/10.1175/1520-0493(2001)129<2884:AEAKFF>2.0.CO;2).
- [5] Jonas E. Arias, Jesús Fernández-Villaverde, Juan F. Rubio-Ramírez, and Minchul Shin. Bayesian estimation of epidemiological models: Methods, causality, and policy trade-offs. *FRB of Philadelphia Working Paper No. 21-18*, 2021. https://www.sas.upenn.edu/~jesusfv/Bayesian_Epidemiological.pdf.
- [6] Jonas E. Arias, Jesús Fernández-Villaverde, Juan F. Rubio-Ramírez, and Minchul Shin. The causal effects of lockdown policies on health and macroeconomic outcomes. *Forthcoming at American Economic Journal: Macroeconomics*, 2022. <https://www.aeaweb.org/articles?id=10.1257/mac.20210367>.

- [7] Jantien A Backer, Liesbeth Mollema, Eric RA Vos, Don Klinkenberg, Fiona RM van der Klis, Hester E de Melker, Susan van den Hof, and Jacco Wallinga. Impact of physical distancing measures against COVID-19 on contacts and mixing patterns: repeated cross-sectional surveys, the Netherlands, 2016-17, April 2020 and June 2020. *Eurosurveillance*, 26(8), 2021. <https://doi.org/10.2807/1560-7917.ES.2021.26.8.2000994>.
- [8] Thomas Bengtsson, Peter Bickel, and Bo Li. Curse-of-dimensionality revisited: Collapse of the particle filter in very large scale systems. *Institute of Mathematical Statistics Collections*, 2:316–334, 2008. <https://doi.org/10.1214/193940307000000518>.
- [9] Otilia Boldea, Adriana Cornea-Madeira, and Joao Madeira. Disentangling the effect of measures, variants and vaccines on sars-cov-2 infections in england: A dynamic intensity model. *The Econometrics Journal, Conditionally accepted*, 2022. <https://doi.org/10.1101/2022.03.09.22272165>.
- [10] Markus Hoffmann, Prerna Arora, and Stefan Pöhlmann. Understanding Omicron: Transmissibility, immune evasion and antiviral intervention. *Clinical and Translational Medicine, Commentary*, 2022. <https://doi.org/10.1002/ctm2.839>.
- [11] Ali Hortaçsu, Jiarui Liu, and Timothy Schwieg. Estimating the fraction of unreported infections in epidemics with a known epicenter: An application to COVID-19. *Journal of Econometrics*, 220(1):106–129, 2021. <https://doi.org/10.1016/j.jeconom.2020.07.047>.
- [12] Max Kozlov. Covid-19: Omicron variant is linked to steep rise in hospital admissions of very young children. *The British Medical Journal*, 376(o110), 2022. <https://doi.org/10.1136/bmj.o110>.
- [13] Theresa Lange. Derivation of ensemble Kalman Bucy filters with unbounded nonlinear coefficients. *Nonlinearity*, 35:1061–1092, 2021. <https://doi.org/10.1088/1361-6544/ac4337>.
- [14] Ruiyin Li, Sen Pei, Bin Chen, Yimeng Song, Tao Zhang, Wan Yang, and Jeffrey Shaman. Substantial undocumented infection facilitates the rapid dissemination of novel coronavirus (SARS-CoV-2). *Science*, pages 489–493, 2020. <https://doi.org/10.1126/science.abb3221>.
- [15] Dina Mistry, Maria Litvinova, Ana Pastore y Piontti, Laura Fumanelli, Marcelo F. C. Gomes, Syed A. Haque, Quan-Hui Liu, Kunpeng Mu, Xinyue Xiong, M. Elizabeth Halloran, Ira M. Longini, Stefano Merler, Marco Ajelli, and Alessandro Vespignani. Inferring high-resolution human mixing patterns for disease modeling. *Nature Communications*, 12:323, 2021. <https://doi.org/10.1038/s41467-020-20544-y>.
- [16] Sen Pei, Teresa K. Yamana, Sasikiran Kandula, Marta Galanti, and Jeffrey Shaman. Burden and characteristics of COVID-19 in the United States during 2020. *Nature*, 598:338–341, 2021. <https://doi.org/10.1038/s41586-021-03914-4>.
- [17] Pablo N. Perez-Guzman, Natsuko Imai, Edward S. Knock, Thomas Rawson, Raphael Sonabend, Divya Thekke Kanapram, Lilith K. Whittles, Erik M. Volz, Neil M. Ferguson, Anne Cori, and Marc Baguelin. Autumn and Winter 2021-2022: potential COVID-19 epidemic trajectories. *Imperial College Reports*, 2021.
- [18] RIVM. Parliament Briefing 7 Jul 2021. 2021. <https://www.tweedekamer.nl/kamerstukken/detail?id=2021D27744&did=2021D27744>, Page 10.
- [19] RIVM. Parliament Report 22 February 2021. 2021. https://www.tweedekamer.nl/zoeken?search_str=Jaap+van+Dissel, Page 9.

- [20] Ganna Rozhnova, Christiaan H. van Dorp, Patricia Bruijning-Verhagen, Martin C. J. Bootsma, Janneke H. H. M. van de Wijgert, Marc J. M. Bonten, and Mirjam E. Kretzschmar. Model-based evaluation of school- and non-school-related measures to control the COVID-19 pandemic. *Nature Communications*, 12:1614, 2021. <https://doi.org/10.1038/s41467-021-21899-6>.
- [21] Raphael Sonabend, Lilith K. Whittles, Pablo N. Perez-Guzman Natsuko Imai, Edward S. Knock, Thomas Rawson, Katy A. M. Gaythorpe, Bimandra A. Djaafara, Wes Hinsley, Richard G. FitzJohn, John A. Lees, Divya Thekke Kanapram, Erik M. Volz, Azra C. Ghani, Neil M. Ferguson, Marc Baguelin, and Anne Cori. Non-pharmaceutical interventions, vaccination, and the SARS-CoV-2 delta variant in England: a mathematical modelling study. *The Lancet*, 398:1825–1835, 2021. [https://doi.org/10.1016/S0140-6736\(21\)02276-5](https://doi.org/10.1016/S0140-6736(21)02276-5).
- [22] RIVM COVID-19 Surveillance Team. Effectivity of COVID-19 vaccines against hospital and intensive-care admissions in netherlands (admissions 11 july 2021 - 25 january 2022). 2022. https://www.rivm.nl/sites/default/files/2022-02/VE%20update%2001-02-2022_20220207.pdf.
- [23] Joao Viana, Christiaan H. van Dorp, Ana Nunes, Manuel C. Gomes, Mirjam E. Kretzschmar, Mark Veldhoen, and Ganna Rozhnova. Controlling the pandemic during the SARS-CoV-2 vaccination rollout. *Nature Communications*, 12:3674, 2021. <https://doi.org/10.1038/s41467-021-23938-8>.
- [24] Wan Yang and Jeffrey Shaman. Development of a model-inference system for estimating epidemiological characteristics of SARS-CoV-2 variants of concern. *Nature Communications*, 12:5573, 2021. <https://doi.org/10.1038/s41467-021-25913-9>.